SCUOLA DI DOTTORATO
UNIVERSITÀ DEGLI STUDI DI MILANO-BICOCCA

Department of Biotechnology & Biosciences
Program in Molecular and Translational Medicine
DIMET
(XXXV Cycle, year 2020-2023)

University of Milano-Bicocca

"Identifying age related changes in the human immune system by using polychromatic flow cytometry"

Christina Pitsillidou

Registration Number: 863994

Supervisor: Alessandra Roberto, PhD

Tutor: Professor Antonella Ellena Ronchi

Co-tutor: Professor Andrea Biondi

Coordinator: Professor Francesco Mantegazza

ACADEMIC YEAR 2021 - 2022

‘Δεν θα διασχίσεις τον ωκεανό,
αν δεν αποκτήσεις το κουράγιο να χάσεις τη θέα της
ακτής’
~ Αντρέ Ζιντ

Αυτή η διδακτορική διατριβή είναι αφιερωμένη στους
παππούδες και τις γιαγιάδες μου,

Ανδρέας Πιτσιλλίδης *Χριστοφής Λαγός*
Ανδρούλα Πιτσιλλίδου *Υβόν Άρτεμις Μαράλ Λαγού*

Acknowledgements

In the following meaningful lines, I would like to express my sincere gratitude to all those who supported me over these past three years.

First and foremost I would like to thank those that whom without I would not have been able to complete this research project and my PhD degree! The whole FlowMetric Europe team was pivotal in my training on flow cytometry and I am truly thankful to have received such knowledge from them. Primarily, I am extremely grateful to my supervisor Dr. Alessandra Roberto for her invaluable advice, guidance, continuous support and patience during my PhD studies. Her immense knowledge and experience has encouraged and inspired me through my project and her work ethic makes her a true role model. Most importantly she has taught me prized life lessons of professionalism and work ethic that I've never seen before in my career. *Grazie mille Ale. Grazie per la tua pazienza, professionalità e per il tempo dedicatomi.*

I would also like to sincerely thank my second supervisor at FME, Dr. Milena Bertolotti as her knowledge and work allowed my studies to go the extra mile. Thank you for always accepting to help me with anything I needed at times when I was under a lot of stress. I am thankful also to Ivan Muradore for his knowledge on flow cytometry and privileged to have been trained by him on the flow cytometers at FME. Thank you for spending your time to order all my reagents and materials that without I would not be able to add content in this thesis. At FME, I would also like to recognise Gianluca Carenzo for giving me the chance to work at FME. I am extremely privileged for this opportunity and I could not have been more thankful.

Next, I would like to thank Dr. Elena Pontarini from Queen Mary University London for supporting me with providing healthy human PBMC samples from my project. I would like to thank her for taking the time to provide valuable information for each subject enrolled in the project. I would also like to thank Dr. Leonid Bystrykh from the University of Groningen for his support in teaching me computational and statistical analysis. Also, I would like to thank Andreas Ioannou FIA, for his support on mathematical questions early on during my degree.

The collaborative work with the ARCH consortium was pivotal for the completion of this project. I am truly thankful to the European Union's Horizon 2020 Research and Innovation Program under the Marie Skłodowska-Curie grant agreement no. 813091 (ARCH, age-related

changes in hematopoiesis). I would also like to take this opportunity to thank Professor Antonella Ellena Ronchi, the coordinator of the ARCH project. I would like to thank her for giving me the opportunity to teach a seminar to students of UNIMIB and for her willingness to collaborate with me to publish an editorial on the struggles faced during the global pandemic with all the PhD students of the ARCH consortium (attached in the epilogue of this thesis).

Throughout this experience I have gained friends for life. Agata Labedz thank you for always being there for me to discuss our worries after work at La Buttiga and always supporting me. I would also like to take this opportunity to thank my new forever friends in Italy, Marco Cocca, Maria Petta and Dobby. Thank you guys for the weekend getaways to the mountains and all the experiences in Italy. To my forever friends, Vasilia Pastella, Antriani Themistokleous, Isabella Georgia Ioannou and Anna Julia Triarou, thank you for always checking in and being there for me. I would also like to acknowledge my therapists, Dr Anna Polyniki and Dr Marta Bottini for helping me find joy and happiness.

To my whole family, thank you for your endless support, but most importantly to my mum, Maria Laghos, my dad, Christos Pitsillides, and my brother Jason Harry Ryles. Without them nothing would be possible. Thank you for believing in me when I never did.

To my partner Christos Pastellas, who moved to Italy with me so that I could pursue this PhD project, I am in debt of gratitude. His presence was irreplaceable, and I forever owe him all the sacrifices he has made. Thank you for your courage, patience and for always trusting and reassuring me that I can make it. *Αγαπώ σε.*

Finally, the following thesis is dedicated to my grandparents, Andreas Pitsillides, Androulla Pitsillidou, Christophis Laghos and Yvonne Artemis Maral Laghos.

This work was supported by the European Union's Horizon 2020 Research and Innovation Program under the Marie Sklodowska Curie grant agreement No. 813091 ("ARCH, Age-related changes in hematopoiesis").

Publications

Protocol - ***Accepted for publication***
Pitsillidou, Christina, et al., "A redox-based characterization of human immune cell subsets by polychromatic flow cytometry." Cell Press - STAR Protocols (2023). – *Attached, Chapter 3*

Editorial - ***Published***
Pitsillidou, Christina, et al., "A Journey Into the Unknown: PhD Students in a European Training Network on Age-related Changes in Hematopoiesis Conduct Their Project During a Global Pandemic." *HemaSphere* 6.8 (2022). – *Attached, Epilogue*

Table of Content

Abbreviations

Analogue-to-digital converter (ACD)

Antigen (Ag)

Antigen-presenting cells (APCs)

Antioxidant Responsive Elements (ARE)

B cell receptor (BCR)

Bone marrow (BM)

C-C chemokine receptor 7 (CCR7)

Central memory (CM)

Chimeric antigen receptor (CAR)

Cluster of differentiation (CD)

Coronavirus disease of 2019 (COVID-19)

Cytomegalovirus (CMV)

Effector memory (EM)

Electron transport chain (ETC)

Endoplasmic reticulum (ER)

Endoplasmic reticulum-associated degradation (ERAD)

Epsein Bar Virus (EBV)

Fluorescent activated cell sorter (FACS)

Flow cytometry (FCM)

Forward scatter (FSC)

Glutathione reductase (GR)

Haematopoietic stem cells (HSCs)

Hydrogen peroxide (H_2O_2)

Immunoglobulins (Ig)

Interferon gamma (IFN-γ)

Interleukins (Il)

Integrated MFI (iMFI)

L-γ-glutamyl-L-cysteinylglycine (GSH)

Lymphoid enhancer-binding factor-1 (LEF1)

Live/Dead Dye (LD)

MitoView Green Dye (MVG)

Natural killer (NK) cells

Natural killer cell cytotoxicity (NKCC)

Natural cytotoxic receptors (NCRs)

Nicotinamide adenine dinucleotide (NADH)

Nuclear factor-E2-related factor (Nrf2)

Paired box gene 5 (PAX5)

Photomultiplier tubes (PMTs)

Polychromatic flow cytometry (PFC)

Precursor B cells (pre-B cells)

Precursor exhausted T (TPEX) cells

Progenitors B cells (pro-B cells),

Programmed cell death protein 1 (PD1)

Red-fluorogenic dye MitoSOX (MSR)

Reduced L-glutathione (GSH)

Reactive oxygen species (ROS)

Side Scatter (SSC)

Stem cell memory (SCM)

Superoxide dismutase 1 (SOD1)

T cell immunoreceptor with Ig and ITIM domains (TIGIT)

T cell receptor (TCR)

Terminal Effector memory (TEM)

ThiolTracker violet (TTV)

Tumour necrosis factor α (TNF- α)

Tyrosine-based activation motif (ITAMs)

Unfolded protein response (UPR)

United Nations (UN)

World Health Organisation (WHO)

X box binding protein 1 (XBP1)

Chapter 1

General Introduction

1.1 Aging and the Immune System

Humankind is living longer than ever. Even though this marks an important accomplishment for the medical and scientific communities worldwide, the increased aging population is to shortly become a historical challenge. What comes to test the scientific community now, is how to manage the predicted 2.1 billion people that will live into their sixties and beyond by 2050 (Figure 1.1.1) (WHO, 2022). The coronavirus disease of 2019 (COVID-19) that caused the recent global pandemic has demonstrated that managing the elderly is already an international challenge (Lambert *et al.*, 2020). Thus, the World Health Organisation (WHO) and the United Nations (UN) have declared the current decade as the 'The Decade of Healthy Aging'(United Nations, 2022a; WHO, 2022). Healthy aging symbolises the process of understanding functional changes with age, and consequently establish functional ability that will enable the wellbeing of the elderly.

Aging, according to the WHO, is when at a biological level, there is molecular and cellular deterioration that happens over a long period of time (WHO, 2022). Ageing is a complicated process that embodies many molecular and cellular mechanisms in different

systems of the human body, including the ***immune system,*** the prime focus of this study**.**

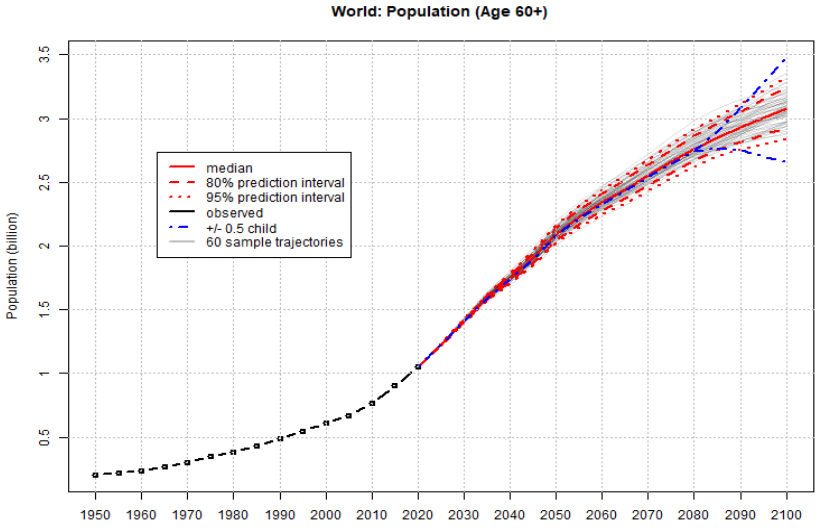

Figure 1.1.1: **The graph shows the estimated projections of the world population over the age of 60.** The probabilistic projections were calculated by conducting the Bayesian Hierarchical Model by using total fertility and life expectancy at birth and used areas where the population is 90,000 or more during the year of 2019. Displayed on the graph is the probable median, the 80% and 95% of the prediction intervals and the deterministic high and low variant (+/- 0.5 child). (United Nations, 2022b)

Gradual age-related deterioration of cellular mechanisms of the immune system has shown to correlate with the increased risk of developing malignant and non-malignant disorders (Goronzy and Weyand, 2013; Barbé-Tuana *et al.*, 2020). Critical components of aging are functional and structural changes of the immune system that involve the decreased ability to fight infections and respond to vaccinations (Barbé-Tuana *et al.*, 2020). Thus, if immunological changes with age can be identified, then we can find solutions to

prevent diseases due to increased longevity and accordingly help predict aging.

Age-related alterations of the immune system are referred to as "immunosenescence" and both the innate and adaptive arms of the immune system are affected, resulting to a decrease of immunocompetences. The main factors involving immunosenescence include persistent inflammation, decreased ability to fight infections or cancer, as well as the impaired ability to respond to newly invading antigens (Goronzy and Weyand, 2013; Furman *et al.*, 2019).

The innate and adaptive immune systems aging process is a consequence of the malfunction of haematopoietic stem cells (HSCs), which are responsible for the production of both the myeloid and lymphoid lineages (Geiger, de Haan and Florian, 2013). Undeniably, there is mounting evidence that immune systems age-related modifications begin at the very top of the haematopoietic hierarchy. HSC ageing, for example, has a direct impact on B cell lymphopoiesis, eliciting a decline in the formation of B cell precursors with age (Rossi, Jamieson and Weissman, 2008; Geiger, de Haan and Florian, 2013). Amongst the human haematopoietic system, aging is also linked with a loss of cellularity in the bone marrow (Pang *et al.*, 2011; Mercier, Ragu and Scadden, 2012).

Other than the malfunction of HSC's, a key trigger of immunosenescence in the T cell compartment of the adaptive immune response is the shrinkage of the thymus (Pawelec, 2018; Thomas, Wang and Su, 2020). Thymic involution begins at birth and continues at rapid rates until adolescence. The organ is mostly replenished with fatty tissue by adulthood, where the contribution to T cell generation decreases from 16% to 1% (Palmer, 2013). Age-related thymic involution is associated with a decrease in naive T cell production (Thomas, Wang and Su, 2020). This is likely to contribute to the decrease in T cell variety found in older people, as well as greater vulnerability to illnesses.

1.1.1 Adaptive Immunity and Age

The main adaptive immune cells are the T and B lymphocytes and they both operate in the presence of two commanding weapons:

1. Antigen-recognizing lymphocyte populations (naïve lymphocytes) and,
2. A Long-lived antigen-experienced population (memory lymphocytes).

The first weapon enables a particular response to any prospective foreign antigen. Naïve cells multiply and develop into effector cells in response to cognate antigen (Ag) encounters, the vast majority of which move to peripheral tissues and inflamed regions to aid in the elimination of infected targets. Following Ag clearance, around 95% of the effector cells die, whereas a tiny pool

of cells matures into long-lived memory cells (Kaech, Wherry and Ahmed, 2002). Memory lymphocytes ensure a more quick and robust response to previously encountered antigens.

Despite the constant decline of naive lymphocytes and preservation or even increase of memory cells, the adaptive immune system 'adapts' to age-related changes and successfully defends the body against most infections for the whole adult life (Weng, 2006).

T cells

T cells are one of two primary types of lymphocytes belonging to the adaptive compartment of the immune system. T cells fully mature in the thymus and are distinctively recognised via their unique multi-chain T cell receptor/CD3 complex (TCR/CD3), which is crucial in antigen recognition, T cell activation and antigen specific immune response (Hwang *et al.*, 2020; Shah *et al.*, 2021). T cell activation involves the binding of the TCR/CD3 complex to the surface of antigen-presenting cells (APCs) by recognising major histocompatibility complexes (MHC) (Clark and Ledbetter, 1994).

There are two types of T cells that acquire either a "killer" response or a "helper" response when encountering APCs (Hwang *et al.*, 2020). T cells that express the CD8 receptor perform cytotoxic functions and can directly kill infected cells by inducing apoptotic effects, while CD4 expressing T cells release cytokines

which further activate or ‘help’ other cells of the immune system like memory B cells to eliminate infected cells (Clark and Ledbetter, 1994; Attanavanich and Kearney, 2004; Hwang *et al.*, 2020; Shah *et al.*, 2021).

However, the assessment and study of T lymphocyte biology has evolved beyond the idea that T cells can be divided into CD4+ and CD8+ subsets alone. The advancement of tools like flow cytometry allowed the discovery of novel markers that have since then reshaped T cell biology, highlighting T cell heterogeneity. Additionally, the implementation of new techniques monitoring cytokine production, enabled comprehensive linkages between T cell functional characteristics (Picker *et al.*, 1995; Hamann *et al.*, 1997). For example, C-C chemokine receptor 7 (CCR7) and has been used in combination with CD45RO to phenotypically define subsets of memory T cells established by their effector functions (Figure1.1.2) (Hamann *et al.*, 1997; Sallusto *et al.*, 1999; Mahnke *et al.*, 2013a). In fact, it was identified that CD45RO+ CD8+ memory T cells expressing CD27, a member of the tumour necrosis factor (TNF) receptor superfamily, secreted both IL-2 and IFN-γ but did not acquire direct cytotoxic activity (Sallusto *et al.*, 1999). Therefore, due to the non-direct effects, cells expressing CD45RO were considered memory subsets. CD4+ and CD8+ memory T cells positive for CCR7 were found to produce IL-2, yet small levels of effector cytokines like IL-4, IL-5, and IFN-γ, while CCR7 negative T cells produce high levels of IL-4 and IL-5 (CD4+ T cells only), and/or IFN-γ (both CD4+ and CD8+ T cells),

and contain perforin granules for employing cytotoxic effects. Therefore CCR7-, CD45RO+ cells are defined as an effector memory (EM) subsets (Sallusto *et al.*, 1999; Mahnke *et al.*, 2013a). Additionally, CCR7 negative cells were named as effector memory cells due to their effector function ex *vivo* and their potential to circulate through the peripheral lymphoid tissues. On the contrary, CCR7+ memory cells were classified as central memory (CM) cells because of their potential to base themselves at secondary lymphoid tissues (Sallusto *et al.*, 1999).

Studies then showed that there was a true relationship amongst CM and EM cells, as CM were able to generate EM cells in vitro, yet EM were unable to convert into CM. This suggested that CM was a precursor of EM and thus another smaller subset was responsible for the regeneration of these subsets (Figure 1.1.2) (Lanzavecchia and Sallusto, 2002). Scientific investigations went on to identify a new subset of T cells that acquired stem cell-like features and thus named T stem cell memory (SCM) cells (Gattinoni *et al.*, 2011; Lugli *et al.*, 2013). TSCM were identified as mainly acquiring a T naïve cell phenotype, yet overexpressing CD95, a marker highly expressed in all memory cells. Genetic and phenotypic characterisation of this subset identified that CM cells differentiated after TSCM, while TSCM cells acquire genes that are associated to self-renewal (Gattinoni *et al.*, 2011). When stimulated *in vivo* with anti-CD3/CD28, TSCM were able to initiate differentiation and create all memory subsets (CM and

EM) while they could also preserve their own phenotype (Gattinoni *et al.*, 2011; Lugli *et al.*, 2013).

Since then, TSCM have marked an important target for treatment, especially for protocols targeting the enrichment of TSCM in chimeric antigen receptor (CAR) T-cell therapy against disease-specific T Cell defects in cancer patients (Kasakovski, Xu and Li, 2018; Arcangeli *et al.*, 2020).TSCM mark as an important subset also in age-related studies of the adaptive immune response, as TSCM have heightened proliferation and differentiation capabilities that are associated with the increased ability of being able to preserve T cell homeostasis (Lugli *et al.*, 2013).

Recently, investigations were centred on TSCM subset in order to understand why T cell homeostasis and differentiation is corrupted under conditions of persistent antigenic stimulation, chronic viral infections, age related diseases and progressive malignancies. By conducting single-cell RNA sequencing, flow cytometry and epigenetic examinations, researchers found a progenitor, amongst CD8+ TSCM cells, that was mostly functional when programmed cell death protein 1 (PD1) and T cell immunoreceptor with Ig and ITIM domains (TIGIT) were not expressed on the cell surface. On the contrary, when PD1 and TIGIT were expressed, an exhausted like-lineage is mostly observed and thus a newly defined subset known as precursor exhausted T (TPEX) cells were discovered (Galletti *et al.*, 2020).

PD1 and TIGIT are immune inhibitory receptors, both expressed on T cells. When PD1 binds to PD-L1 (its receptor found on basal tissue) signalling pathways are activated to prevent a T cell immune response. Some cancer cells have large amounts of PD-L1, which allows them to conceal from an immune attack. Monoclonal antibodies that target either PD1 or PD-L1 can block this binding and boost the immune response against cancer cells. TIGIT works in a similar way, however it binds to two other ligands, CD155 and CD112, that are also expressed by tumorigenic tissue (Raphael *et al.*, 2021; Shive *et al.*, 2021; Banta *et al.*, 2022).

Thus far, age-related research on T cells has identified that there is a transfer from a naive to a memory or activated effector T cells phenotype with age, based on a heightened antigen exposure over one's lifetime (Hu *et al.*, 2020). Memory T cells are notorious for experiencing cellular expansion and activation, while they are also very active upon re-exposure to antigens. Due to these complex features, memory T cells are also hindered throughout the aging process due to persistent infections, like cytomegalovirus (CMV) or the Epsein Bar Virus (EBV) (Pita-Lopez *et al.*, 2009; Martin-Ruiz *et al.*, 2020). This persistence of infections tends to promote T cell exhaustion, that is characterised by the lack of effector functions, diminished proliferative capacity, and an increased expression of inhibitory markers like PD1 and TIGIT.

Overall, the phenotypic profile of the T cell differentiation pattern with age and sex has still yet to be fully understood since emerging subpopulations have been defined. The definition of the cellular changes that occur in the immune system is an important goal for aging research, as this information has provided the rationale for many clinical trials to rejuvenate the aging immune system.

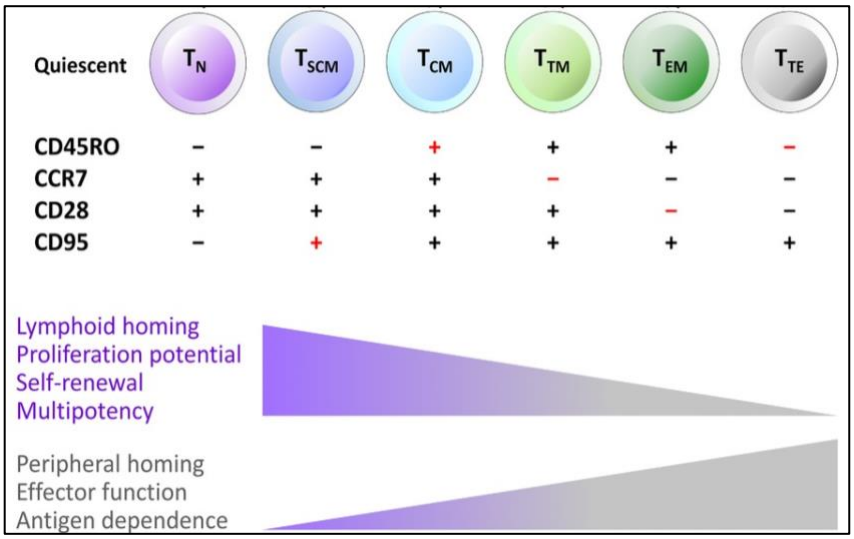

Figure 1.1.2: **The expression of CD45RO, CCR7, CD28, and CD95 determines six major subsets of quiescent T cells.** Plus or minus signs in red indicate the markers that change when T cells differentiate from one subset to another. Memory T cells loss or gain specific functions as they differentiate from SCM to CM, TM, EM, and finally TTE cells (Mahnke *et al.*, 2013b).

B cells

B cells are the only cells of the immune system able to produce and express immunoglobulins (Ig). These proteins acquire high levels of specificity and have two separate functions: one is to bind specifically to molecules from the pathogen and the other is to recruit other cells and molecules to destroy the pathogen once it is bound to it. These functions are structurally separated in the antibody molecule, one part of which specifically recognizes and binds to the antigen whereas the other engages different effector mechanisms. The antigen-binding region varies extensively among Ig and thus is known as the variable region (V region). The region of the antibody that engages the effector function of the immune system does not vary in the same way and is thus defined constant region (C region). It's important to highlight that antibodies are structurally the secreted form of the B cell receptor (BCR), and they have identical structure to the BCR, except for a small portion of the C-terminus of the heavy-chain constant region. This exception is a hydrophobic membrane-anchoring sequence and in the antibody it is a hydrophilic sequence that allows secretion (Saper, 2009).

Immunoglobulins are divided into five classifications (IgG, IgM, IgA, IgD, and IgE) (Owen A. Judith *et al.*, 2013). According to their biological characteristics, distribution, target specificity, chemical composition, and functions, each Ig separately differs. Specifically, IgM and IgD are membrane bound immunoglobulins mainly found on naïve B cells, however, IgM is also identified on

immature B cells. IgM is known to fight the initial response to an antigen while the main function of IgD is still yet to be fully understood, however, it is primarily found on most B cell subsets. IgG is known as the most abundant immunoglobulin as it is found in the serum as non-membrane bound protein, however, IgG is also found on the membrane of memory B cells (Owen A. Judith *et al.*, 2013). The second most abundant Ig is IgA, which is mostly associated with bacterial colonisation and is found in secondary lymphoid organs. The production of IgE from B cells is mainly associated to pathogenesis of allergic diseases (Schroeder and Cavacini, 2010; Owen A. Judith *et al.*, 2013; Chi, Li and Qiu, 2020).

During B cell development, rearrangement of the Ig heavy chain occurs first, commencing with *pre-pro B cells*, the earliest B cell progenitors after the multipotent hematopoietic stem cells (HSCs). Subsequently, at the *pro-B cell* stage, CD20 (cluster of differentiate 20) starts to be expressed and then progressively increases in concentration until maturity in the bone marrow. Together with the activator co-receptor CD79a (Igα), CD20 represents the most specific markers for B-lineage derivation.

The Igα/β dimer and the recombined heavy chain associated to a surrogate light chain then form the pre-B cell receptor (pre-BCR), which is expressed on the cell surface. At this stage, the now called *pre-B cells* start to express CD19, under the control of the B cell master regulator known as the transcription factor paired box

gene 5 (PAX5) (Cobaleda *et al.*, 2007; Medvedovic *et al.*, 2011). The expression of PAX5 commences at the pre-pro-B cell stage and is preserved at a stable level throughout B-cell differentiation, being then downregulated during plasma cell terminal differentiation (Figure 1.1.3)(Holmes, Pridans and Nutt, 2008). PAX5 has also been associated to human B cell diseases, as chromosomal translocations of the gene trigger acute lymphoblastic leukaemia and non-Hodgkin lymphomas, interfering with the proper development of B cells (Gu *et al.*, 2019).

Signalling through the pre-BCR drives intense proliferation and differentiation into the small pre-B cell stage. Quiescent small pre-B cells then undergo rearrangements of the Ig light chain, allowing the production of a complete functional BCR with a unique specificity that is expressed as IgM on the surface of immature B cells. In a bid to prevent autoreactivity, immature B cells which encounter Ag capable of cross-linking their newly expressed BCRs are eliminated by a variety of mechanisms. After production in the BM, immature surface IgM+ B cells migrate to the spleen, where they differentiate through distinct transitional B cell stages, before differentiating into long-lived mature follicular (FO) or marginal zone (MZ) B cells. Thus, B cells experience both antigen-dependent and independent phases of selection, which are tightly regulated through signalling events.

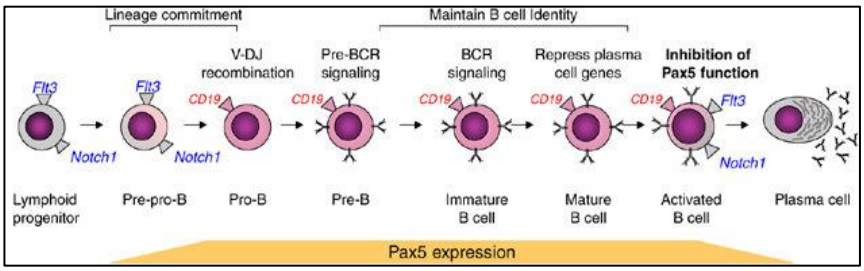

Figure: 1.1.3: **The development of B-cells and its mast regulator paired box gene 5 (PAX5).** A schematic diagram of the stages of B-cell development. The expression of PAX5 starts at the pre and pro B cell phases and remains constant throughout B cells expansion, before being silenced during plasma cell development. The upper part of the figure shows the main functions of PAX 5 thought B cell development. It is shown that the protein products of two PAX5-repressed genes, Flt3 and Notch1 (in blue), and one activated gene, CD19 (in red), are expressed on the cell surface. The manifestation of Flt3 and Notch is made possible by the post-translational inhibition of PAX5 in antigen exposed (activated) B cells. In plasma cells, PAX5 is transcriptionally silenced (Holmes, Pridans and Nutt, 2008).

In normal circumstances mature B cells, also known as naïve B cells (CD19+, CD21+, CD27-), migrate to the peritoneal cavity or lymphoid follicles of secondary lymphoid organs where they confront foreign antigens (Hua and Hou, 2020; de Mol *et al.*, 2021). Once an antigen binds to the BCR, in combination with innate and costimulatory signals (among which CD19 and reactive oxygen species plays an important role, as explained also in paragraph 1.1.3), it contributes to triggering the MAPK, NF-κB, PI3K signalling pathways.

As a consequence, B cells present the antigenic protein on the surface as APCs using MHCs, and further differentiate into antibody-secreting plasma cells in the periphery, while long lived memory B cells also generate in response (CD19+, CD21+, CD27+) (Adler *et al.*, 2017; Wieczorek *et al.*, 2017; Hong *et al.*, 2018a).

Plasma cells can thus develop either from naive marginal-zone B cells and follicular B cells, from activated germinal-centre B cells or from memory B cells. Which B-cell subsets becomes terminally differentiated depends on the nature of the antigen, its dose and form, and the location of the encounter.

Whatever their origin, all plasma cells undergo a dramatic transformation during differentiation: a prominent endoplasmic reticulum (ER) expansion, accompanied by an enlargement of the Golgi complex (Lewis et al, 1985; Rush et al, 1991; Shohat et al, 1973; Wiest et al, 1990), which are necessary to accommodate the increase in Ig synthesis. This transformation is accomplished by the interplay between B lineage-specific transcriptional programs that control plasma cell differentiation and the unfolded protein response (UPR) (Todd, Lee and Glimcher, 2008; Todd *et al.*, 2009). Specifically, UPR is an adaptive reaction that reduces unfolded protein load within the endoplasmic reticulum to maintain cell viability and function (Grootjans *et al.*, 2016). Transcription factor X box binding protein 1 (XBP1) mediates one branch of the unfolded protein response (UPR) whereby it controls

the transcription of UPR target genes involved in protein folding, like ER-associated degradation (ERAD), protein quality control and phospholipid synthesis (Hetz, 2012; Janssens, Pulendran and Lambrecht, 2014; Grootjans *et al.*, 2016). An age-related decline in retinal function and neurodegeneration has been identified in the absence of XBP1, yet little is known about XBP1 function in B cell subsets with age (McLaughlin *et al.*, 2018) . Therefore, we included this transcription factor in our B cell assessment of age-related changes.

Age-related studies on B cell immunity has demonstrated that the peripheral B cell pool fills up with memory cells resulting in restricted variety in the B cell repertoire, causing lower vaccination efficacy, and rise in circulating autoreactive antibodies (de Mol *et al.*, 2021). Studies have shown that with aging, pro–B cells remain intact while pre-B cells decrease in number with age (Bulati *et al.*, 2011; Rodriguez-Zhurbenko *et al.*, 2019). On the contrary, how the frequency of Immature B cells (CD10+) changes with age still remains to be fully understood. Gerontological studies have determined that mature B cells within the circulating blood of healthy donors can vary in abundance significantly, yet why this is the case still remains unanswered(Seita and Weissman, 2010). However studies have demonstrated an overall loss of naïve B cells (CD21+,CD27-) while there is a significant expansion of memory B cells (CD21+,CD27+) and exhausted B cells, also known as age associated B cells (ABCs) or atypical B cells (CD21-,CD27-)(Fogli *et al.*, 2012; Rubtsova *et al.*, 2015;

Corrente *et al.*, 2022). These ABCs have determent to alter the B cell immune response with age(Rubtsova *et al.*, 2013, 2015).

In relation to sex, ATAC-seq and RNA-seq data on healthy donors spanning all ages, found that the B cell specific genes (PAX5, CD79A) were modestly activated with age in females yet significantly inactivated in men (Márquez *et al.*, 2020) . These findings indicate the presence of sex-differences within the immune response with age. However, further investigations are required to define these findings, as similar studies on age immunomodulation tend to overlook the influence of gender. Overall, B cell assortment and plasticity marks as one of the most important attributes of the immune system, thus it is important to keep working on how aging alters their functional potential (Molnarfi *et al.*, 2013; Hong *et al.*, 2018b).

The complexity of the adaptive immune system, its heterogeneity and constant growth of knowledge in science highlights the importance of follow up in age associated studies. It's vital to go deep into immune heterogeneity (both adaptive and innate) and thus further unravel how the immune system is being affected with age to target healthy aging.

1.1.2 Innate Immunity and Age

Innate immunity is the first defensive mechanism of the immune system in fighting against invading pathogens and foreign substances. In fact, innate immunosenescence plays an important role upon the health and well-being of the elderly population as well as the adaptive immune response. In the following study, other than the most abundant adaptive immune cell subsets (T and B lymphocytes) we also focus our attention on the most abundant innate immune cells, Natural Killer (NK) cells.

NK cells

NK cells encompass 10-15% of the human peripheral blood and are large granular cells capable of distinguishing and eradicating target cells (viral infected cells, cancers cells etc) (Hazeldine and Lord, 2013). Moreover, NK cells, mainly defined as CD3-, CD56+, secrete cytokines that attract other immune cell subsets to the site of infection or inflammation, such as interferon gamma (IFNγ) or tumour necrosis factor alpha (TNF-α). Specifically, IFNγ activates macrophages for phagocytosis and lysis, and TNFα acts to promote direct NK death receptor-mediated cytotoxicity cytotoxocity. (Hazeldine and Lord, 2013; Michel *et al.*, 2016)

Two main subsets can be identified: $CD56^{DIM}$ and $CD56^{BRIGHT}$ (Cooper *et al.*, 2001; Cooper, Fehniger and Caligiuri, 2001; Hazeldine and Lord, 2013). $CD56^{DIM}$ NK cells are known as the cytotoxic subset, while $CD56^{BRIGHT}$ NK cells are mainly responsible for the secretion of cytokines.. NK-mediated

cytotoxicity acts through surface expression of Tumor Necrosis Factor-Related Apoptosis Inducing Ligand (TRAIL/TNFSF10) and Fas Ligand (FasL/TNFSF6), which engage and activate their respective receptors. This results in caspase activation, mitochondrial dysfunction, and consequently apoptosis of target cells (Prager and Watzl, 2019) (Figure 1.1.4). CD16 is also a renown marker used to describe NK cells, and is mostly expressed on $CD56^{DIM}$ NK cells, as it is involved in antibody dependent cell cytotoxicity (ADCC) (Hazeldine and Lord, 2013) .

There are a variety of different ligands expressed on both major NK cell subsets, that interact with the target cell to either induce inhibitory or activator functions (Le Garff-Tavernier *et al.*, 2010). For example, NKG2D and natural cytotoxicity receptors (NCRs) like NKp46 and NKp30 are numbered among the primary activating ligands of NK cells (Bauer *et al.*, 1999; Hazeldine and Lord, 2013). Specifically, NKG2D receptor on NK cells interacts with its ligand on target cells and induces the phosphorylation of tyrosine-based activation motif (ITAMs) via tyrosine kinases. This function encourages a signalling pathway that allows the release of perforins and granzymes through granule exocytosis or degranulation, guided by CD107A, a process that will then activate apoptosis within the target cell (Bauer *et al.*, 1999). In fact perforin forms holes like pores within the cell membrane of the target cell, allowing granzyme and other perforin molecules to enter (Figure 1.1.4). Once inside the cytosol of the target cell, perforin induces endosomal lysis and encourages the release of

granzyme into the cytosol (Thiery *et al.*, 2010). NK cell express five different granzyme types (A, B, H, K and M), but granzyme B has predominantly been the one to uphold scientific interest (Hazeldine and Lord, 2013). Granzyme B has the potential to induce the activation of many caspases (3 and 7) which directly drive mitochondrial permeabilization and help the release of the pro-apoptotic protein cytochrome c into the target cells cytoplasm (Goping *et al.*, 2003).

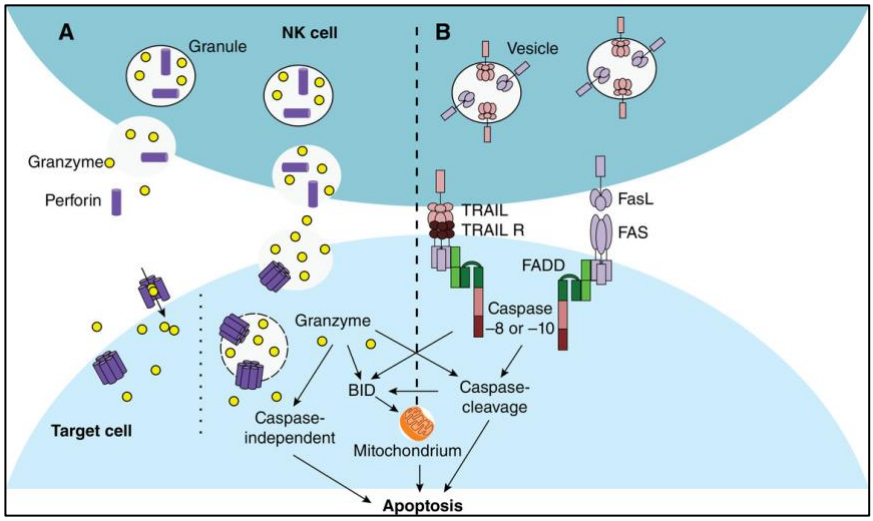

Figure 1.1.4: **NK cell related induction of apoptosis. (A)** A simplified diagram demonstrating cytotoxicity via the targeted release of lytic granules like granzymes and perforin towards target cell. Granzymes enter the target cell by pores generated by perforin in the plasma membrane or by endocytosis and endosomes. Once granzymes enter the target cell they induce caspase activation, mitochondrial dysfunction and/or caspase-independent apoptosis. **(B)** Death receptor-mediated cytotoxicity is induced by surface expression of FasL or TRAIL, which activate their respective receptor on the target cell and consequently inducing apoptosis (Prager and Watzl, 2019).

In contrast, NKG2A and killer cell immunoglobulin-like receptors (KIRs) are NK inhibitory receptors (Lee *et al.*, 1998). Respectively, these ligands also bind to tyrosine-based inhibitory motifs (ITIMs), which consequently encourage the deactivation of NK cells (Pegram *et al.*, 2011). Consequently, it has been determined that inhibitory NK receptors act as immune checkpoints controlling anti-tumour NK cell function by the recognition of specific ligands on tumour cells, thus aiding tumour escape from NK cell cytotoxicity. Subsequently, inhibitory NK cell receptors have now been a target for immunotherapeutic studies (Sivori *et al.*, 2020).

$CD56^{DIM}$ NK cells themselves are heterogeneous cells which mature from an early stage with high CD94/NKG2A expression to later stages with less CD94/NKG2A expression and more CD57 (Pegram *et al.*, 2011; Hazeldine, Hampson and Lord, 2012). High expression of CD94/NKG2A is primarily for recognising self-major histocompatibility complex (MHC) class I molecules and initiate inhibitory signals through ITIMs (Bauer *et al.*, 1999).

CD57 has been associated with a fully differentiated subset of NK cells, that marks as senescent cells. The CD57+ NK cell subset actually upsurges with age, and recent documentations suggest that its increase is also coupled with human cytomegalovirus (HCMV) chronic infections (Bigley *et al.*, 2012; Hazeldine, Hampson and Lord, 2012; Brauning *et al.*, 2022a).

An ample variety of age related studies assessing NK cells have identified an absolute increase in the number of NK cells in the peripheral blood, while the distribution of NK cell subsets remains arbitrary (Brauning *et al.*, 2022b) . In some studies, however, age appears to have no significant effect on NK cell progenitors, thus no significant alterations are reported in the peripheral blood. While there is a strong debate within the field, many research studies conclude that NK cells significantly increase with age, where specifically there is a change amongst the $CD56^{DIM}/CD56^{BRIGHT}$ circulating ratio (Hazeldine, Hampson and Lord, 2012). Numerous experimental research studies imply that the NK cell number and subpopulations vary with age, with an increase of the $CD56^{DIM}$ population and a reduction of the $CD56^{BRIGHT}$ NK cells (Hazeldine, Hampson and Lord, 2012; Brauning *et al.*, 2022a, 2022b).

Other than the distribution of the cell subsets, functional components of NK cell biology are also hindered with aging. Specifically several studies have reported that perforins protein expression declines with age, while others contradict this study, outlining no impaired perforin expression with age (Mariani, 1996; Almeida-Oliveira *et al.*, 2011; Hazeldine, Hampson and Lord, 2012). These opposing studies stimulate our curiosity as to what truly are the age related functional changes that occur which instigate the altered functions of NK cell cytotoxicity.

1.1.3 Oxidative stress and Immunity

It is now clear that immune related pathways are regulated by oxidative alterations (Forman and Torres, 2002; Franchina, Dostert and Brenner, 2018). Specifically, immune cell activation involves metabolic changes that go from high energy demand to a glycolytic one by using their mitochondrial respiratory mechanism and thus releasing adenosine triphosphate (ATP) and superoxide anions (reactive oxygen species – ROS) (Finkel and Holbrook, 2000).

One of the most important roles of ROS in the immune system is their response to pathogens during an acute inflammatory response via innate immunity, where they accumulate to perform what is known as the "respiratory burst", that kills invading pathogens (Forman and Torres, 2002; Franchina, Dostert and Brenner, 2018; Nolfi-Donegan, Braganza and Shiva, 2020). When this occurs, the rapid loss of the respiratory mechanism and hyperpolarisation alters mitochondrial membrane potential and leads to the accumulation of mitochondrial superoxide's. Therefore, redox homeostasis is crucial as the accumulation of oxygen metabolites can damage essential cellular components (Kuilman *et al.*, 2010; Davalli *et al.*, 2016a). Antioxidants are hence responsible for balancing correct redox levels to avoid host cell related damage. In particular, oxidoreductase enzymes have been demonstrated to be essential for normalizing immune cell signalling (Zuo *et al.*, 2019; Nolfi-Donegan, Braganza and Shiva, 2020).

The over production of ROS via this process is referred to as oxidative stress, as this process is also characterised by the incapability of the cell to mount an effective antioxidant response. A dysregulation of this fine balance can stimulate and retain cellular senescence and the accumulation of high levels of ROS have been found to correlated with disease progression, inflammatory diseases and aging (Finkel and Holbrook, 2000; Davalli *et al.*, 2016b; Zuo *et al.*, 2019).

ROS

ROS (commonly called free radicals) have unstable atoms that can damage cells. They are produced in response to mitochondrial oxidative metabolism and can also be generated in response to xenobiotics, cytokines, and bacterial invasion (Liu, Fiskum and Schubert, 2002; Zhao *et al.*, 2019). Specifically, ROS are produced within the electron transport chain (ETC) in the mitochondria, where electrons are transferred to complex I by nicotinamide adenine dinucleotide (NADH) and then too complex II. Both complexes are found in the membrane of mitochondria. Following these steps electrons are transferred to complex III and IV by ubiquinone and cytochrome C and by the end of this process H_2O_2 is produced by electrons transferred onto O_2. This complicated transfer of electrons can result to the leakage of electrons, which result to the formation of partial reduced O_2, which is also characterised as superoxide anion (O_2^-) (Bertolotti *et al.*, 2010, 2013; Sies and Jones, 2020).

All cells have a mechanism that counterbalances excess ROS (like O_2^-), called antioxidant response, which involves a variety of compounds that can neutralise ROS (Finkel and Holbrook, 2000). Antioxidants come in small molecular forms or in enzymatic form. For example, small molecules involve vitamins C, A, and E, uric acid or minerals like copper, zinc and magnesium. In the small molecule category L-γ-glutamyl-L-cysteinyl glycine (GSH) is also included. As a tripeptide of glutamic acid, cysteine, and glycine, GSH represents one of the most prevalent and important thiol buffers in the cell. The ratio of GSH (reduced) and its disulphide, GSSG (oxidized) contributes to the redox potential of the cell and thereby contributes to redox homeostasis (Nolfi-Donegan, Braganza and Shiva, 2020; Sies and Jones, 2020). On the contrary enzymatic antioxidants include superoxide dismutase (SOD), glutathione reductase (GR), and thioredoxin reductase. Once leaked O_2^- through the electron transport chain are present, O_2^- is converted into hydrogen peroxide (H_2O_2) via the enzymatic functions of SOD1. An electron and two protons are added to O_2^-. At this point, reduce glutathione comes along and donates electrons that will allow glutathione peroxidase to produce H_2O (Zhao *et al.*, 2019; Sies and Jones, 2020).

The majority of the antioxidant enzymes are expressed and controlled by the transcription factor nuclear factor-E2-related factor (Nrf2) (Sies and Jones, 2020; Tavassolifar *et al.*, 2020). Nrf2 is a redox-sensitive transcription factor that induces the transcription of some antioxidant enzymes, like glutathione-S-

transferase, glutamyl-cysteine ligase, heme oxygenase and phase II detoxifying enzymes (Owuor & Kong, 2002). Under non stressed conditions, the majority of Nrf2 resides in the cytoplasm and associates with a dimeric inhibitory protein, Kelch-like ECH-associated protein-1 (Keap1) (Itoh et al, 1999); Keap1 interacts with the cullin-3 E3 ubiquitin ligase (Cul3) and serves as a platform for the ubiquitination and resultant proteasomal degradation of Nrf2.

Redox homeostasis perturbations in the intracellular environment induce conformational changes in oxidized Keap1, so that Nrf2 is not sequestered to the cytoplasm anymore; anyway, for Nrf2 to be activated and migrate into the nucleus, a specific phosphorylation on a N-terminal Ser is needed. Once in the nucleus, Nrf2 dimerizes with members of another b-zip family and binds Antioxidant Responsive Elements (ARE) enhancers, activating ARE-dependent transcription of target genes, which serve mainly as antioxidants.
ROS mark as targets in measuring cellular functionality in the immune system and mitochondria are one of the most important contributors to cellular ROS pools. In the current study, measurements of ROS related metabolites are assessed using a novel flow cytometry assay, that has been particularly designed for this study.

1.2 Flow Cytometry

The etymology of flow cytometry describes its exact purpose. The word cytometry derives from the Greek words ‘Κύτος - kútos’, which means ‘receptacle’ or a hollow object thus defining a cell. On the other hand, ‘metry’ comes from the word ‘Μετρία - metria’ which means measure. Therefore, **flow cytometry** is the **measurement** of physical and/or chemical characteristics of **single cells or particles** that **flow** through a fluidic stream and are excited by a beam of light (Howard M. Shapiro, 2003).

The technology of flow cytometry (FCM) emerged during the 1960’s and 1970’s at Stanford University were Bonner, Sweet, Hulett and Herzenberg pioneered the first Fluorescence Activated Cell Sorter (FACS) instrument, while German researcher Wolfgang Göhde discovered the fluorescent based flow cytometer that would then go on to be commercialised (Bonner *et al.*, 1972; Herzenberg *et al.*, 2002) . Shortly came the commercialisation of monoclonal antibodies labelled with fluorescent dyes specialised for FCM that could tag proteins of interest, and since then flow cytometry has revolutionised research and diagnosis. FCM offers many advantages over other laboratory techniques (Doerr, 2011). For example, FCM can measure many parameters at once and simultaneously for each individual cell that passes through the instrument. Therefore, this quality allows the differentiation of cell types or populations present within a heterogeneous sample and can offer instant quantitative measurements. Additionally, a high

number of cells can be analysed in seconds where measuring rates can range from 10^3 to 10^7 events per second (depending on the model of the instrument) (Nigel P. Carter and Michael G. Ormerod, 2000; Givan Alice Longobardi, 2001; Howard M. Shapiro, 2003). Fast acquisition facilitates the generation of statistically significant data, while the ability to acquire high number of cells aids in the detection of rare cell subsets.

The machine that conducts traditional flow cytometry is known as a flow cytometer and is made up of a 1) fluidic, 2) optics, and 3) electronic system (Howard M. Shapiro, 2003).

1.2.1 The principles of Conventional Flow Cytometry

The Fluidic System

The fluidic system uses pressure that passes ready prepared suspended cells that are in a buffered salt-based solution through the flow cytometers nozzle. The pressurized fluidic system of a flow cytometer consists of liquid called sheath fluid, a buffer that is suitable for preserving the physiological state of the cells that pass through the machine to reach the lasers interrogation point (Nigel P. Carter and Michael G. Ormerod, 2000; Givan Alice Longobardi, 2001; McKinnon, 2018).

The suspended cells that are in FACS tubes seal onto the O-ring and air is introduced to force the sample through the injection tube. Therefore the fluidic system is composed of two fluidic inlets that

feed the flow cell funnel: the sheath fluid inlet and the sample inlet (Figure 1.2.1). The funnel is comprised of a wider inlet that is designated for the sheath fluid and within it there is a smaller funnel for the sample. This allows the sample to be injected slowly (10-60 µl/min) into the central wilder sheath fluid stream (20 km/h) (Veal *et al.*, 2000; Cho *et al.*, 2010). The combined sheath fluid and sample together with the pressure generated by the fluidic system move towards a narrow channel. Here the pressure, together with the narrowing shape of the machine's nozzle allows the passage of the cells to be constricted enough to flow one by one and precisely be aligned. This process of hydrodynamic focusing allows the uniform alignment of the cells and allows them to be illuminated in single file when reaching the interrogation point and the light beams from the lasers. The fluid stream then is hit by a laser beam which construct the optical system of the flow cytometer (Nigel P. Carter and Michael G. Ormerod, 2000; Givan Alice Longobardi, 2001; Howard M. Shapiro, 2003). The fluidic system described above resembles the fluidic mechanisms of most flow cytometers with no sorting capabilities. Sorters on the other hand have a different shaped flow cell (quartz cuvette shape) that is perpendicular to the lasers.

The fluidic system marks as an important one for flow cytometers as any malfunctions of the fluidics can affect the positioning of the cells with the laser beams resulting in inconsistent optical signals. For example, the presence of bubbles, or clogs within the fluid stream can change the pressure and thus yield falsified signals. The

increased flow rate of the fluidics can also disturb the positioning of the cells with the laser beams (Givan Alice Longobardi, 2001). Specifically, when the flow rate is too high the stream widens, and this leads to more cells passing through the interrogation point. Consequently, this may lead to cells flowing too close to one another and thus passing in doublets through the laser beam(Howard M. Shapiro, 2003). These issues, however, can be identified and excluded when analysing the data (to be explained in Chapter 2).

The Optical System

Within the instrument, the optical system handles the illumination of lighting via lasers and the collection of the light refracted. The lasers which are part of the optical system are responsible for the production of powerful yet coherent light. In modern flow cytometers one can find diode or diode-pumped solid-state lasers (DPSS) which have many advantages, as they offer a compact setup, are efficient, and offer noble beam quality (Howard M. Shapiro, 2003; Telford, 2018). The laser diodes are driven by the voltage of the electric current that is pumped into a solid medium to generate light. The blue laser generating light at the wavelength of 488 nm is the most commonly used light source in flow cytometry. Yet, the red lasers (640 nm, Yellow/Green (561 nm), Violet laser (405 nm) and UV laser (355 nm) are also very prominent light sources (Nigel P. Carter and Michael G. Ormerod, 2000; Givan Alice Longobardi, 2001; Howard M. Shapiro, 2003; Cho *et al.*, 2010; Telford, 2018; Telford *et al.*, 2019). Common

laser lines and their wavelengths used in flow cytometry are defined in Table 2.1 below.

The laser beams that hit the cells one by one scattering light into two different directions: Forward and Side. The forward scattering of light (FSC) defines the size of the cell, while the side scattered light (SSC) that is refracted at a 90° angle defines the complexity and granularity of a cell(Shapiro and Perlmutter, 2001; Telford, 2018). Yet the scatter of light is independent of the fluorescence. Fluorescence can be naturally emitted by a cell or particle, while there may also be one or many attached fluorescent probes or compounds excited simultaneously by the lasers.

The optical filters then come into play, where their role is to separate the SSC from the fluorescent light and thus direct specific wavelengths to their designated photodetectors. The optical filters are defined by their transmissivity, for example (i) short-pass filters are responsible for transmitting light below a defined wavelength (ii) long-pass filters pass wavelengths that are longer (Nigel P. Carter and Michael G. Ormerod, 2000). These two types are known as dichroic filters which navigate the fluorescent signal to specific detectors. To do this the dichroic filters allow light through that has a short or long wavelength and reflect the remaining light with mirrors through a specific angle (right angle), splitting the lights wavelengths to reach the designated detector. Finally, the (iii) bandpass filters, will only detect a small window of specific wavelengths of light. Specifically, a 450/50 bandpass

filter only allows fluorescent signals that have a wavelength of 450 nm (+/- 25 nm) to pass through and measured by the detector. Therefore, bandpass filters are placed in front of the photodetectors to further limit the lights wavelength it registers to a distinct colour (Nigel P. Carter and Michael G. Ormerod, 2000). The number of detectors per instrument varies thus complex optical layouts are available in flow cytometers. Figure 1.2.1 demonstrates a scheme of the principles of flow cytometry as described above.

The Electronic System

The emitted scattered light is measured by the collection optics composed of the photomultiplier tubes (PMTs) and photodiodes. As the electron exits the detector, it moves in the form of an electric current entering the electronic system of the flow cytometer, which goes to the amplifier (amp)(Nigel P. Carter and Michael G. Ormerod, 2000). The amp is responsible for amplifying the signal to form a voltage pulse that then goes on to be further transformed by the analogue-to-digital converter (ACD) into a digit. This digit is now in the form of a .fcs file and can be transferred to the computer, where it can be analysed by distinct flow cytometry software (Nigel P. Carter and Michael G. Ormerod, 2000; Snow, 2004).

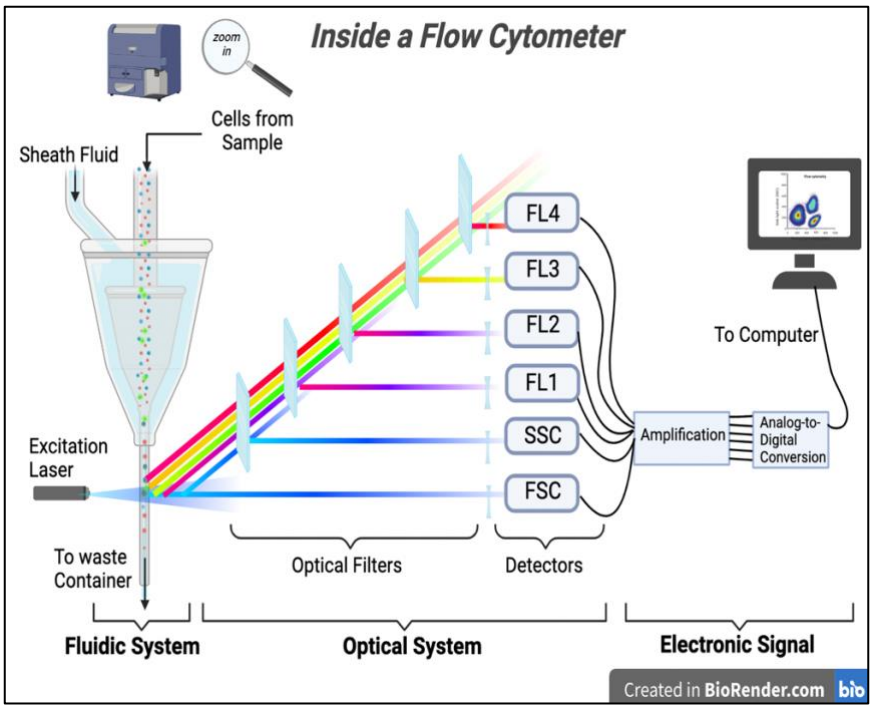

Figure 1.2.1: **A schematic diagram of the main principles of flow cytometry.** Zooming into a BD LSR Fortessa X20 the Fluidic system is composed of two fluidic inlets that feed the flow cell funnel. One inlet is called the sheath fluid inlet and the other is the sample inlet. The funnel is made up of a wider funnel and within it is a smaller funnel for the sample. The combined sheath fluid and sample together with the fluidic pressure allow the cells to move towards a narrow channel in single file towards the excitation laser. Now optical system handles the illumination of lighting emitted via the lasers and the collection of the light refracted. The scatter light moves into two different directions: Forward and Side (FSC & SSC respectively). Now the optical filters separate the SSC from the fluorescent light and direct specific wavelengths to their designated detectors (FL1, FL2, FL3, FL4). The emitted scattered light is measured by the detectors composed of PMTs and photodiodes. The electron exits the detector and moves in electronic form to the amplifier (amp) that then goes on to be further transformed by the ACD and into a digit. This digit acquires now the form of a .fcs file is transferred to the computer where it can be analysed.

1.2.2 Immunophenotyping with Flow Cytometry

Flow Cytometry has revolutionised the medical and scientific field. Since the discovery of flow cytometry, clinicians, especially haemato-oncologists and immunologists, routinely use the technology to define and classify haematological malignancies as well as assess treatment outcomes (Doerr, 2011; Cossarizza *et al.*, 2021; Robinson, 2022). The capability to characterise, quantify and recognize immune cells and their subsets has helped in the continues availability of new scientific information. Deep characterisation of cell subsets has also aided the identification of diverse disease variations via immunophenotyping (McKinnon, 2018).

Flow cytometry's ability to detect the presence or lack of cell-surface markers is the foundation of immunophenotyping (Bleesing and Fleisher, 2001). Immunophenotyping is a type of flow cytometry testing where the technique involves the measurement of specific protein expression within a cell population in combination with specific antibodies with fluorescent compounds. Immunophenotyping with flow cytometry involves scattered light signals that pick up the fluorescent compounds of interest and report the presence or absence of a target cell protein (Cossarizza *et al.*, 2021).

With the advancement of flow cytometry and the ability to measure 20 to 30 colours and more simultaneously, it is possible to detect specific cell lineages of the immune system which permits

direct diagnosis for a variety of immunodeficiency disorders (Craig and Foon, 2008; Chen and Cherian, 2017; Dworzak *et al.*, 2018). Immunophenotyping by flow cytometry helped the elucidation of the impact of the SARS-CoV-2 during the recent COVID-19 pandemic, marking an important classification of the disease, while helping in the understanding of how the whole immune system is affected by the virus (Cossarizza *et al.*, 2020; de Biasi *et al.*, 2020; Lee *et al.*, 2020). Creating an immunophenotyping profile of a disease is required to determine which therapies, if any, will benefit the patient. (Wojas-Krawczyk *et al.*, 2019). Thus, immunophenotyping by flow cytometry marks as a useful technology to profile age related changes of the immune system, the principal aim of the following study.

1.3 Scope of Thesis

The aim of the following thesis is to describe how to design and optimise state-of-the-art polychromatic flow cytometry panels and subsequently utilise them to reveal age-related changes and sexual dimorphism in the healthy human adaptive and innate immune responses. The objective of the designed panels are to dive deep into the heterogeneity of the most abundant immune cell compartments (T, B and NK cells), and thus address the changes of these subsets with age and sex, potentially answering certain questions that still remain unresolved. To fulfil this aim, we perform a classical immune cell characterization, through a polychromatic flow cytometry-based investigation of cell surface molecules known as Clusters of differentiation (CD). However, analysing the expression levels of cell surface molecules alone offers only a partial picture of immune cell functionality. For this reason, we include markers that help us define also functional changes for each cell that could impact age related immunosenescence.

It is now evident that oxidative alterations regulate many immune related pathways. Therefore, immunologists have been widely engaged in the metabolism of immune cells and how it may influence the immune response. In fact, immune cells activate due to the recognition of antigens or tissue damage where their metabolism changes from high energy demand using the mitochondrial respiratory mechanism to glycolytic releasing ATP.

Consequently, the rapid loss of the respiratory mechanism and hyperpolarisation alters mitochondrial membrane potential and leads to the accumulation of mitochondrial superoxide's. In general mitochondria from senescent cells show a decreased mitochondrial membrane potential, increased proton leak and increased generation of ROS. Moreover, during aging, damaged mitochondria, that produce less ATP and more ROS accumulate. We thus aim at studying the link between these redox homeostasis alterations and immune cells functionality. Therefore we develop a novel polychromatic flow cytometry panel that can allow the measurement of redox related regulators throughout ageing immune cell subsets, combining ROS-specific dyes, antioxidant markers and lineage-specific surface molecules.

Below we discuss the scope of the thesis following the introducing chapter:

- In Chapter 2 we describe the intricate process of developing and standardise polychromatic flow cytometry panels. We explain the importance of each step from titration to standardisation.
- In Chapter 3 we describe the importance of ROS in the immune system and how a novel staining protocol allows us to define greater the immune cell oxidative alterations. Redox related measurements have been traditionally investigated using conventional immunoblot assays and microscopy. Never before has a protocol been designed to

measure age related redox alterations using polychromatic flow cytometry within the heterogenous immune system.

- In Chapter 4 we define age and sex related changes of the adaptive immune response using our newly designed polychromatic flow cytometry panels on T and B lymphocytes, while we also assess ROS related markers by utilising our novel panel. We discuss the main changes that we see amongst a cohort of 54 healthy participants and show the frequencies and MFI targets of different immune cell subsets and their functional markers and how they change with age and sex.
- Chapter 5 includes high dimensional single cell analysis of flow cytometry data to address age related changes on the major cell type of the innate immune response - NK cells. After the development of a multiparametric polychromatic flow cytometry panel capable of simultaneously investigating 17 parameters on thousands of single cells, we assess the peripheral blood of 45 healthy donors. UMAP analysis is performed followed by PhenoGraph analysis to assess such high dimensional single cell data.
- Chapter 6 denotes concluding remarks for the whole thesis.

1.4 Bibliography

Adler, L.N. *et al.* (2017) "The Other Function: Class II-Restricted Antigen Presentation by B Cells," *Frontiers in Immunology*, 8. Available at: https://doi.org/10.3389/fimmu.2017.00319.

Almeida-Oliveira, A. *et al.* (2011) "Age-related changes in natural killer cell receptors from childhood through old age," *Human Immunology*, 72(4), pp. 319–329. Available at: https://doi.org/10.1016/j.humimm.2011.01.009.

Arcangeli, S. *et al.* (2020) "Next-Generation Manufacturing Protocols Enriching TSCM CAR T Cells Can Overcome Disease-Specific T Cell Defects in Cancer Patients," *Frontiers in Immunology*, 11. Available at: https://doi.org/10.3389/fimmu.2020.01217.

Attanavanich, K. and Kearney, J.F. (2004) "Marginal Zone, but Not Follicular B Cells, Are Potent Activators of Naive CD4 T Cells," *The Journal of Immunology*, 172(2), pp. 803–811. Available at: https://doi.org/10.4049/jimmunol.172.2.803.

Banta, K.L. *et al.* (2022) "Mechanistic convergence of the TIGIT and PD-1 inhibitory pathways necessitates co-blockade to optimize anti-tumor CD8+ T cell responses," *Immunity*, 55(3), pp. 512-526.e9. Available at: https://doi.org/10.1016/j.immuni.2022.02.005.

Barbé-Tuana, F. *et al.* (2020) "The interplay between immunosenescence and age-related diseases," *Seminars in Immunopathology*, 42(5), pp. 545–557. Available at: https://doi.org/10.1007/s00281-020-00806-z.

Bauer, S. *et al.* (1999) "Activation of NK Cells and T Cells by NKG2D, a Receptor for Stress-Inducible MICA," *Science*, 285(5428), pp. 727–729. Available at: https://doi.org/10.1126/science.285.5428.727.

Bertolotti, M. *et al.* (2010) "B- to Plasma-Cell Terminal Differentiation Entails Oxidative Stress and Profound Reshaping

of the Antioxidant Responses," *Antioxidants & Redox Signaling*, 13(8), pp. 1133–1144. Available at: https://doi.org/10.1089/ars.2009.3079.

Bertolotti, M. *et al.* (2013) "Tyrosine Kinase Signal Modulation: A Matter of H 2 O 2 Membrane Permeability?," *Antioxidants & Redox Signaling*, 19(13), pp. 1447–1451. Available at: https://doi.org/10.1089/ars.2013.5330.

de Biasi, S. *et al.* (2020) "Marked T cell activation, senescence, exhaustion and skewing towards TH17 in patients with COVID-19 pneumonia," *Nature Communications*, 11(1), p. 3434. Available at: https://doi.org/10.1038/s41467-020-17292-4.

Bigley, A.B. *et al.* (2012) "NK-cells have an impaired response to acute exercise and a lower expression of the inhibitory receptors KLRG1 and CD158a in humans with latent cytomegalovirus infection," *Brain, Behavior, and Immunity*, 26(1), pp. 177–186. Available at: https://doi.org/10.1016/j.bbi.2011.09.004.

Bleesing, J.J.H. and Fleisher, T.A. (2001) "Immunophenotyping," *Seminars in Hematology*, 38(2), pp. 100–110. Available at: https://doi.org/10.1016/S0037-1963(01)90044-7.

Bonner, W.A. *et al.* (1972) "Fluorescence Activated Cell Sorting," *Review of Scientific Instruments*, 43(3), pp. 404–409. Available at: https://doi.org/10.1063/1.1685647.

Brauning, A. *et al.* (2022a) "Aging of the Immune System: Focus on Natural Killer Cells Phenotype and Functions," *Cells*, 11(6), p. 1017. Available at: https://doi.org/10.3390/cells11061017.

Brauning, A. *et al.* (2022b) "Aging of the Immune System: Focus on Natural Killer Cells Phenotype and Functions," *Cells*, 11(6), p. 1017. Available at: https://doi.org/10.3390/cells11061017.

Bulati, M. *et al.* (2011) "B cells and immunosenescence: A focus on IgG+IgD−CD27− (DN) B cells in aged humans," *Ageing Research Reviews*, 10(2), pp. 274–284. Available at: https://doi.org/10.1016/j.arr.2010.12.002.

Chen, X. and Cherian, S. (2017) "Acute Myeloid Leukemia Immunophenotyping by Flow Cytometric Analysis," *Clinics in Laboratory Medicine*, 37(4), pp. 753–769. Available at: https://doi.org/10.1016/j.cll.2017.07.003.

Chi, X., Li, Y. and Qiu, X. (2020) "V(D)J recombination, somatic hypermutation and class switch recombination of immunoglobulins: mechanism and regulation," *Immunology*, 160(3), pp. 233–247. Available at: https://doi.org/10.1111/imm.13176.

Cho, S.H. *et al.* (2010) "Review Article: Recent advancements in optofluidic flow cytometer," *Biomicrofluidics*, 4(4), p. 043001. Available at: https://doi.org/10.1063/1.3511706.

Clark, E.A. and Ledbetter, J.A. (1994) "How B and T cells talk to each other," *Nature*, 367(6462), pp. 425–428. Available at: https://doi.org/10.1038/367425a0.

Cobaleda, C. *et al.* (2007) "Pax5: the guardian of B cell identity and function," *Nature Immunology*, 8(5), pp. 463–470. Available at: https://doi.org/10.1038/ni1454.

Cooper, M.A. *et al.* (2001) "Human natural killer cells: a unique innate immunoregulatory role for the CD56bright subset," *Blood*, 97(10), pp. 3146–3151. Available at: https://doi.org/10.1182/blood.V97.10.3146.

Cooper, M.A., Fehniger, T.A. and Caligiuri, M.A. (2001) "The biology of human natural killer-cell subsets," *Trends in Immunology*, 22(11), pp. 633–640. Available at: https://doi.org/10.1016/S1471-4906(01)02060-9.

Corrente, F. *et al.* (2022) "CD21– CD27– Atypical B Cells in a Pediatric Cohort Study: An Extensive Single Center Flow Cytometric Analysis," *Frontiers in Pediatrics*, 10. Available at: https://doi.org/10.3389/fped.2022.822400.

Cossarizza, A. *et al.* (2020) "SARS-CoV-2, the Virus that Causes COVID-19: Cytometry and the New Challenge for Global Health,"

Cytometry Part A, 97(4), pp. 340–343. Available at: https://doi.org/10.1002/cyto.a.24002.

Cossarizza, A. *et al.* (2021) "Guidelines for the use of flow cytometry and cell sorting in immunological studies (third edition)," *European Journal of Immunology*, 51(12), pp. 2708–3145. Available at: https://doi.org/10.1002/eji.202170126.

Craig, F.E. and Foon, K.A. (2008) "Flow cytometric immunophenotyping for hematologic neoplasms," *Blood*, 111(8), pp. 3941–3967. Available at: https://doi.org/10.1182/blood-2007-11-120535.

Davalli, P. *et al.* (2016a) "ROS, Cell Senescence, and Novel Molecular Mechanisms in Aging and Age-Related Diseases," *Oxidative Medicine and Cellular Longevity*, 2016, pp. 1–18. Available at: https://doi.org/10.1155/2016/3565127.

Davalli, P. *et al.* (2016b) "ROS, Cell Senescence, and Novel Molecular Mechanisms in Aging and Age-Related Diseases," *Oxidative Medicine and Cellular Longevity*, 2016, pp. 1–18. Available at: https://doi.org/10.1155/2016/3565127.

Doerr, A. (2011) "A flow cytometry revolution," *Nature Methods*, 8(7), pp. 531–531. Available at: https://doi.org/10.1038/nmeth0711-531.

Dworzak, M.N. *et al.* (2018) "AIEOP-BFM Consensus Guidelines 2016 for Flow Cytometric Immunophenotyping of Pediatric Acute Lymphoblastic Leukemia," *Cytometry Part B: Clinical Cytometry*, 94(1), pp. 82–93. Available at: https://doi.org/10.1002/cyto.b.21518.

Finkel, T. and Holbrook, N.J. (2000) "Oxidants, oxidative stress and the biology of ageing," *Nature*, 408(6809), pp. 239–247. Available at: https://doi.org/10.1038/35041687.

Fogli, M. *et al.* (2012) "Emergence of Exhausted B Cells in Asymptomatic HIV-1-Infected Patients Naïve for HAART is Related to Reduced Immune Surveillance," *Clinical and*

Developmental Immunology, 2012, pp. 1–10. Available at: https://doi.org/10.1155/2012/829584.

Forman, H.J. and Torres, M. (2002) "Reactive Oxygen Species and Cell Signaling," *American Journal of Respiratory and Critical Care Medicine*, 166(supplement_1), pp. S4–S8. Available at: https://doi.org/10.1164/rccm.2206007.

Franchina, D.G., Dostert, C. and Brenner, D. (2018) "Reactive Oxygen Species: Involvement in T Cell Signaling and Metabolism," *Trends in Immunology*, 39(6), pp. 489–502. Available at: https://doi.org/10.1016/j.it.2018.01.005.

Furman, D. *et al.* (2019) "Chronic inflammation in the etiology of disease across the life span," *Nature Medicine*, 25(12), pp. 1822–1832. Available at: https://doi.org/10.1038/s41591-019-0675-0.

Galletti, G. *et al.* (2020) "Two subsets of stem-like CD8+ memory T cell progenitors with distinct fate commitments in humans," *Nature Immunology*, 21(12), pp. 1552–1562. Available at: https://doi.org/10.1038/s41590-020-0791-5.

Le Garff-Tavernier, M. *et al.* (2010) "Human NK cells display major phenotypic and functional changes over the life span," *Aging Cell*, 9(4), pp. 527–535. Available at: https://doi.org/10.1111/j.1474-9726.2010.00584.x.

Gattinoni, L. *et al.* (2011) "A human memory T cell subset with stem cell–like properties," *Nature Medicine*, 17(10), pp. 1290–1297. Available at: https://doi.org/10.1038/nm.2446.

Geiger, H., de Haan, G. and Florian, M.C. (2013) "The ageing haematopoietic stem cell compartment," *Nature Reviews Immunology*, 13(5), pp. 376–389. Available at: https://doi.org/10.1038/nri3433.

Givan Alice Longobardi (2001) *Instrumentation: into the black box. In Flow cytometry. First Principles.* a. New York: Wiely-Liss.

Goping, I.S. *et al.* (2003) "Granzyme B-Induced Apoptosis Requires Both Direct Caspase Activation and Relief of Caspase Inhibition," *Immunity*, 18(3), pp. 355–365. Available at: https://doi.org/10.1016/S1074-7613(03)00032-3.

Goronzy, J.J. and Weyand, C.M. (2013) "Understanding immunosenescence to improve responses to vaccines," *Nature Immunology*, 14(5), pp. 428–436. Available at: https://doi.org/10.1038/ni.2588.

Grootjans, J. *et al.* (2016) "The unfolded protein response in immunity and inflammation," *Nature Reviews Immunology*, 16(8), pp. 469–484. Available at: https://doi.org/10.1038/nri.2016.62.

Gu, Z. *et al.* (2019) "PAX5-driven subtypes of B-progenitor acute lymphoblastic leukemia," *Nature Genetics*, 51(2), pp. 296–307. Available at: https://doi.org/10.1038/s41588-018-0315-5.

Hamann, D. *et al.* (1997) "Phenotypic and Functional Separation of Memory and Effector Human CD8+ T Cells," *Journal of Experimental Medicine*, 186(9), pp. 1407–1418. Available at: https://doi.org/10.1084/jem.186.9.1407.

Hao, Y. *et al.* (2011) "A B-cell subset uniquely responsive to innate stimuli accumulates in aged mice," *Blood*, 118(5), pp. 1294–1304. Available at: https://doi.org/10.1182/blood-2011-01-330530.

Hazeldine, J., Hampson, P. and Lord, J.M. (2012) "Reduced release and binding of perforin at the immunological synapse underlies the age-related decline in natural killer cell cytotoxicity," *Aging Cell*, 11(5), pp. 751–759. Available at: https://doi.org/10.1111/j.1474-9726.2012.00839.x.

Hazeldine, J. and Lord, J.M. (2013) "The impact of ageing on natural killer cell function and potential consequences for health in older adults," *Ageing Research Reviews*, 12(4), pp. 1069–1078. Available at: https://doi.org/10.1016/j.arr.2013.04.003.

Herzenberg, Leonard A *et al.* (2002) "The History and Future of the Fluorescence Activated Cell Sorter and Flow Cytometry: A

View from Stanford," *Clinical Chemistry*, 48(10), pp. 1819–1827. Available at: https://doi.org/10.1093/clinchem/48.10.1819.

Hetz, C. (2012) "The unfolded protein response: controlling cell fate decisions under ER stress and beyond," *Nature Reviews Molecular Cell Biology*, 13(2), pp. 89–102. Available at: https://doi.org/10.1038/nrm3270.

Holmes, M.L., Pridans, C. and Nutt, S.L. (2008) "The regulation of the B-cell gene expression programme by Pax5," *Immunology & Cell Biology*, 86(1), pp. 47–53. Available at: https://doi.org/10.1038/sj.icb.7100134.

Hong, S. *et al.* (2018a) "B Cells Are the Dominant Antigen-Presenting Cells that Activate Naive CD4+ T Cells upon Immunization with a Virus-Derived Nanoparticle Antigen," *Immunity*, 49(4), pp. 695-708.e4. Available at: https://doi.org/10.1016/j.immuni.2018.08.012.

Hong, S. *et al.* (2018b) "B Cells Are the Dominant Antigen-Presenting Cells that Activate Naive CD4+ T Cells upon Immunization with a Virus-Derived Nanoparticle Antigen," *Immunity*, 49(4), pp. 695-708.e4. Available at: https://doi.org/10.1016/j.immuni.2018.08.012.

Howard M. Shapiro (2003) *Practical Flow Cytometry*. 4th edn.
Hu, B. *et al.* (2020) "Distinct Age-Related Epigenetic Signatures in CD4 and CD8 T Cells," *Frontiers in Immunology*, 11. Available at: https://doi.org/10.3389/fimmu.2020.585168.

Hua, Z. and Hou, B. (2020) "The role of B cell antigen presentation in the initiation of CD4+ T cell response," *Immunological Reviews*, 296(1), pp. 24–35. Available at: https://doi.org/10.1111/imr.12859.

Hwang, J.-R. *et al.* (2020) "Recent insights of T cell receptor-mediated signaling pathways for T cell activation and development," *Experimental & Molecular Medicine*, 52(5), pp. 750–761. Available at: https://doi.org/10.1038/s12276-020-0435-8.

Janssens, S., Pulendran, B. and Lambrecht, B.N. (2014) "Emerging functions of the unfolded protein response in immunity," *Nature Immunology*, 15(10), pp. 910–919. Available at: https://doi.org/10.1038/ni.2991.

Kaech, S.M., Wherry, E.J. and Ahmed, R. (2002) "Effector and memory T-cell differentiation: implications for vaccine development," *Nature Reviews Immunology*, 2(4), pp. 251–262. Available at: https://doi.org/10.1038/nri778.

Kasakovski, D., Xu, L. and Li, Y. (2018) "T cell senescence and CAR-T cell exhaustion in hematological malignancies," *Journal of Hematology & Oncology*, 11(1), p. 91. Available at: https://doi.org/10.1186/s13045-018-0629-x.

Kuilman, T. *et al.* (2010) "The essence of senescence," *Genes & Development*, 24(22), pp. 2463–2479. Available at: https://doi.org/10.1101/gad.1971610.

Lambert, H. *et al.* (2020) "COVID-19 as a global challenge: towards an inclusive and sustainable future," *The Lancet Planetary Health*, 4(8), pp. e312–e314. Available at: https://doi.org/10.1016/S2542-5196(20)30168-6.

Lanzavecchia, A. and Sallusto, F. (2002) "Progressive differentiation and selection of the fittest in the immune response," *Nature Reviews Immunology*, 2(12), pp. 982–987. Available at: https://doi.org/10.1038/nri959.

Lee, J.S. *et al.* (2020) "Immunophenotyping of COVID-19 and influenza highlights the role of type I interferons in development of severe COVID-19," *Science Immunology*, 5(49). Available at: https://doi.org/10.1126/sciimmunol.abd1554.

Lee, N. *et al.* (1998) "HLA-E is a major ligand for the natural killer inhibitory receptor CD94/NKG2A," *Proceedings of the National Academy of Sciences*, 95(9), pp. 5199–5204. Available at: https://doi.org/10.1073/pnas.95.9.5199.

Liu, Y., Fiskum, G. and Schubert, D. (2002) "Generation of reactive oxygen species by the mitochondrial electron transport

chain," *Journal of Neurochemistry*, 80(5), pp. 780–787. Available at: https://doi.org/10.1046/j.0022-3042.2002.00744.x.

Lugli, E. *et al.* (2013) "Superior T memory stem cell persistence supports long-lived T cell memory," *Journal of Clinical Investigation* [Preprint]. Available at: https://doi.org/10.1172/JCI66327.

Mahnke, Y.D. *et al.* (2013a) "The who's who of T-cell differentiation: Human memory T-cell subsets," *European Journal of Immunology*, 43(11), pp. 2797–2809. Available at: https://doi.org/10.1002/eji.201343751.

Mahnke, Y.D. *et al.* (2013b) "The who's who of T-cell differentiation: Human memory T-cell subsets," *European Journal of Immunology*, 43(11), pp. 2797–2809. Available at: https://doi.org/10.1002/eji.201343751.

Mariani, E. (1996) "Perforins in human cytolytic cells: the effect of age," *Mechanisms of Ageing and Development*, 92(2–3), pp. 195–209. Available at: https://doi.org/10.1016/S0047-6374(96)01829-5.

Márquez, E.J. *et al.* (2020) "Sexual-dimorphism in human immune system aging," *Nature Communications*, 11(1), p. 751. Available at: https://doi.org/10.1038/s41467-020-14396-9.

Martin-Ruiz, C. *et al.* (2020) "CMV-independent increase in CD27−CD28+ CD8+ EMRA T cells is inversely related to mortality in octogenarians," *npj Aging and Mechanisms of Disease*, 6(1), p. 3. Available at: https://doi.org/10.1038/s41514-019-0041-y.

McKinnon, K.M. (2018) "Flow Cytometry: An Overview," *Current Protocols in Immunology*, 120(1). Available at: https://doi.org/10.1002/cpim.40.

McLaughlin, T. *et al.* (2018) "Loss of XBP1 accelerates age-related decline in retinal function and neurodegeneration," *Molecular Neurodegeneration*, 13(1), p. 16. Available at: https://doi.org/10.1186/s13024-018-0250-z.

Medvedovic, J. *et al.* (2011) “Pax5,” in, pp. 179–206. Available at: https://doi.org/10.1016/B978-0-12-385991-4.00005-2.

Mercier, F.E., Ragu, C. and Scadden, D.T. (2012) “The bone marrow at the crossroads of blood and immunity,” *Nature Reviews Immunology*, 12(1), pp. 49–60. Available at: https://doi.org/10.1038/nri3132.

Michel, T. *et al.* (2016) “Human CD56 ^{bright} NK Cells: An Update,” *The Journal of Immunology*, 196(7), pp. 2923–2931. Available at: https://doi.org/10.4049/jimmunol.1502570.

de Mol, J. *et al.* (2021) “The Dynamics of B Cell Aging in Health and Disease,” *Frontiers in Immunology*, 12. Available at: https://doi.org/10.3389/fimmu.2021.733566.

Molnarfi, N. *et al.* (2013) “MHC class II–dependent B cell APC function is required for induction of CNS autoimmunity independent of myelin-specific antibodies,” *Journal of Experimental Medicine*, 210(13), pp. 2921–2937. Available at: https://doi.org/10.1084/jem.20130699.

Nigel P. Carter and Michael G. Ormerod (2000) *Introduction to the principles of flow cytometry. In Flow cytometry. A practical approach*. 3rd edn. Edited by Michael Ormerod. Oxford: Oxford University Press.

Nolfi-Donegan, D., Braganza, A. and Shiva, S. (2020) “Mitochondrial electron transport chain: Oxidative phosphorylation, oxidant production, and methods of measurement,” *Redox Biology*, 37, p. 101674. Available at: https://doi.org/10.1016/j.redox.2020.101674.

Owen A. Judith *et al.* (2013) *Kuby Immunology*. 7th edn. Edited by Champion Erica. New York: W.H Freeman and Company. Available at: https://doi.org/10.1084/jem.20091739.

Palmer, D.B. (2013) “The Effect of Age on Thymic Function,” *Frontiers in Immunology*, 4. Available at: https://doi.org/10.3389/fimmu.2013.00316.

Pang, W.W. *et al.* (2011) "Human bone marrow hematopoietic stem cells are increased in frequency and myeloid-biased with age," *Proceedings of the National Academy of Sciences*, 108(50), pp. 20012–20017. Available at: https://doi.org/10.1073/pnas.1116110108.

Pawelec, G. (2018) "Age and immunity: What is 'immunosenescence'?," *Experimental Gerontology*, 105, pp. 4–9. Available at: https://doi.org/10.1016/j.exger.2017.10.024.

Pegram, H.J. *et al.* (2011) "Activating and inhibitory receptors of natural killer cells," *Immunology & Cell Biology*, 89(2), pp. 216–224. Available at: https://doi.org/10.1038/icb.2010.78.

Picker, L. *et al.* (1995) "Direct demonstration of cytokine synthesis heterogeneity among human memory/effector T cells by flow cytometry," *Blood*, 86(4), pp. 1408–1419. Available at: https://doi.org/10.1182/blood.V86.4.1408.bloodjournal8641408.

Pita-Lopez, M.L. *et al.* (2009) "Effect of ageing on CMV-specific CD8 T cells from CMV seropositive healthy donors," *Immunity & Ageing*, 6(1), p. 11. Available at: https://doi.org/10.1186/1742-4933-6-11.

Prager, I. and Watzl, C. (2019) "Mechanisms of natural killer cell-mediated cellular cytotoxicity," *Journal of Leukocyte Biology*, 105(6), pp. 1319–1329. Available at: https://doi.org/10.1002/JLB.MR0718-269R.

Raphael, I. *et al.* (2021) "TIGIT and PD-1 Immune Checkpoint Pathways Are Associated With Patient Outcome and Anti-Tumor Immunity in Glioblastoma," *Frontiers in Immunology*, 12. Available at: https://doi.org/10.3389/fimmu.2021.637146.

Robinson, J.P. (2022) "Flow cytometry: past and future," *BioTechniques*, 72(4), pp. 159–169. Available at: https://doi.org/10.2144/btn-2022-0005.

Rodriguez-Zhurbenko, N. *et al.* (2019) "Human B-1 Cells and B-1 Cell Antibodies Change With Advancing Age," *Frontiers in*

Immunology, 10. Available at: https://doi.org/10.3389/fimmu.2019.00483.

Rossi, D.J., Jamieson, C.H.M. and Weissman, I.L. (2008) "Stems Cells and the Pathways to Aging and Cancer," *Cell*, 132(4), pp. 681–696. Available at: https://doi.org/10.1016/j.cell.2008.01.036.

Rubtsov, A. V. *et al.* (2011) "Toll-like receptor 7 (TLR7)–driven accumulation of a novel CD11c+ B-cell population is important for the development of autoimmunity," *Blood*, 118(5), pp. 1305–1315. Available at: https://doi.org/10.1182/blood-2011-01-331462.

Rubtsova, K. *et al.* (2013) "T-box transcription factor T-bet, a key player in a unique type of B-cell activation essential for effective viral clearance," *Proceedings of the National Academy of Sciences*, 110(34). Available at: https://doi.org/10.1073/pnas.1312348110.

Rubtsova, K. *et al.* (2015) "Age-Associated B Cells: A T-bet–Dependent Effector with Roles in Protective and Pathogenic Immunity," *The Journal of Immunology*, 195(5), pp. 1933–1937. Available at: https://doi.org/10.4049/jimmunol.1501209.

Sallusto, F. *et al.* (1999) "Two subsets of memory T lymphocytes with distinct homing potentials and effector functions," *Nature*, 401(6754), pp. 708–712. Available at: https://doi.org/10.1038/44385.

Saper, C.B. (2009) "A Guide to the Perplexed on the Specificity of Antibodies," *Journal of Histochemistry & Cytochemistry*, 57(1), pp. 1–5. Available at: https://doi.org/10.1369/jhc.2008.952770.

Schroeder, H.W. and Cavacini, L. (2010) "Structure and function of immunoglobulins," *Journal of Allergy and Clinical Immunology*, 125(2), pp. S41–S52. Available at: https://doi.org/10.1016/j.jaci.2009.09.046.

Seita, J. and Weissman, I.L. (2010) "Hematopoietic stem cell: self-renewal versus differentiation," *WIREs Systems Biology and Medicine*, 2(6), pp. 640–653. Available at: https://doi.org/10.1002/wsbm.86.

Shah, K. *et al.* (2021) "T cell receptor (TCR) signaling in health and disease," *Signal Transduction and Targeted Therapy*, 6(1), p. 412. Available at: https://doi.org/10.1038/s41392-021-00823-w.

Shapiro, H.M. and Perlmutter, N.G. (2001) "Violet laser diodes as light sources for cytometry," *Cytometry*, 44(2), pp. 133–136. Available at: https://doi.org/10.1002/1097-0320(20010601)44:2<133::AID-CYTO1092>3.0.CO;2-S.

Shive, C.L. *et al.* (2021) "Markers of T Cell Exhaustion and Senescence and Their Relationship to Plasma TGF-β Levels in Treated HIV+ Immune Non-responders," *Frontiers in Immunology*, 12. Available at: https://doi.org/10.3389/fimmu.2021.638010.

Sies, H. and Jones, D.P. (2020) "Reactive oxygen species (ROS) as pleiotropic physiological signalling agents," *Nature Reviews Molecular Cell Biology*, 21(7), pp. 363–383. Available at: https://doi.org/10.1038/s41580-020-0230-3.

Sivori, S. *et al.* (2020) "Inhibitory Receptors and Checkpoints in Human NK Cells, Implications for the Immunotherapy of Cancer," *Frontiers in Immunology*, 11. Available at: https://doi.org/10.3389/fimmu.2020.02156.

Snow, C. (2004) "Flow cytometer electronics," *Cytometry*, 57A(2), pp. 63–69. Available at: https://doi.org/10.1002/cyto.a.10120.

Tavassolifar, M. javad *et al.* (2020) "The Influence of Reactive Oxygen Species in the Immune System and Pathogenesis of Multiple Sclerosis," *Autoimmune Diseases*, 2020, pp. 1–14. Available at: https://doi.org/10.1155/2020/5793817.

Telford, W. *et al.* (2019) "Deep ultraviolet lasers for flow cytometry," *Cytometry Part A*, 95(2), pp. 227–233. Available at: https://doi.org/10.1002/cyto.a.23640.

Telford, W.G. (2018) “Overview of Lasers for Flow Cytometry,” in, pp. 447–479. Available at: https://doi.org/10.1007/978-1-4939-7346-0_19.

Thiery, J. *et al.* (2010) “Perforin activates clathrin- and dynamin-dependent endocytosis, which is required for plasma membrane repair and delivery of granzyme B for granzyme-mediated apoptosis,” *Blood*, 115(8), pp. 1582–1593. Available at: https://doi.org/10.1182/blood-2009-10-246116.

Thomas, R., Wang, W. and Su, D.-M. (2020) “Contributions of Age-Related Thymic Involution to Immunosenescence and Inflammaging,” *Immunity & Ageing*, 17(1), p. 2. Available at: https://doi.org/10.1186/s12979-020-0173-8.

Todd, D.J. *et al.* (2009) “XBP1 governs late events in plasma cell differentiation and is not required for antigen-specific memory B cell development,” *Journal of Experimental Medicine*, 206(10), pp. 2151–2159. Available at: https://doi.org/10.1084/jem.20090738.

Todd, D.J., Lee, A.-H. and Glimcher, L.H. (2008) “The endoplasmic reticulum stress response in immunity and autoimmunity,” *Nature Reviews Immunology*, 8(9), pp. 663–674. Available at: https://doi.org/10.1038/nri2359.

United Nations (2022a) *Ageing*, *https://www.un.org/en/UN-system/ageing*.

United Nations (2022b) *World Population Prospects 2022*, *https://population.un.org/wpp/Graphs/Probabilistic/POP/80*.

Veal, D.A. *et al.* (2000) “Fluorescence staining and flow cytometry for monitoring microbial cells,” *Journal of Immunological Methods*, 243(1–2), pp. 191–210. Available at: https://doi.org/10.1016/S0022-1759(00)00234-9.

Weng, N. (2006) “Aging of the Immune System: How Much Can the Adaptive Immune System Adapt?,” *Immunity*, 24(5), pp. 495–499. Available at: https://doi.org/10.1016/j.immuni.2006.05.001.

WHO (2022) *Ageing and health*, *https://www.who.int/news-room/fact-sheets/detail/ageing-and-health*.

Wieczorek, M. *et al.* (2017) "Major Histocompatibility Complex (MHC) Class I and MHC Class II Proteins: Conformational Plasticity in Antigen Presentation," *Frontiers in Immunology*, 8. Available at: https://doi.org/10.3389/fimmu.2017.00292.

Wojas-Krawczyk, K. *et al.* (2019) "Beyond PD-L1 Markers for Lung Cancer Immunotherapy," *International Journal of Molecular Sciences*, 20(8), p. 1915. Available at: https://doi.org/10.3390/ijms20081915.

Zhao, R. *et al.* (2019) "Mitochondrial electron transport chain, ROS generation and uncoupling (Review)," *International Journal of Molecular Medicine* [Preprint]. Available at: https://doi.org/10.3892/ijmm.2019.4188.

Zuo *et al.* (2019) "Inflammaging and Oxidative Stress in Human Diseases: From Molecular Mechanisms to Novel Treatments," *International Journal of Molecular Sciences*, 20(18), p. 4472. Available at: https://doi.org/10.3390/ijms20184472

Chapter 2

Polychromatic Flow Cytometry Panel Optimisation

2.1 Introduction

Assays for immunophenotyping established by flow cytometry have evolved to be more multiparametric and thus are able to simultaneously evaluate a variety of cellular parameters. This advancement of flow cytometry, however, comes with a thorough optimisation process before advancing to the main experimental assays. The optimisation of polychromatic flow cytometry (PFC) takes time, but is worth it as the process yields reliable antibody conjugate panels (Mahnke and Roederer, 2007; Mura *et al.*, 2020).

In order to successfully design and develop PFC panels, there are a number of crucial considerations and steps that must be taken into account, which will be explained in this chapter. These practices described have been applied for designing the PFC panels of this study, that are utilised to define age and sex related changes in the immune system.

2.2 Designing PFC panels

2.2.1 Before Starting

Before starting to design a PFC panel, it is fundamental to know the configuration of the flow cytometer accessible. The laser availability, filters present and detectors determine the flow cytometers configuration, and these components define how many colours can be detected simultaneously (Holmberg-Thyden et al., 2021, Cossarizza et al., 2021). Additionally, it is important that the voltages' detector has been optimized to define the minimally acceptable voltage that can give the optimal resolution for each detector (Cossarizza *et al.*, 2021). In this study we use a fully equipped BD LSR Fortessa 20X, where its configuration is shown in table 2.1 below.

Table 2.1: Configuration of LSR Fortessa 20X

Laser Name	*Laser Wavelength*	*Bandpass Filter*	*Parameter name*	*Example of fluorochrome detected*
Blue	488nm	N/A	FSC	Forward Scatter
Blue	488nm	488/10	SSC	Side Scatter
Blue	488nm	530/30	B530	FITC, Alexa Fluor488
Blue	488nm	710/50	B710	PerCP-Cy5.5
Red	640nm	670/30	R670	APC
Red	640nm	730/45	R730	Alexa Fluor 700
Red	640nm	780/60	R780	APC-H7, APC-Cy7
Violet	405nm	450/50	V450	Brilliant Violet 421
Violet	405nm	525/50	V525	Brilliant Violet 510
Violet	405nm	610/20	V610	Brilliant Violet 605
Violet	405nm	670/30	V670	Brilliant Violet 650
Violet	405nm	710/50	V710	Brilliant Violet 711
Violet	405nm	780/60	V780	Brilliant Violet 786
UV	355nm	379/28	U379	Brilliant UV 395
UV	355nm	450/50	U450	Live/Dead Blue
UV	355nm	730/45	U730	Brilliant UV 737
UV	355nm	800/40	U800	Brilliant UV 805
Yellow/Green	561nm	586/15	G586	PE
Yellow/Green	561nm	610/20	G610	PE-CF594
Yellow/Green	561nm	780/60	G780	PE-Cy7

2.2.2 Selection of Markers and Fluorochrome-conjugated antibodies

The initial step in designing a PFC panel, is to consider the aims of the study, which define the markers needed to isolate the main populations of interests. This study aims to analyse T, B, NK and redox related markers thus there are antigens unique for identifying these subsets of interest. Each marker was ranked by prominence as suggested by Mahnke and Roederer (2007), and segregated into three categories:

I. Lineage antigens that identify the populations of interest. Examples: CD3, CD4, CD8 (T cells) CD19 or CD20 (B cells) and CD56 (NK cells).

II. Markers that define differentiation and provide a profounder characterization of major populations. Examples: CD45RO, CCR7, CD95 (T cell differentiation) CD21, CD27, IgD, IgG (B cells maturation), CD16, perforin (NK cells).

III. Any antigens of interest whose expression level is unknown and needs to be assessed by PFC in specific subsets or conditions Examples: activation markers (HLA-DR), markers of functionality (Granzyme B) and transcription factors (XBP1, PAX5).

Once the list of the markers is outlined and their level of priority is well-defined, markers are assigned to fluorochrome-conjugated antibodies on the basis of both the markers' expression level and the fluorophores brightness. Precisely, antibodies specific for highly expressed antigens, which generally belong to the primary group, were matched with dim fluorophores, leaving bright fluorophores for antigens with low or unknown expression, which generally belong to the third group (like XBP1, PAX5 etc.).

2.2.3 Titrations

The reagent concentration suggested by the supplier it is not always appropriate, thus antibody titrations are an essential step in the optimisation of PFC panel. The positive population must be well defined from the negative one(Mahnke and Roederer, 2007;

Kalina, Lundsten and Engel, 2020; Cossarizza *et al.*, 2021). Additionally, titrations can be a useful tool if fluorochrome-conjugated antibodies show "spreading error". Spreading error is the consequence of imprecise measurement and compensation, that generates artifacts, which impact the analysis and data interpretation (M Roederer, 2001). Since the impact of "spreading error" is more with high fluorescence levels, it useful to know the lower titre that can be used without losing separation between the positive and the negative signal. Therefore, to identify the correct concentration of fluorophore-conjugated antibodies in this current study all antibodies have been titrated. Spreading errors were monitored in all the detectors, and where possible, antibody combination were changed to prevent spreading error effects. In the other circumstances, a lower titre was selected with caution of not losing in separation capacity.Below we describe the process of titrations and how the optimal concentration was defined.

Method

The recommended vendor concentration was used as the highest titre for each fluorophore-conjugated antibody and serial dilutions were performed to define the optimal titre. For example, if the suggested quantity is 5 µl per test in 100 µl, then 10 µl of antibody was added and topped up with 90 µl BD BSA Staining Buffer (Cat: 554657) giving a total of 100 µl in the first tube. Then, 50 µl was extracted and diluted in another 50 µl of buffer six times formulating a serial dilution. It's important to note that for intracellular markers, permeabilization buffers were used instead

of BSA Staining Buffer. Overall, it's important to use usual assay conditions for each antibody when titrations are conducted. An equal volume of cells was added to each tube to generate a 1:1 concentration of antibody mix to cells. Staining was done for 20 minutes protected from light. The temperature used for the staining was decided based on the vendor's recommendation. Washing steps were conducted after staining cells and re-suspended in appropriate volume for acquisition.

Analysis

When analysing this data, a minimal gating strategy is applied (Figure 2.1, A) where doublets are eliminated by plotting cells against FSC-H vs. FSC-A parameters. Following doublet discrimination, dead cells are eliminated by excluding cells that are positive for the viability dye (Live/Dead dye - LD), while lymphocytes are then selected on the basis of physical parameters (FSC-A vs. SSC-A). For antigens known to be expressed on just small cell subsets, samples are also stained for markers that facilitate subsequent analysis. After selecting the population of interest, dot plots are created to compare the performance of the reagent for each titre. The median fluorescent intensities (MFIs) of the positive and negative populations are graphed for each titration as a ratio against the antibody concentration to conclude the peak signal-to-background ratio (Figure 2.1 B). The highest ratio indicates the optimal concentration as it defines the highest difference amongst the positive and the negative populations and indicates the antibodies saturation point. Additionally, titrations

can be plotted as concatenate graphs for a visual observations of each titre (Figure 2.1 C).

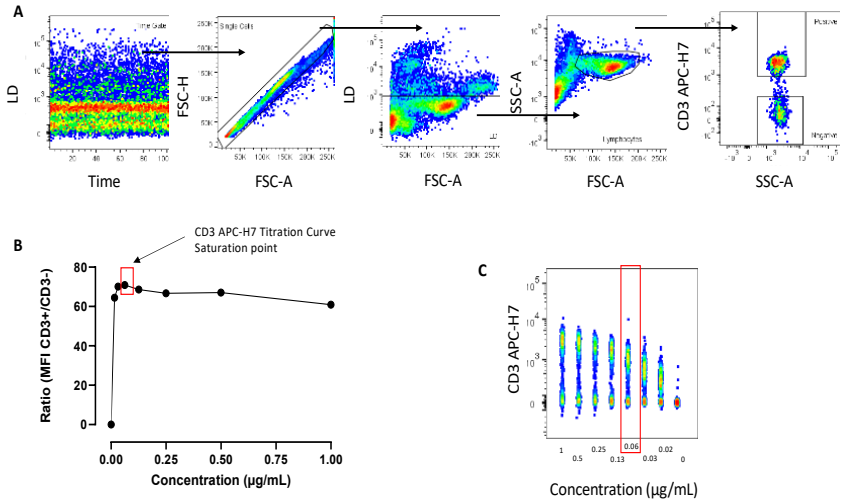

Figure 2.1: **Example of process of fluorochrome-conjugated antibody titration analysis. A)** Minimal gating strategy defining the population of interest for CD3 APC-H7 antibody titration: Doublets are eliminated in the FSC-H vs. FSC-A plot, dead cells are eliminated excluding cells that are positive for the viability dye (LD), lymphocytes are selected on physical parameters, and then , the expression of the marker of interest (CD3 APC-H7) is valuated gating on positive and negative cells. **B)** Following ratio calculations of MFI+/MFI-, results are plotted to determine the peak signal-to-background ratio. The highest ratio is 70.9 of MFI for CD3 APC-H7, which is the fifth serial dilution with a concentration of 0.06 µg/mL. **C)** Concatenate graph of all the dilutions.

2.2.4 Compensation and Spreading Error

When referring to flow cytometry , the term "compensation" denotes the practise of eliminating the fluorescent signal of a fluorochrome from all detectors, aside from the one used to measure that dye (Mario Roederer, 2001) . This is done by a complex and automated mathematical method to correct for fluorescence spillover (Figure 2.2 A, B). On the contrary, spreading error refers to an error that is visible after compensation has been applied (Mario Roederer, 2001; Herzenberg *et al.*, 2006). The reason spreading error occurs after compensation is because inevitably counting photons is challenging and can be unavoidably detected by different wavelengths (Figure 2.2) (Roederer, 2002). Therefore, when designing a PFC panel it is important to first perfect compensation related difficulties and then work to eliminate or minimise spreading error.

Applying Compensation

In this study we utilised compensation beads to eliminate spill over in our PFC panels. Compensation beads are a helpful experimental tool in flow cytometry as they offer a higher fluorescent intensity alone and therefore have a clear positive and negative control that increases the accuracy of the automated calculation (Perfetto *et al.*, 2012; Brummelman *et al.*, 2019; Cossarizza *et al.*, 2021). Additionally, their choice is useful especially if there is limited sample availability and there is a need to avoid wasting valuable cells when configuring an experiment procedure.

Method

For each fluorochrome conjugated antibody for each PFC panel one compensation control is prepared. Specifically, in this study UltraComp eBeads™ (Cat#01-3333-42) were used, and stained for 15 minutes protected from light. Usually the same amount of antibody used to stain the cells is used for compensation. In case of volume lower the 1 µL, 1 µL was used for convenience.

Assessing Spreading Error

Background fluorescence and spreading error are major contributors of variability in PFC. As already explained, spreading error is visible only after compensation has been applied and is known as the "trumpet effect" since the positive population forms a funnel shaped structure which can make it difficult to determine the double positive population (Figure 2.2 C) (Nguyen *et al.*, 2013; Cossarizza *et al.*, 2021).

In PFC spreading error is inevitable, however, in this study we used a variety of strategies to avoid or minimise this effect:

I. Allocated highly expressed markers like CD3, or CD19 to dim fluorophores and low or unknown expression of markers to bright fluorochrome conjugated antibodies.

II. When assessing many markers on a single cell type choose fluorochromes with minimal spreading on co-expressed markers.

III. When applicable, decrease titres of fluorochrome conjugated antibodies that cause spreading to minimise their fluorescent intensity and consequently the spreading error. It could be also useful to increase the titre of the fluorochrome conjugated antibody in the channel in which spreading error is occurring, to maximize the positive signal, but keeping attention to not increase the negative signal too much).

For example, as seen in Figure 2.2C if PE-Cy7 has a low titre, then the double positive populations of PE-Cy7 and APC-H7 will be undetectable. In this case, the solution is to decrease the titre of APC-H7 and, if possible, increase the titre of PE-Cy7.

IV. To assess the spreading error of each panel, each fluorophore conjugated antibody with its selected titre was assessed by performing a spreading error assay (Method below).

Method

Once titres per fluorophore conjugated antibodies are initially selected a spreading error assay was executed. To do this, healthy donor PBMC's were used, and cells were single stained with the

selected titre alone. All compensation controls for all the antibodies were conducted and complete compensation matrix for all fluorophore conjugated antibodies was applied to each single stained simple. This allowed the visualisation of spreading error in channel after compensation is corrected.

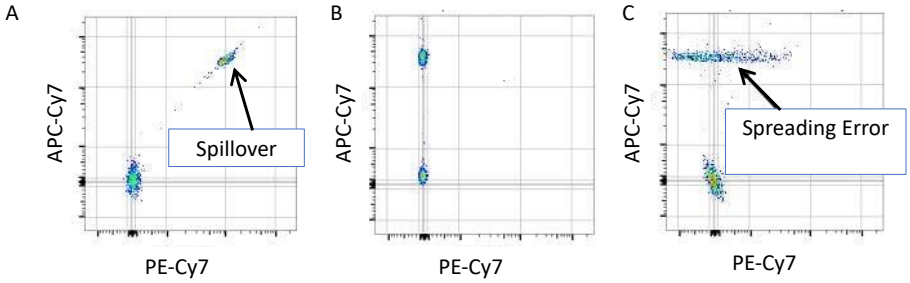

Figure 2.2: **The difference of spillover and spreading error. A)** Uncompensated dot plot where the fluorochrome APC-H7 fluorescence spills into the PE-Cy 7 channel. **B)** After applying compensation a straight line should be generated amongst the positive and the negative populations. **C)** In some cases, after compensation the positive population has a funnel shape also known as the "trumpet effect" which is the indications that there is spreading of APC-H7 channel in the PE-Cy 7 channel.

2.2.5 Machine Standardisation

Amongst the field of flow cytometry, there is an overall agreement that to encourage reproducibility and accuracy instrument standardisation is essential (Perfetto *et al.*, 2012). There are a variety of methods that can be applied to encourage standardization, which can give a foundation for better cytometry result reproducibility over extended time periods, between various sites, and amongst various instruments. Additionally, standardisation is essential for decreasing instrument user set-up variation among replicates when studies focus on evaluation protein expression levels by utilising the mean fluorescence intensity (MFI) (Le Lann *et al.*, 2020).

Rainbow Beads

There are several non-biological factors that influence fluorescent intensity on flow cytometers such as laser power, laser alignment and optical efficiency (Perfetto *et al.*, 2006, 2012). When a flow cytometer is being set up for an experiment, detector sensitivity is adjusted to optimise instrument performance per run, however these voltages being altered may not be optimal for the following experiments (Mahnke and Roederer, 2007; Perfetto *et al.*, 2012; Le Lann *et al.*, 2020; Holmberg-Thyden *et al.*, 2021). Therefore to eliminate this bias, in this study uses hard-dyed fluorescent beads known as rainbow beads (Spherotech, Cat. RCP-30-20A Rainbow Calibration Particles, 8 peaks) which are capable of emitting light through a series of eight peaks in each channel. Acquisition of

rainbow beads allows one to fix target values that reflect the instruments sensitivity as done for each panel designed in the following study (Perfetto *et al.*, 2012). Each experimental run then involves the initial acquisition of rainbow beads and voltages are adjusted until the designated bead peak reaches the initial target value. In this study a threshold of ±10% has been established. This particular method of experimental harmonization is highly reliable and can allow users to adapt to any changes in performance after cytometer maintenance or laser alignment (Le Lann *et al.*, 2020).

The set-up of the target values is done either during a test experiment for the panel. The stained sample with chosen titres is acquired first to set the voltages first and then the rainbow beads are acquired (Mahnke and Roederer, 2007; Perfetto *et al.*, 2012). In figure 2.2A we show as representative example the gating strategy to define the rainbow beads, and then gate on the 8^{th} peak (or peak of choice) of detector B710-A to indicate the target value that will always be measured for each experiment. In Figure 2.2B we demonstrate an example of a series of eight experiments to show how each designated peak for each detector attains a comparable MFI per experiment, not exceeding the ±10% threshold. Rainbow bead results as shown in figure 2.2B confirm that the experimental procedures done for the study reduce instrumental related biases.

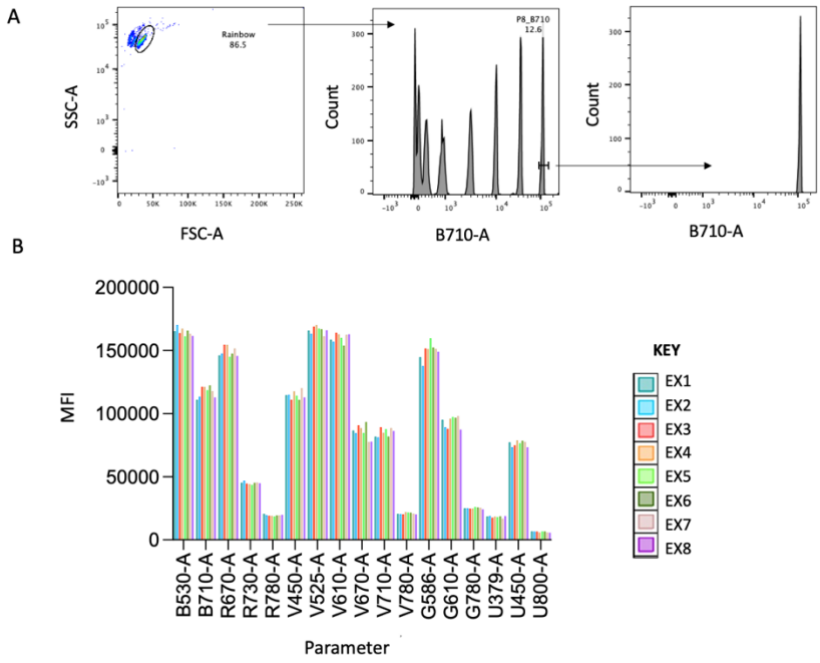

Figure 2.2: **Rainbow calibration bead set up and examples. A)** Gating strategy of rainbow calibration beads detected by plotting against SSC-A and FSC-A physical parameters. Histogram representation of Rainbow gate against the B710-A parameter to determine peaks of interest. Gate on the 8th peak is set to determine the target MFI of B710-A. **B)** Example of a series of 8 experiments after setting the target MFI values for each parameter in all the lasers available for the flow cytometer used in this study (BD LSR Fortessa 20X). For all experiments the designated target peak per detector achieves comparable MFI per experiment not exceeding the ±10% threshold.

2.3 Conclusion

In this study, we establish and optimise the PFC panels used to address age and sex related changes in T, B and NK cells (Chapter 4 and 5). Using the configuration of the flow cytometer BD LSR Fortessa 20X, thoughtful matching of fluorochromes to antigens of interest was applied to achieve the studies aims and objectives. Following this, optimisation experiments were conducted to identify the finest concentrations for each fluorochrome-conjugated antibody used and to determine spreading error, while compensation controls were established to correct any fluorescence spillover. Machine standardisation was also established to encourages experimental reproducibility. The overall procedure of implementing and optimising a PFC panel for conventional flow cytometry can be challenging, however, crucial in eliminating experimental biases, and yielding accurate results.

2.4 Bibliography

Brummelman, J. *et al.* (2019) 'Development, application and computational analysis of high-dimensional fluorescent antibody panels for single-cell flow cytometry', *Nature Protocols*, 14(7), pp. 1946–1969. Available at: https://doi.org/10.1038/s41596-019-0166-2.

Cossarizza, A. *et al.* (2021) 'Guidelines for the use of flow cytometry and cell sorting in immunological studies (third edition)', *European Journal of Immunology*, 51(12), pp. 2708–3145. Available at: https://doi.org/10.1002/eji.202170126.

Herzenberg, Leonore A *et al.* (2006) 'Interpreting flow cytometry data: a guide for the perplexed', *Nature Immunology*, 7(7), pp. 681–685. Available at: https://doi.org/10.1038/ni0706-681.

Holmberg-Thyden, S. *et al.* (2021) 'A user's guide to multicolor flow cytometry panels for comprehensive immune profiling', *Analytical Biochemistry*, 627, p. 114210. Available at: https://doi.org/10.1016/j.ab.2021.114210.

Kalina, T., Lundsten, K. and Engel, P. (2020) 'Relevance of Antibody Validation for Flow Cytometry', *Cytometry Part A*, 97(2), pp. 126–136. Available at: https://doi.org/10.1002/cyto.a.23895.

Le Lann, L. *et al.* (2020) 'Standardization procedure for flow cytometry data harmonization in prospective multicenter studies', *Scientific Reports*, 10(1), p. 11567. Available at: https://doi.org/10.1038/s41598-020-68468-3.

Mahnke, Y.D. and Roederer, M. (2007) 'Optimizing a Multicolor Immunophenotyping Assay', *Clinics in Laboratory Medicine*, 27(3), pp. 469–485. Available at: https://doi.org/10.1016/j.cll.2007.05.002.

Mura, M. *et al.* (2020) 'Optimized flow cytometric protocol for the detection of functional subsets of low frequency antigen-specific

CD4+ and CD8+ T cells', *MethodsX*, 7, p. 101005. Available at: https://doi.org/10.1016/j.mex.2020.101005.

Nguyen, R. *et al.* (2013) 'Quantifying spillover spreading for comparing instrument performance and aiding in multicolor panel design', *Cytometry Part A*, 83A(3), pp. 306–315. Available at: https://doi.org/10.1002/cyto.a.22251.

Perfetto, S.P. *et al.* (2006) 'Quality assurance for polychromatic flow cytometry', *Nature Protocols*, 1(3), pp. 1522–1530. Available at: https://doi.org/10.1038/nprot.2006.250.

Perfetto, S.P. *et al.* (2012) 'Quality assurance for polychromatic flow cytometry using a suite of calibration beads', *Nature Protocols*, 7(12), pp. 2067–2079. Available at: https://doi.org/10.1038/nprot.2012.126.

Roederer, Mario (2001) 'Spectral compensation for flow cytometry: Visualization artifacts, limitations, and caveats', *Cytometry*, 45(3), pp. 194–205. Available at: https://doi.org/10.1002/1097-0320(20011101)45:3<194::AID-CYTO1163>3.0.CO;2-C.

Roederer, M. (2002) 'Compensation in Flow Cytometry', *Current Protocols in Cytometry*, 22(1). Available at: https://doi.org/10.1002/0471142956.cy0114s22.

Chapter 3

A redox based characterization of immune cell subsets by polychromatic flow cytometry

3.1 Introduction

Redox metabolites fulfil key functions in immunity and it is now evident that redox-related enzymes are essential for normalizing immune cell signalling. The majority of the main cellular redox state determinants have been traditionally studied using fluorescent microscopy and immunoblot analysis, yet thus far, no complete polychromatic flow cytometry (PFC) panel and assay has been developed allowing their simultaneous measurement in various immune cell subsets. Here we present a flow cytometry assay that can measure simultaneously key antioxidant defence systems and reactive oxygen species (ROS) in the different subsets of T, B and NK lymphocytes, thus allowing a deep investigation of the Redox status of the immune system.

3.2 Graphical Abstract

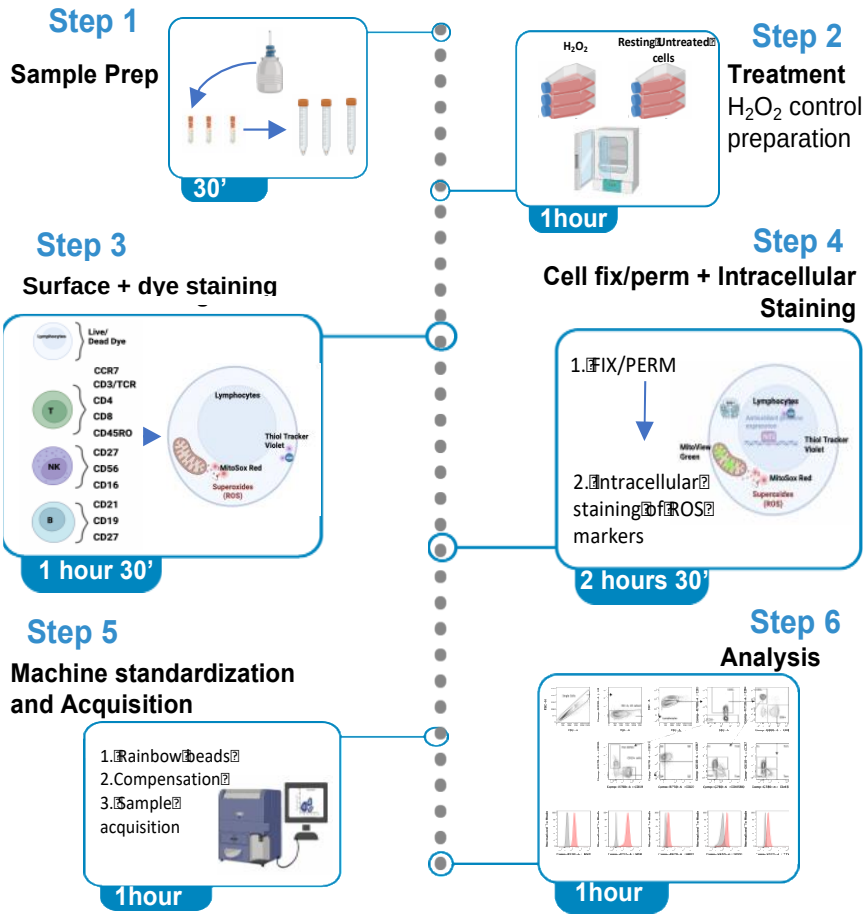

3.3 Before you begin

The polychromatic flow cytometry (PFC) assay described here allows the simultaneous measurement of cell-surface markers of immune cell subsets (T, B and NK cells) and their key redox homeostasis players (ROS and antioxidant systems). This protocol is unique as it uses fluorescent conjugated monoclonal Antibodies (mAbs), in combination with redox-related dyes and markers. We demonstrate a quick way of evaluating key parameters of redox homeostasis in immune cells, useful for research associated with immune-related diseases.

The objective of the designed panel is to dive deep into the heterogeneity of the most abundant immune cell compartments and measure their redox status. For example, the T cell immune compartment is comprised of T cells subpopulation and subsets that differs in terms of phenotypic composition, functional activity and capacity to respond to homeostatic or antigenic stimulation (Appay *et al.*, 2008). Therefore we used mAbs specific for CD4 and CD8, to detect helper and cytotoxic T cells, respectively. To identify the different T cell subsets, we used a combination of mAbs specific for detection T naïve (T_n CD45RO- CCR7+), T central memory (T_{cm}CD45RO+ CCR7+), T effector memory T_{em} CD45RO+ CCR7-), T terminal effector (T_{tem} CD45RO- CCR7-)(Roberto et al., 2015). Following the identification of T cells we centre our attention on CD3- cells to analyse B and NK cells. B cells also acquire a heterogenic phenotype following the identification of the main B cell subset as (CD3−CD14−CD19+)

(A Roberto *et al.*, 2015). For example Naïve B cells are further defined as CD21+, CD27- while memory B cells can be defined as CD21+, CD27+. We also include CD56 in our panel to define NK cells predominantly as CD3- CD56+. NK cells are another heterogeneous population of lymphocytes which are characterised into two main subsets: $CD56^{DIM}$ and $CD56^{BRIGHT}$ (Roberto *et al.*, 2018).

To detect superoxide anion molecules within the mitochondria of the heterogenous populations of lymphocytes mentioned above, we take advantage of the highly selective red-fluorogenic dye MitoSOX (MSR). As an internal control, we identify the mitochondria using a green-fluorogenic dye (MitoView Green – MVG) that stains mitochondria in live cells and provides normalization with respect to the mitochondrial mass. To get a more comprehensive view of the intracellular redox homeostasis, we also analyse some representative defence systems, harboured in cells against excessive ROS exposure. Therefore, superoxide dismutase 1 (SOD1) can be detected in each immune subset mentioned above. It is a highly conserved and abundant antioxidant enzymes, known for its scavenging activity, maintaining redox balance and regulation of transcription (Zelko, Mariani and Folz, 2002). The nuclear factor erythroid 2-related factor 2 (Nrf2), which is a key regulator of antioxidant responses, is also ubiquitously expressed by immune cells (Kaspar, Niture and Jaiswal, 2009; Milani *et al.*, 2013)and it plays a key role in the differentiation and functionality of B cells in particular (Bertolotti

et al., 2010). Sequestered by cytoplasmic Keap1 and targeted to proteasomal degradation in basal conditions, in case of oxidative stress Nrf2 detaches from Keap1 and translocates to the nucleus, where it activates the transcription of some crucial defense mechanisms to counteract oxidative stress (Keum and Choi, 2014). Additionally, we also use a thiol reactive dye to measure the cellular levels of reduced glutathione (GSH), which plays a role in preventing damage to cellular components by ROS (Townsend, Tew and Tapiero, 2003; Brasil *et al.*, 2013). Likewise, GSH is fundamental to protect SOD1 residues under mild oxidative stress enabling SOD1 activation (Brasil *et al.*, 2013). To confirm that the panel can detect redox-related changes, appropriate redox-homeostasis modulators should be used as controls (Bertolotti *et al.*, 2013, 2016). In this assay we used Hydrogen Peroxide (H_2O_2), as it is the easiest to source and use. However, H_2O_2 generators (like t-BHP) or O2- inducers (like PB) can also be used as alternative.

The protocol has been optimized and described using Peripheral Blood Mononuclear cells (PBMC's) from healthy human whole blood. Any human PBMC's either fresh or stored in liquid nitrogen can be used for this protocol. However, in case of different biological sources (peripheral blood, lymph nodes, tissues etc), the panel can be easily adjusted with the addition of an anti-CD45 antibody to specifically select lymphocytes.

For the development of the assay, mAbs and Dyes have to be titrated for identifying the best concentration that allows to distinguish the populations of interest (Cossarizza *et al.*, 2021b). It is highly advised that all antibodies and dyes used are titrated before conducting the assay, as the optimal titre can change.

The panel presented here has been optimised on a BD LSR Fortessa X-20 fully equipped with five lasers -blue (488 nm), Red (635 nm), Violet (405 nm), Ultraviolet (355 nm), Yellow/Green (561 nm). However, the protocol can be used with any flow cytometer that can detect all the fluorochromes listed (Refer to key resources table for a complete list of reagents and tools). We recommend to set up the Flow cytometer by completing instrument quality control before beginning and report the performance of the machine. For BD LSR Fortessa X-20, we used CS&T beads. Finally, before beginning, use any Rainbow calibration beads to standardise the acquisitions (Kalina *et al.*, 2012) . Rainbow calibration beads allow the setting of a peak MFI target and that this target is close to identical every time a new experiment is acquired. Adjusting the voltages for each channel to reach the MFI target set is important for standardizing acquisitions. For more information and details on how to setup the ideal MFI targets, refer to previously published protocols (Perfetto *et al.*, 2006, 2012)

Institutional permissions

Sample collection from healthy donors was approved by the ethics committee: REC 17WS0172 at the Experimental Medicine and Rheumatology department, Queen Mary University of London. Healthy volunteers signed informed consent.

3.4 Preparation of Dye Stock solutions and buffers

Timing: 30 min

Refer to materials and equipment for all the recipes that need to be prepared prior to starting.

Key resources table

REAGENT or RESOURCE	SOURCE	IDENTI
Antibodies		
Anti-Nrf2 Antibody A-10	Santa Cruz	Cat#sc-365949
APC-H7 Mouse Anti-Human CD3	BD Pharmingen™	Cat# 560275
BV711 Mouse Anti-Human CD4	BD Horizon™	Cat#563913
BUV805 Mouse Anti-Human CD8	BD Horizon™	Cat#612890
PE-CF594 Mouse Anti-Human CCR7 (CD197)	BD Horizon™	Cat#566769
PE-Cy™7 Mouse Anti-Human CD45RO	BD Pharmingen™	Cat#560608
Alexa Fluor® 700 Mouse Anti-Human CD27	BD Pharmingen™	Cat#560611
BV786 Mouse Anti-Human CD19	BD Horizon™	Cat#563325

BV650 Mouse Anti-Human CD21	BD OptiBuild™	Cat#740569
BUV395 Mouse Anti-Human CD56	BD Horizon™	Cat#563554
SOD1/Cu-Zn SOD Antibody	Novus Biologicals	Cat#JF1005
Goat anti-Rabbit IgG (H+L) Secondary Antibody, DyLight™ 405	Thermo Fisher Scientific	Cat#35551
Human samples		
Cryopreserved human Peripheral Blood Mononuclear Cells (PBMC's)	n/a	n/a
Chemicals, peptides, and recombinant proteins		
Dulbecco's Phosphate Buffer Saline (DPBS) Solution without calcium and magnesium	Gibco	Cat#14190-144
RPMI 1640 Medium (RPMI)	Thermo Fisher	Cat#11875093
Penicillin-Streptomycin (10,000 U/mL)	Thermo Fisher	Cat#15140122
Fetal bovine serum (FBS)	EueoClone	EUS00AY
Distilled Cell Culture Water	Gibco	Cat#A12873-01
Viability Dye - LIVE/DEAD™ Fixable Blue	Thermo Fisher Scientific	Cat#L34962
ThiolTracker™ Violet (TTV)	Thermo Fisher Scientific	Cat#T10096
MitoSOX™ RED	Thermo Fisher Scientific	Cat#M36008
MitoView™ Green (MVG)	Biotium	Cat#70054
Brilliant Stain Buffer	BD Horizon™	Cat#566349
Stain Buffer (BSA)	BD	Cat#554657

Foxp3 / Transcription Factor Fixation/Permeabilization Concentrate and Diluent kit	eBioscience™	Cat#00-5521-00
Permeabilization Buffer (10X)	eBioscience™	Cat#00-8333-56
UltraComp eBeads™ Plus	Thermo Fisher	Cat#01-3333-42
ArC Reactive Beads	Thermo Fisher	Cat#A10346
DIVA CS&T RUO BEAD 150	BD	Cat#655051
Trypan Blue	BioWhittaker	Cat#17-942E
H_2O_2	DR MARCUS	02083626000200
Software and algorithms		
FACSDiva™ 8.0.3		
FlowJoTM v10 Software		

3.5 Materials and equipment

Supplemented RPMI 1640 media (R10)

Reagent	**Final concentration**	**Amount**
RPMI	N/A	445 mL
FBS	10%	50 mL
Penicillin-Streptomycin (10,000 U/mL)	100U/mL	5 mL
Total		500 mL
Media is filtered (0.22µm) and stored at 4°C up to 1 month.		

Live/Dead Fixable Blue Stock Solution

Reagent	**Final concentration**	**Amount**

LIVE/Dead Fixable Blue	n/a	1 vial
DMSO	n/a	50 µL
Total		50 µL
Vortex well after preparation. Store the reconstituted stock solution for up to 2 weeks at -20°C, protected from light and humidity. Prepare small aliquots to avoid freeze-thaw cycles.		

ThiolTracker™ Stock Solution

Reagent	**Final concentration**	**Amount**
ThiolTracker™ Violet	10 mM	1 vial
DMSO	n/a	30 µL
Total		30 µL
Vortex well. Prepare small aliquots of stock to avoid multiple freeze-thaw cycles. Store at -20ºC.		

MitoSOX™ RED Stock solution

Reagent	**Final concentration**	**Amount**
MitoSOX™ RED	5 mM	1 vial
DMSO	n/a	13 µL
Total		13 µL
Vortex well. Prepare small aliquots of stock to avoid multiple freeze-thaw cycles. Store at -20ºC.		

MitoView™ Green Stock solution

Reagent	**Final concentration**	**Amount**
MitoView™ Green 5M	200 µM	1 vial
DMSO	n/a	400 µL
Total		400 µL

Vortex well. Prepare small aliquots of stock to avoid multiple freeze-thaw cycles. Store at -20ºC.

Foxp3 / Transcription Factor Fixation/Permeabilization Concentrate and Diluent kit (1:4) Dilution

Reagent	**Final concentration**	**Amount**
Transcription Factor Fixation/Permeabilization Concentrate	n/a	1 µL
Transcription Factor Fixation/Permeabilization Diluent	n/a	3 µL
Total		4 µL
CRITICAL: Prepare fresh and in a chemical hood each time. The Transcription Factor Fixation/Permeabilization Concentrate contains formaldehyde and should be used with caution. Acute exposure to formaldehyde is highly irritating to the eyes, nose, and throat while long-term exposure to low levels in the air or on the skin can cause asthma-like respiratory problems, skin irritation and even cancer.		

Permeabilization Buffer (1X)

Reagent	**Final concentration**	**Amount**
Permeabilization Buffer (10X)	1X	5 mL
Cell culture water	n/a	45 mL
Total		50 mL
Prepare fresh each time.		

Blocking solution

Reagent	**Final concentration**	**Amount**
DPBS	n/a	9.8 mL
FBS	n/a	200 µL
Total		10 mL
Store at 4°C.		

Flow cytometer (BD LSR Fortessa X-20)

Reagent	**Laser (excitation nm)**	**Emission filter (nm)**
Viability Dye - LIVE/DEAD™ Fixable Blue	UV (355)	450/50
MitoSOX™ RED (MSR)	Blue (488)	710/50
MitoView™ Green (MVG)	Blue (488)	530/30
ThiolTracker™ Violet (TTV)	Violet (405)	
SOD1/Cu-Zn SOD Antibody / Goat anti-Rabbit IgG (H+L) Secondary Antibody, DyLight™ 405	Violet (405)	450/50
Brilliant Violet 605™ anti-human CD16 Antibody	Violet (405)	610/20
BUV395 Mouse Anti-Human CD56	UV (355)	379/28
BV650 Mouse Anti-Human CD21	Violet (405)	670/30
BV786 Mouse Anti-Human CD19	Violet (405)	780/60
Alexa Fluor® 700 Mouse Anti-Human CD27	Red (640)	730/45
PE-Cy™7 Mouse Anti-Human CD45RO	Yellow/Green (561)	780/60
PE-CF594 Mouse Anti-Human CCR7 (CD197)	Yellow/Green (561)	610/20
BUV805 Mouse Anti-Human CD8	UV (355)	800/40
BV711 Mouse Anti-Human CD4	Violet (405)	710/50
APC-H7 Mouse Anti-Human CD3	Red (640)	780/60
Anti-Nrf2 Antibody A-10	Red (640)	670/30

Alternatives: BD LSR Fortessa X-20 fully equipped with five lasers -blue (488 nm), Red (635 nm), Violet (405 nm), Ultraviolet (355 nm), Yellow/Green (561 nm) - was used in this assay. Any other flow cytometers equipped with the same lasers and similar emission filters can also be used.

Alternatives: In the key resources table, the mAbs used for the detection of the different markers were validated ad titrated for this protocol. However, depending on the configuration of the instrument, the fluorochromes of the mAbs can be exchanged, and, if required, any other markers can be incorporated.

3.6 Step-by-step method details

PBMC's thawing

Timing: 1h

This section describes how PBMC's are thawed before starting the staining procedure. This step must be fast to allow good sample recovery.

1. Thawing PBMCs

    a. Prepare and warm R10 in a water bath at 37°C.
    b. In a biological hood add 5 mL of warm R10 in a 15 mL tube.
    c. Take PBMC vials from the Liquid Nitrogen tanks and transfer them to the water bath on dry ice. Do this quickly. If the liquid nitrogen is not close to the water bath, cells can be temporarily kept in dry ice before the thawing.
    d. Swivel the vials in the water bath until no ice crystals are seen.

e. Transfer the vials into the biological hood and dropwise add warm RPMI to each vial, resuspending the cell-medium solution very well using a pipette.
f. Transfer the single cell suspension with leukocytes cells in the previously prepared 15 mL tube with the warm medium.

CRITICAL: Add warm RPMI to minimize the risk of osmotic shock dropwise. *However,* don't take too long to complete this process. PBMC's that are stored in liquid nitrogen have cryopreservatives (like 10% DMSO) that can be toxic to the cells once thawed so be relatively fast to avoid cell death.

g. Top up the tube with R10 and wash the cells at 400g for 10 mins at Room Temperature (RT).
h. Discard the supernatant carefully without losing the pellet.
i. Resuspend the cells in appropriate volume and count the number of cells.

Note: Any cell counter or traditional trypan blue cell counting methods can be conducted.

CRITICAL: Each washing step may lead to losing cells. In this assay we started with about 5 x 10^6 live cells per donor in order to have 1 x 10^6 cells acquired per donor. This number of cells was

enough to detect the populations of interest. The starting number of cells can be scaled down to 1 x 10^6 live cells, if necessary.

3.7 In vitro H_2O_2 - treatment of human PBMC's to generate redox-positive controls

Timing: 1 h

This section describes how generate positive controls to confirm that the assay can detect redox-related changes. Additionally, resting cells after a thawing is also important as thawing can be a stressful process.

2. Treating PBMC's

    a. Once counted, resuspend the cells at a concentration of 1 x 10^6 cells/mL and split the suspension in 2 flasks, tubes or plates.
    b. Label one flask as the oxidative control and add H_2O_2 to reach a 50 µM final concentration.
    c. Keep the other flask untreated and place both flasks in an incubator for 1h at 37°C

Note: To find the optimal H_2O_2 concentration and time of treatment for your experiment and type of cells, conduct appropriate test experiments. Here we tested a variety of concentrations and times and found that a 1h treatment and a 50

µM concentration of H_2O_2 was enough to demonstrate a redox related shift after staining with redox related markers.

3.8 Sample and staining control preparation

Timing: 10 min

This section of the protocol lists the samples and the controls necessary for the assay.

Together with the full stained samples, additional staining controls have to be prepared. A Fluorescence Minus One (FMO) or FMX control is a tube of cells labelled with all but one of more fluorophores respectively. In multi-colour immunofluorescent investigations, FMO or FMX controls are employed to define the cut-off point between background fluorescence and positive populations during analysis. In this assay, we used an FMX control labelled for all the marker with the exception of MVG, MSG, NRF2, TTV, SOD1.

Preparing Controls

a. Collect treated and untreated cells in 15 mL tubes
b. From the untreated sample take about 0.5 x 10^6 cells, place them into a separate 15 mL tube and label it as a FMX tube. The other cells (about 2 x 10^6 cells in our case) will be used for the full staining, to detect the redox status in the population of interest.

c. From the treated sample, keep aside about 0.5 x 10^6 cells to use for compensation controls * (see step 12)
d. The other treated cells (about 2 x 10^6 cells in our case) will be used for the full staining in treated sample, as positive controls of the redox markers in the population of interest.

Live/Dead staining

Timing: 30 min

This section of the protocol describes the staining procedure for excluding dead cells from the analysis.

3. Live/dead staining
    a. top up all the samples with R10 to wash the cells
    b. Spin at 500 g for 10 minutes at RT.
    c. Prepare 1:1000 dilution of LIVE/Dead Fixable Blue mix (1 µl LIVE/Dead Fixable Blue stock solution and 999 µl of DPBS).
    d. Discard supernatant carefully not disrupting the pellet (use a pipette to remove ALL the residual supernatant).
    e. Stain pelleted cells with 100 µl of viability mix (diluted Live/Dead Fixable Staining Solution) directly in the 15 mL tubes

f. Vortex cell pellet with viability mix and stain for 15 mins at RT protected from light.
g. Wash cells with 2ml of BSA and centrifuge at 500g for 5 minutes

CRITICAL: Live/Dead staining is essential as to most flow cytometry-based investigations. Use it to exclude debris and dead cells from analysis especially after optimal H_2O_2 treatment. Viability dyes are sensitive to light and can lose their fluorescence, so make sure to keep the dyes very well protected from light.

Cell Staining Assay

Timing: 4 h

This section of the protocol describes the staining procedure of immune cells subsets and redox markers using Dyes and Monoclonal antibodies.

4. CCR7 staining
    a. Discard supernatant and transfer the cells into FACS tubes
    b. Prepare CCR7 panel as indicated in Table 1
    c. Stain both treated, untreated and FMX control cells with 100 µL cell suspension of CCR7 mixture for 20 minutes at 37^{o}C, protected from light.

Table 1: CCR7 mix

Marker and Clone	**Fluorophore**	**Volume (for 100 µL cell suspension)**
CCR7 (2-L1-A)	PE-CF594	0.6 µL
BV stain buffer	n/a	99.4 µL
Total		100 µL
Note: The preparation provided here is for 1 tube. The volume has to be multiplied by the number of tubes: for one sample you would have to make the surface mix times 3 (untreated sample full staining, untreated sample FMX, treated sample full staining). In case of a higher amount of samples, it is suggested to prepare a master mix with at least 10% extra volume (e.g. if 10 tubes are required, calculate on the basis of 11), so that even the last tube is filled properly avoiding the effect of sample loss when dosing. The mAbs have to be titrated for identifying the best concentration that allows to distinguish the populations of interest.		

CRITICAL: CCR7 is a molecule better detected at 37ºC due to plasma membrane recovery, hence why it vital to stain CCR7 separately at 37ºC (Berhanu *et al.*, 2003).

NOTE: An incubator can be used to keep cells at 37°C, during the CCR7 staining.

5. **Surface staining**

   a. After staining cells with CCR7, wash the cells with 2 mL of PBS and centrifuge at 500g for 5 minutes
   b. Discard supernatant carefully without disrupting the pellet and prepare a mix for all the other Surface Abs using Table 2

Table 2: Surface mix

Marker and Clone	**Fluorophore**	**Volume (for 100 µL cell suspension per sample)**
CD3 (SK7)	APC-H7	0.6 µL
CD4 (L200)	BV711	0.3 µL
CD8 (SK1)	BUV805	0.6 µL
CD45RO (UCHL1)	PE-Cy™7	2.5 µL
CD19 (SJ25C1)	BV786	0.6 µL
CD56 (NCAM16.2)	BUV395	0.6 µL
CD27 (M-T271)	Alexa Fluor® 700	5 µL
CD21 (B-ly4)	BV650	1.25 µL
BV stain buffer	n/a	88.55 µL
TOTAL		**100 µL**

The preparations provided here is for 1 tube. The volume has to be multiplied by the number of tubes: for one sample you would have to make the surface mix times 3 (untreated sample full staining, untreated sample FMX, treated sample full staining). In case of a higher amount of samples, it is suggested to prepare a master mix with at least 10% extra volume (e.g. if 10 tubes are required, calculate on the basis of 11), so that even the last tube is filled properly avoiding the effect of sample loss when dosing.

The mAbs have to be titrated for identifying the best concentration that allows to distinguish the populations of interest.

c. Stain each dry pellet with 100 µL of surface marker staining mixture to create a 100 µL cell suspension per sample.
d. Stain surface markers for 20 mins at RT protected from light.

6. **Redox markers staining**

a. Prepare the ThiolTracker™ & MitoSOX™ RED Dye Mix as indicated in Table 3

Table 3: ThiolTracker™ & MitoSOX™ RED Dye Mix

Reagent - Stock solution concentration	**Final concentration**	**Volume (for 1 mL mix)**
ThiolTracker™ Violet (TTV) - 10 mM	10 µM	1 µL
MitoSOX™ RED (MSR)- 5 mM	5 µM	1 µL
RPMI with 2% FBS	n/a	998 µL
Total		**1 mL**
Note: The required volume of the mix is 100µL per tube. For one p sample you would have to make the redox markers staining times 2 (untreated sample full staining, treated sample full staining§). Here we prepared 1 mL of Mix, enough for 9 tubes with 10% of extra volume. Vortex well and prepare fresh before using.		

b. Once surface markers are stained wash with 1 mL of PBS and centrifuge at 500g for 5 minutes
c. Discard supernatant being careful not to disrupt the pellet.

d. Stain dry pellets, except the FMX tube, with 100 µL of ThiolTracker™ & MitoSOX™ RED Dye Mix immediately. Resuspend the FMX dry pellet in 100uL RPMI with 2% FBS.
e. Incubate cells for 15min at 37ºC protected from light
f. Wash with 1 mL of PBS and centrifuge at 500g for 5 minutes

7. **Fixation**

a. Discard supernatant being careful not to disrupt the pellet
b. Add 1mL of diluted (1:4) Foxp3 / Transcription Factor Fixation/Permeabilization Concentrate (refer to Materials and Equipment for further instructions on how to prepare the fixative)
c. Fix for 30 minutes at 4^{O}C protected from light

Note: Remember to add the fixative in a chemical hood due to the presence of formaldehyde.

8. **Intracellular staining**

a. Prepare MVG staining concentration as indicated in Table 4.

Table 4: MitoView™ Green Mixture

Reagent - Stock solution concentration	**Final concentration**	**Volume**
MitoView™ Green - 200 µM	50 nM	1 µL
1X Perm Buffer	n/a	3999 µL
Total		**4 mL**
Note: The required volume of the mix is 100µL per tube. For one p sample you would have to make the redox markers staining times 2 (untreated sample full staining, treated sample full staining). Here we prepared 4 mL of Mix because of the high dilution factor of the stock solution.		

b. After 30 mins of fixation, wash cells with 2mL of 1X Perm Buffer (refer to Materials and Equipment)
c. Spin at 500g for 5 minutes
d. wash cells again with 2mL of 1X Perm Buffer
e. Spin at 500g for 5 minutes
g. Decant supernatant and stain all tubes except the FMX one with 100 µL of MVG per sample. Resuspend the FMX dry pellet in 100uL 1X Perm Buffer.
f. Stain cells for 15 minutes at RT protected from light.
g. Prepare NRF2 intracellular mix as indicated in Table 5.

Table 5: NRF2 Intracellular staining mix

Marker and Clone	**Fluorophore**	**Final Dilution**	**Volume (for 100 µL cell suspension)**
NRF2 (A-10)	APC	1:40	2.5 µL
1X Perm Buffer	n/a	n/a	97.5 µL
Total			100 µL
Note: The required volume of the mix is 100µL per tube. The final volume has to be multiplied by the number of tubes. For one sample you would have to make the redox markers staining times 2 (untreated sample full staining, treated sample full staining). In case of a higher amount of samples, it is suggested to prepare a master mix with at least 10% extra volume (e.g. if 10 tubes are required, calculate on the basis of 11), so that even the last tube is filled properly avoiding the effect of sample loss when dosing.			

e. After MVG incubation, wash cells with 2mL of 1x Perm Buffer and spin at 500 g for 5 minutes.
f. Repeat washing step
g. Decant supernatant and resuspend all samples except the FMX tube with 100 µL of Intracellular NRF2 mix per sample
h. Resuspend the FMX dry pellet in 100uL 1X Perm Buffer.
i. Stain for 30 minutes in RT protected from light
j. Wash cells with 2 mL of 1x Perm Buffer and spin at 1500 rpm for 5 minutes
k. Repeat washing step
l. Use 1 mL of BSA to perform a blocking step

Alternatives: use PBS with 2% FBS instead of BSA

m. Perform blocking for 30 minutes at RT protected from light

Note: The blocking step here is to avoid any unspecific binding of the SOD1 staining that follows.

n. Prepare SOD1 primary intracellular mix as indicated in Table 6.

Table 6: Primary SOD1 Antibody Mixture

Marker and Clone	**Fluorophore**	**Final Dilution**	**Volume (for 100 µL cell suspension)**
SOD1/Cu-Zn SOD Antibody	n/a	1:25	4 µL
1X Perm Buffer	n/a	n/a	96 µL
Total n/a			**100 µL**
Note: The required volume of the mix is 100µL per tube. The final volume has to be multiplied by the number of tubes. For one sample you would have to make the redox markers staining times 2 (untreated sample full staining, treated sample full staining). In case of a higher amount of samples, it is suggested to prepare a master mix with at least 10% extra volume (e.g. if 10 tubes are required, calculate on the basis of 11), so that even the last tube is filled properly avoiding the effect of sample loss when dosing.			

o. Wash cells with 2 mL of 1x Perm Buffer and spin at 1500 rpm for 5 minutes
p. Stain all tubes, except the FMX one, with 100 µL primary antibody mix.
q. Resuspend the FMX dry pellet in 100uL 1X Perm Buffer.
r. Incubate al samples 30 minute at RT.
s. Prepare the secondary Antibody Mixture Targeting SOD1 as indicated in Table 7.

Table 7: Secondary Antibody Mixture Targeting SOD1

Marker and Clone	**Fluorophore**	**Final Dilution**	**Volume (for 100 µL cell suspension)**
Goat anti-Rabbit IgG (H+L) Secondary Antibody,	DyLight™ 405	1:1000	1 µL
1X Perm Buffer	n/a	n/a	999 µL
Total			1 mL
Note: The required volume of the mix is 100µL per tube. For one sample you would have to make the redox markers staining times 2 (untreated sample full staining, treated sample full staining). Here we prepared 1 mL of Mix, enough for 9 tubes with 10% of extra volume.			

t. Wash cells with 2 mL of 1x Perm Buffer and spin at 500 g for 5 minutes
u. Decant supernatant and repeat washing step

v. Stain all samples with 100 µL Goat anti-Rabbit IgG (H+L) Secondary Antibody each sample for 30 minutes at RT

Note: The FMX control sample has to be stained with secondary Antibody Mixture Targeting SOD1 to prove the specificity of the primary staining.

w. Wash cells with 2 mL of 1x Perm Buffer and spin at 500 g for 5 minutes
x. Decant supernatant and repeat washing step
y. Re-suspend cells with 200 µL of BD Stabilising Fixative
z. Samples are ready for acquisition

Note: Store at 4^{o}C until ready to acquire. Acquire within 4 h after staining completion.

Preparation of Compensation Controls

Timing: 40 mins

Compensation controls for flow cytometry are very important. Compensation is a mathematical calculation that removes unwanted fluorescence signal that is coming into a primary channel and overlapping in a secondary channel. Here we use both

compensation beads and single stained cells to calculate compensation.

Note: the compensation controls can be prepared the same day of the staining, in any moment prior of the acquisition (before, during or after the samples staining).

9. Compensation controls for fluorophore conjugated antibodies.

    a. Prepare 1 FACS tube for each fluorophore conjugated antibody and prepare also an unstained tube.
    b. Vortex well UltraComp eBeads™ (Cat#01-3333-42) for 2 minutes very well and allow them to reach RT.
    c. Add one drop of UltraComp eBeads™in each tube for each fluorophore conjugated antibody. Add one drop of UltraComp eBeads™ also in the unstained tube.
    d. Use at least 1 µL of fluorophore conjugated antibody to stain the beads. If the volume of fluorophore conjugated antibody used per 100 µL cell suspension is higher than 1 µL use the same amount used per cell suspension. Refer to Table 1, 2 and 7 for verifying the amount of antibody
    e. Vortex the FACS tubes and incubate at RT for 15 minutes protected from light

f. Wash beads in 2 mL of BSA and spin at 500g for 5 minutes
g. Resuspend in 300 uL of BSA
h. Store at +4-8°C until samples are ready to be acquired.

10. Compensation controls for Viability Dye - LIVE/DEAD™ Fixable Blue

    a. Prepare and label one FACS tube for the Viability Dye and one FACS tube for the respective unstained compensation control.
    b. Gently vortex ArC™ Amine Reactive Compensation Bead Kit components for 30 seconds to completely resuspend before use.
    c. Add 1 drop of ArC™ Amine Reactive (+) to the FACS tube for the Viability Dye.
    d. Add 1 drop of ArC™ Amine Reactive (-) to the FACS tube for the unstained compensation control.
    e. Allow ArC™ reactive beads to sit in the tube for 5 minutes to warm to room temperature.
    f. Allow ArC™ Amine Reactive (+) and ArC™ Amine Reactive (-) beads to reach RT
    g. Vortex both ArC™ Amine Reactive (+) and ArC™ Amine Reactive (-) beads. for 2 minutes very well.

h. Add one drop of ArC™ Amine Reactive beads in the for each dye and one drop of negative beads (-) to the unstained compensation control.
i. Add 1 µL of undiluted dye to the FACS tube for the Viability Dye.
j. Vortex the FACS tubes and incubate at RT for 15 minutes protected from light
k. Wash beads in 2 mL of BSA and spin at 500g for 5 minutes
l. Resuspend in 300 µL of BSA
m. Store at +4-8°C protected from light until samples are ready to be acquired

11. Compensation controls for TTV, MVG, and MSR *

a. Divide the 0.5 x 10^6 cells into three separate FACS tubes. Designate one tube for each dye (TTV, MVG, and MSR)
b. Wash cells in each tube by adding 1 mL and spin at 500g
c. First stain cells for TTV for a final concentration of 10 µM and the tube for MSR with 5 µM (dilute in RPMI with 2% FBS (as done for Table 3 for the full stain)
d. Incubate cells for 15 minutes at 37°C protected from light

e. Wash with 1 mL of PBS and centrifuge at 500g for 5 minutes
f. Discard supernatant being careful not to disrupt the pellet Add 1mL of diluted (1:4) Foxp3 / Transcription Factor Fixation/Permeabilization Concentrate (refer to Materials and Equipment for further instructions on how to prepare the fixative)
g. Fix for 30 minutes at 4^{O}C protected from light – do this also for the cells in the tube for MVG
h. Wash cells with 2 mL of 1x Perm Buffer and spin at 500 g for 5 minutes
i. Decant supernatant and repeat washing step
j. Resuspend the TTV and MSR tubes with 200 µL of BD Stabilising Fixative. These compensation controls are ready for acquisition.
k. Stain the cells designated for MVG with a 50 nM concentration as prepared for the full stain in Table 4. (use perm buffer as a dilutant)
l. Stain cells for 15 minutes at RT protected from light.
m. Wash cells with 2 mL of 1x Perm Buffer and spin at 500 g for 5 minutes
n. Decant supernatant and repeat washing step
o. Resuspend MVG tube with 200 µL of BD Stabilising Fixative. All compensation controls are now ready for acquisition.

Note: Remember to add and prepare the fixative in a chemical hood due to the presence of formaldehyde.

CRITICAL: It is important to check the quality of the compensation controls: make sure the positive peaks are well resolved and have higher signal compared to that one observed in the fully stained samples.

3.9 Expected outcomes

This protocol allows to clearly identify the main populations of lymphocytes: CD4+ CD3+ T helper, CD8+ CD3+ cytotoxic T cells, CD19+ B cells, CD56+ NK cells. By gating on the total CD3+ cells, both CD4+ T helper and CD8+ cytotoxic T cells we can look deep in the T cell differentiation subsets (T_N, T_{CM}, T_{EM}, T_{TEM}). Likewise, within the CD19+ B cells we can identify Naïve B cells (CD21+, CD27-) and memory B cells (CD21+, CD27+). Other than CD19+ cells, amongst the CD3- cells we can also dive into defining NK cells (CD56+) (Figure 2.1A). All redox related marker of interest can be clearly identified amongst the total lymphocytes (Figure 2.1B). The FMX control allows to distinguish the positive signals from the background. The H_2O_2 controls demonstrate a change in redox related shift proving that we are truly identifying redox related markers and not a specific signals (Figure 2.1 C, B).

3.10 Quantification and statistical analysis

The Median Fluorescence Intensity (MFI) of TTV, NRF2 and SOD1 can be used to study the redox status on the population of interest. For the analysis of MSR, it is important to normalize the MFI of MSR with the MFI of MVG. MVG is strategically included as an internal control as it detects mitochondrial mass overall, independently of the status of the organelles themselves or of the cells, and the dye localizes mitochondria regardless of mitochondrial membrane potential. Therefore, MVG can be used to normalize the MSR median fluorescence intensity that instead detects mainly mitochondrial ROS, specifically anion superoxide. Therefore, by calculating the ratio between MSR and MVG MFI, the mitochondrial ROS would be normalized for the mitochondrial mass, meaning that the residual relative differences among samples (comparing the ratios) would be only ROS-dependent (and not due to a random shift of the mitochondrial mass or to a differential dye- uptake/metabolism by the cells) (Figure 2.1D).

3.11 Limitations

Many notes and crucial consideration points throughout this protocol illustrate the procedure's varied shortcomings. While this approach allows for the standardized measurement and simultaneous comparison of many redox-related markers, it cannot detect the absolute oxidative stress level of any given cell or sample. To do this, use this panel in parallel to other appropriate controls (like knock outs for antioxidant enzymes). Also,

comparisons using this approach can only be done between redox-related markers from one single cell population or from one sample to another. To this aim, ratios of redox-related markers can be calculated. This approach does not allow an absolute quantification of cellular levels of ROS molecules or redox-related markers, as this would imply usage of standard reference samples and controlled experimental conditions (e.g. nitrogen/oxygen monitoring and continuous pH evaluation).

3.12 Troubleshooting

Problem 1:
Issues with compensation.

Potential solution:
If you notice that there are issues with compensation controls, re-prepare the compensation tubes and re-run them using the same machine settings used to acquire the samples. For cell-based compensation tubes, it is suggested to use a different donor (biological source).

Problem 2:
Clumps in sample.

Potential solution:
PBMC'S are sensitive to thawing, thus it's possible that some samples are not of the best quality. If clumps are found in the

sample while resuspending, pass the cell suspension through filtered FACS tubes before acquisition (For example: Corning™ Falcon™ Round-Bottom Polystyrene Tubes with Cell Strainer Snap Cap, 5mL - Catalog No.08-771-23). It's important that no clumps are passed through the flow cytometer as this may block it.

Problem 3:
No shift with H_2O_2 control

Potential solution:
It is possible that you may see no H_2O_2 shift or one that is no expected for each sample. This can be expected as the chemical reaction is fragile and may not yield the expected result. To combat this, it is important to test for the appropriate H_2O_2 concentration needed for the cell type of interest and use better oxidative controls as mentioned in limitations. You should also check the effectiveness of your H_2O_2, as redox reagents tend to be air sensitive and repeated opening/closing cycles should be minimized. In case of doubts, replace all the reagents with fresh ones.

3.13 Resource availability

Lead contact

Further information and requests for resources and reagents should be directed to and will be fulfilled by the lead contact, Alessandra Roberto (aroberto@flowmetric.com)

Materials availability

This study did not generate new unique materials or reagents.

Data and code availability

This study does not have data or codes available.

Acknowledgments

This project has received funding from the European Union's Horizon 2020 Research and Innovation Program under the Marie Skłodowska-Curie grant agreement no. 813091 (ARCH, age-related changes in hematopoiesis).

Author contributions

C.P. has developed and collected the data for this report with the input of M.B. and A.R. M.B. conceived the original idea. C.P. wrote the manuscript with support from M.B. and A.R. I.M. helped with the instrument setting and maintenance. E.P. and J.A.B. provided part of the human PBMC samples. All authors discussed the results and contributed to the final manuscript.

Declaration of interests

The authors declare no competing interests.

3.14 Bibliography

Appay, V. *et al.* (2008) 'Phenotype and function of human T lymphocyte subsets: Consensus and issues', *Cytometry Part A*, 73A(11), pp. 975–983. Available at: https://doi.org/10.1002/cyto.a.20643.

Berhanu, D. *et al.* (2003) 'Optimized lymphocyte isolation methods for analysis of chemokine receptor expression', *Journal of Immunological Methods*, 279(1–2), pp. 199–207. Available at: https://doi.org/10.1016/S0022-1759(03)00186-8.

Bertolotti, M. *et al.* (2010) 'B- to Plasma-Cell Terminal Differentiation Entails Oxidative Stress and Profound Reshaping of the Antioxidant Responses', *Antioxidants & Redox Signaling*, 13(8), pp. 1133–1144. Available at: https://doi.org/10.1089/ars.2009.3079.

Bertolotti, M. *et al.* (2013) 'Tyrosine Kinase Signal Modulation: A Matter of H 2 O 2 Membrane Permeability?', *Antioxidants & Redox Signaling*, 19(13), pp. 1447–1451. Available at: https://doi.org/10.1089/ars.2013.5330.

Bertolotti, M. *et al.* (2016) 'AQP8 transports NOX2-generated H2O2 across the plasma membrane to promote signaling in B cells', *Journal of Leukocyte Biology*, 100(5), pp. 1071–1079. Available at: https://doi.org/10.1189/jlb.2AB0116-045R.

Brasil, A.A. *et al.* (2013) 'The involvement of GSH in the activation of human Sod1 linked to FALS in chronologically aged yeast cells', *FEMS Yeast Research*, 13(5), pp. 433–440. Available at: https://doi.org/10.1111/1567-1364.12045.

Kalina, T. *et al.* (2012) 'EuroFlow standardization of flow cytometer instrument settings and immunophenotyping protocols', *Leukemia*, 26(9), pp. 1986–2010. Available at: https://doi.org/10.1038/leu.2012.122.

Kaspar, J.W., Niture, S.K. and Jaiswal, A.K. (2009) 'Nrf2:INrf2 (Keap1) signaling in oxidative stress', *Free Radical Biology and*

Medicine, 47(9), pp. 1304–1309. Available at: https://doi.org/10.1016/j.freeradbiomed.2009.07.035.

Keum, Y.-S. and Choi, B. (2014) 'Molecular and Chemical Regulation of the Keap1-Nrf2 Signaling Pathway', *Molecules*, 19(7), pp. 10074–10089. Available at: https://doi.org/10.3390/molecules190710074.

Lamoreaux, L., Roederer, M. and Koup, R. (2006) 'Intracellular cytokine optimization and standard operating procedure', *Nature Protocols*, 1(3), pp. 1507–1516. Available at: https://doi.org/10.1038/nprot.2006.268.

Milani, P. *et al.* (2013) 'SOD1 and DJ-1 Converge at Nrf2 Pathway: A Clue for Antioxidant Therapeutic Potential in Neurodegeneration', *Oxidative Medicine and Cellular Longevity*, 2013, pp. 1–12. Available at: https://doi.org/10.1155/2013/836760.

Perfetto, S.P. *et al.* (2006) 'Quality assurance for polychromatic flow cytometry', *Nature Protocols*, 1(3), pp. 1522–1530. Available at: https://doi.org/10.1038/nprot.2006.250.

Perfetto, S.P. *et al.* (2012) 'Quality assurance for polychromatic flow cytometry using a suite of calibration beads', *Nature Protocols*, 7(12), pp. 2067–2079. Available at: https://doi.org/10.1038/nprot.2012.126.

Roberto, A *et al.* (2015) 'B-cell reconstitution recapitulates B-cell lymphopoiesis following haploidentical BM transplantation and post-transplant CY', *Bone Marrow Transplantation*, 50(2), pp. 317–319. Available at: https://doi.org/10.1038/bmt.2014.266.

Roberto, Alessandra *et al.* (2015) 'Role of naive-derived T memory stem cells in T-cell reconstitution following allogeneic transplantation', *Blood*, 125(18), pp. 2855–2864. Available at: https://doi.org/10.1182/blood-2014-11-608406.

Roberto, A. *et al.* (2018) 'The early expansion of anergic NKG2A ^{pos} /CD56 ^{dim} /CD16 ^{neg} natural killer represents a therapeutic target in haploidentical hematopoietic stem cell transplantation',

Haematologica, 103(8), pp. 1390–1402. Available at: https://doi.org/10.3324/haematol.2017.186619.

Townsend, D.M., Tew, K.D. and Tapiero, H. (2003) 'The importance of glutathione in human disease', *Biomedicine & Pharmacotherapy*, 57(3–4), pp. 145–155. Available at: https://doi.org/10.1016/S0753-3322(03)00043-X.

Zelko, I.N., Mariani, T.J. and Folz, R.J. (2002) 'Superoxide dismutase multigene family: a comparison of the CuZn-SOD (SOD1), Mn-SOD (SOD2), and EC-SOD (SOD3) gene structures, evolution, and expression', *Free Radical Biology and Medicine*, 33(3), pp. 337–349. Available at: https://doi.org/10.1016/S0891-5849(02)00905-X.

3.15 Figure Legends

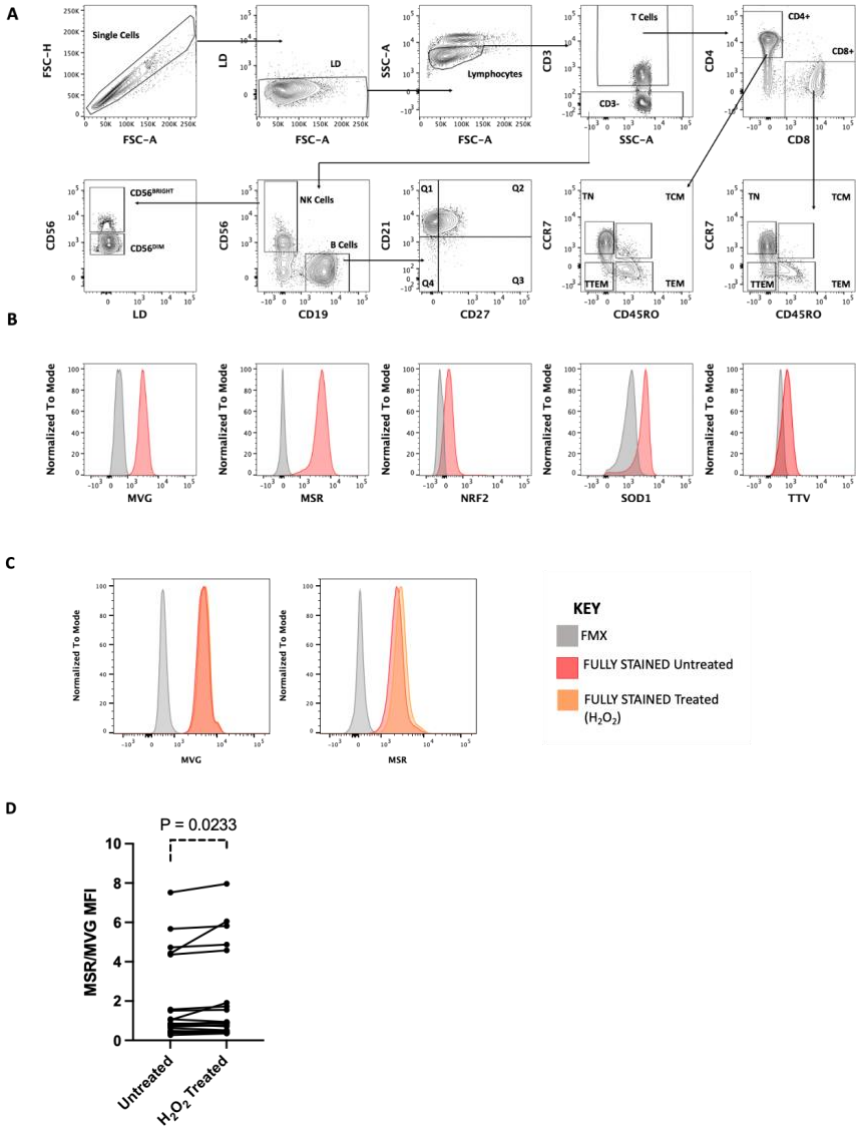

Figure 2.1: **Flow cytometry analysis of redox makers on human immune cell subsets. A)** Gating strategy to detect T, B and NK cell subsets. Singlets are defined by gating FSC-A against FSC-H. Live cells are identified by gating on viability dye (LD) negative cells . Morphological parameters FSC-A and SSC-A then define the Lymphocyte gate. T cells are identified as CD3+ cells. On the CD3+ cells, CD4 and CD8 markers allow to identify the major T cell populations (CD4+ helper T cells and CD8+ Cytotoxic T cells). In both

CD4+ and CD8+ compartment, T naïve-like (NL, CCR7+CD45RO-), T central memory (CM, CCR7+CD45RO+), T effector Memory (EM, CCR7- CD45RO+), T terminal effector memory (TE, CCR7-CD45RO-) are defined. On CD3- cells, B cell are defined as CD19+. On CD19+ cells, B Naïve are defined as CD21+,CD27- (Q1), and B cell Memory are defined as CD21+,CD27+ (Q2). On CD3- cells, total NK cells are defined as CD56+ cells. From the CD56+ population we can move further into defining $CD56^{BRIGHT}$and $CD56^{DIM}$. **B)** Redox markers represented by histograms. Compensated redox related markers on the total gate of lymphocytes with the red peaks defining the fully stained (MVG - MitoView™ Green, MSR - MitoSOX™ Red, NRF2 - nuclear factor erythroid 2–related factor 2, SOD1 - superoxide dismutase 1, TTV -ThiolTracker™ Violet) and the grey peak defines the FMX controls. **C)** Histograms representing the superoxide anion detection in FMX(grey peak), untreated (red peak) and H_2O_2 treated (orange peak) control of a single subject. **D)** Normalised MSR values of 20 healthy PBMC's showing a significant increase in H_2O_2 treated against untreated samples ($p = 0.0233$).

Chapter 4

Multiparametric Flow Cytometry-Based Immunophenotyping defines age and sex related changes

4.1 Introduction

The immune system of aged individuals is severely impaired when compared to the young (Goronzy and Weyand, 2013). Differences in immune function also contribute to health and life-span discrepancies between sexes, where the role of sex in the immune system is still not very well understood (Márquez et al., 2020). Therefore, a detailed investigation of the immune response on healthy human donors spanning different ages and sexes is required to unravel knowledge on the aged immune system.

In order to monitor the changes of the immune response with age, we utilise our own standardized multiparametric flow cytometry panels to assess T and B cells in order to address the adaptive immune response. In the following chapter we have employed a flow cytometry approach to analyse T and B lymphocytes from 54 healthy participants of different ages. We were able to combine the measurement of cell-surface markers with the assessment of mitochondrial fitness and of some key redox homeostasis players in the different immune subsets.

We show that, with age, healthy subjects have an overall weakened T cell compartment in both sexes and display several alterations, mostly involving CD8+ T cell subsets. We also define changes in markers of exhaustion (PD1 and TIGIT) and senescence (CD57). Meanwhile, we assess a rare subsets of memory T cell (CCR7+, CD45RO-, CD95+, TIGIT+, PD1+), that has been recently discovered amongst CD8+ TSCM memory cells and it is committed to a reduced functionality and a decreased proliferative capacity in response to activation. This subset is a progenitor exhausted-like T cell subset (Tpex). It has been hypothesised that persistent antigenic stimulation is preferentially associated with the development of Tpex cells, while it is thought that the Tpex subsets' exhausted phenotype obstructs T cell differentiation. (Galletti et al., 2020). Nevertheless, this subsets has still to be assessed in age related studies and we are the first to our knowledge to do so.

In B cell subsets, we evaluate transcription factors PAX5 and XBP1 and we report a decrease in the frequencies of XBP1 with age. XBP1 is a major component of the unfolded protein response (UPR) and is essential for maintaining protein homeostasis and reducing cellular stresses (McLaughlin *et al.*, 2018). Our analysis of age-associated redox markers revealed indeed a significant increase in mitochondrial superoxide which specify an impaired redox balance and mitochondrial fitness with age.

Overall, our standardized polychromatic flow cytometry assays can provide information about the changes of the main adaptive immune cells with age. By utilising the panels, a better understanding of age-related diseases and immunosenescence can be distinguished, thus offering a powerful target for interventions to improve the health of the elderly.

4.2 Materials and Methods

4.2.1 Sample information and cell preparation

Peripheral blood mononuclear cells (PBMC's) were obtained from Queen Mary University London, FlowMetric Inc USA or isolated from whole blood purchased from European vendors by density gradient centrifugation. Then, PBMC's were frozen and stored in liquid nitrogen. A total of fifty-four healthy participants were enrolled in the study where all were free from infectious diseases, malignant conditions and immunodeficiencies. We categorised our cohort in three different age groups with a span of an average of 20-23 years. The characteristics and composition of each group are displayed in Table 4.1. To minimize technical variability, samples were analysed in nine batches (6 subjects per batch). An internal control was used in each experiment to test the experimental variability and avoiding experiment related bias. Frozen cells were thawed in RPMI1640 (containing a stable form of L-glutamine), supplemented with 10% foetal bovine serum (FBS) and 1% penicillin streptomycin -(all from Life Technologies). Cells were divided in 3 subsamples: one used for T cell characterization (T

cell panel), one for B cell characterization (B cell panel), one for Redox investigation (Redox panel) and one for CMV positivity testing.

Table 4.1: Characteristics of healthy participants

Variable	Sex		
Age	**Male**	**Female**	**Total**
Young 18-35	6	15	21
Middle Aged 36-59	7	15	22
Old 60+	7	4	11
Total	20	34	**54**

4.2.2 Polychromatic flow cytometry

Cells were first stained for 15 min at room temperature (RT) with live/dead fixable dead cell stain kit (Invitrogen™) to eliminate dead cells, which may influence the analysis. LIVE/DEAD™ Fixable Aqua Dead Cell Stain Kit, a viability dye for 405 nm excitation was used in T and B cells panel. The ROS panel includes the Invitrogen™ LIVE/DEAD™ Fixable Blue Dead Cell Stain Kit, for UV excitation instead. After live/dead staining, cells were washed with PBS and then stained for the panel of interest.

Monoclonal antibodies were purchased from different providers (BD Biosciences, BioLegend, ThermoFisher Scientific and Abcam) and titrated on human PBMCs to identify the concentration proper for the assay (see Chapter 2 for details).

Table 4.2 lists all the antibodies used in each panel with their staining condition.

Table 4.2: List and staining information of all antibodies used for the T, B and ROS panel

Panel	Marker	Fluorochrome	Clone	Type of marker	Incubation time (mins)	Temperature	Dilution buffer
T cell	Live Dead	Aqua	–	Dye	15	RT	PBS
	CD3	APC-H7	SK7	Surface	20	RT	PBS
	CD4	BV711	L200	Surface	20	RT	PBS
	CD8	BV786	RPA-T8	Surface	20	RT	PBS
	CCR7	PE-CF594	2-L1-A	Surface	20	37°C	PBS
	CD45RO	PE-Cy7	UCHL1	Surface	20	RT	PBS
	CD27	Alexa Fluor® 700	M-T271	Surface	20	RT	PBS
	CD95	BV605	DX2	Surface	20	RT	PBS
	PD1	BV421	EH12.1	Surface	20	RT	PBS
	Granzyme B	FITC	GB11	Intracellular	30	RT	Perm buffer
	CD57	APC	NK-1	Surface	20	RT	PBS
	TIGIT	BV650	741182	Surface	20	RT	PBS
B cell	Live Dead	Aqua	–	Dye	15	RT	PBS
	CD19	BV786	SJ25C1	Surface	20	RT	PBS
	CD20	APC-H7	2H7	Surface	20	RT	PBS
	CD27	BV711	L128	Surface	20	RT	PBS
	CD10	BUV737	HI10a	Surface	20	RT	PBS
	CD21	BV650	B-ly4	Surface	20	RT	PBS
	CD38	Pe-Cy7	Clone HIT2	Surface	20	RT	PBS
	CD43	PerCPcy5.5	1G10	Surface	20	RT	PBS
	IgM	PE-CF594	G20-127	Surface	20	RT	PBS
	IgD	FITC	IA6-2	Surface	20	RT	PBS
	IgG	BV605	RUO	Surface	20	RT	PBS
	CD79A	APC	HM47	Intracellular	30	RT	Perm buffer
	PAX5	PE	1H9	Intracellular	30	RT	Perm buffer
	XBP-1	BV421	Q3-695	Intracellular	30	RT	Perm buffer
ROS Panel	Live Dead	Blue	–	Dye	15	RT	PBS
	Nrf2	Alexa Fluor® 647	A-10	Intracellular	30	RT	Perm buffer
	ThiolTracker™	BV510	–	Dye	15	37°C	PBS + 2% RPMI
	SOD1	DyLight405	JF1005	Intracellular	30	RT	Perm buffer
	MitoView™	FITC	–	Dye	15	RT	Perm buffer
	MitoSOX™	RED	–	Dye	15	37°C	PBS + 2% RPMI
	CD3	APC-H7	SK7	Surface	20	RT	PBS
	CD4	BV711	L200	Surface	20	RT	PBS
	CD8	BUV800	SK1	Surface	20	RT	PBS
	CCR7	PE-CF594	2-L1-A	Surface	20	37°C	PBS
	CD45RO	PE-Cy7	UCHL1	Surface	20	RT	PBS
	CD27	Alexa Fluor® 700	M-T271	Surface	20	RT	PBS
	CD19	BV786	SJ25C1	Surface	20	RT	PBS
	CD21	BV650	B-ly4	Surface	20	RT	PBS
	CD56	BUV395	NCAM16.2	Surface	20	RT	PBS
	CD16	BV605	3G8	Surface	20	RT	PBS

When required, cells were first stained for chemokine receptor expression (e.g CCR7 in the T and ROS cell panel) by incubating cells at 37°C for 20 minutes (Berhanu *et al.*, 2003). Staining for all the other surface protein was then performed at RT for 20 minutes. Intracellular markers (e.g GrB) were investigated after the surface staining upon fixation/permeabilization process performed with Cytofix/Cytoperm™ Fixation/Permeabilization Solution Kit (BD Biosciences Cat no.: 554714). Transcription factor (e.g. NRF2, XBP1, PAX5) were assessed after fixation/permeabilization process with eBioscience™ Foxp3/Transcription Factor Fixation/Permeabilization Concentrate and Diluent kit (Cat no.: 00-5523-00.

Redox panel was performed as reported in chapter 3. Fluorogenic MitoSOX™ Red, ThiolTracker™Violet and MitoView™Green (MVG) dyes were used to detect redox related systems.

After staining cells were acquired with a BD LSR Fortessa X-20 flow cytometer (BD, Biosciences, USA), fully equipped with blue, red, yellow/green, violet and ltraviolet (UV) lasers. Samples were acquired using BD FACSDiva™ Software (V 8.0.3).

4.2.3 Cell treatments

H_2O_2

To confirm that the Redox panel can detect redox-related changes a positive control was prepared treating 2 x 10^6 cells from each subject with a 50 µM final concentration of H_2O_2 (BioWhittaker Cat#17-942E) (Bertolotti *et al.*, 2013, 2016) . Cells were seeded at at 37ºC for 1 hour before staining.

Antigen-specific stimulation

To detect if subjects were positive for cytomegalovirus (CMV), PBMCs were stimulated in 96-well plate for 16 hours with PepTivator® CMV pp65 (Cat:130-093-435; 1 mg/mL per peptide). Staphylococcal enterotoxin B from Staphylococcus aureus (SEB; Cat: S488; 200 µg/mL) was used as a positive control. CMV pp65-specificity was determined measuring the frequency of cells positive for inflammatory cytokines IFN-γ, IL-2, and TNF-α.

4.2.4 Statistical analyses

Data analysis was performed using FlowJo software (V10.8.2): cells of interest were identified using gating strategy based on two-dimensional identification of cell types, and then frequencies and mean fluorescence intensity (MFI) of specific markers were calculated in each population of interest.

Data processing was performed by GraphPad Prism software (V.9.5.1). Simple linear regression models were applied to define age and sex related trends for T and B cell subsets where *P* values were considered significant when ≤0.05. Ordinary one way ANOVA multiple comparisons test were completed to compare different age groups.

4.3 Results

4.3.1 T Cells

We studied CD4+ and CD8+ T cells in fifty-four healthy participants using multiparametric flow cytometry. The analysis of the data involved a classic approach based on two-dimensional identification of a cell type, followed by an initial gate that was essential to define major populations of interest. Within the major populations of interest for T cells we continue gating by identifying markers of differentiation, senescence, exhaustion and cytotoxicity (Shive *et al.*, 2021). Frequencies from these gates were then used to plot linear regression models and scatter plots to define age and sex related changes amongst each subset and each functional marker of interest. Figure 4.1 shows the gating strategy that we used to identify the T cells subsets to compare young and old healthy subjects. A first gate was set on the singlets followed by the identification of viable cells by using a viability dye (LD). Then, we identify the lymphocytes based on the morphological parameters (FSC-A, SSC-A). CD3 positivity defines the T lymphocytes, among which we classify CD8+ and CD4+ T lymphocytes. Within CD4+ and CD8+ T lymphocytes we categorise T cell differentiation by gating against CCR7, CD45RO and CD95. Specifically, we can isolate Naive T cells (TN: CCR7+CD45-), stem cell memory T cells (TSCM: CCR7+,CD45RO-,CD95+) central memory T cells (TCM: CCR7+CD45+), effector memory T cells (TEM: CCR7-CD45+) and terminal effector memory T cells (TTEM: CCR7-CD45-),

(Roberto *et al.*, 2015). We then go on to analyse markers commonly related to T cell exhaustion (PD1, TIGIT) and senescence (CD57) (de Biasi *et al.*, 2020; Shive *et al.*, 2021) in specific populations of interest.

4.3.1.1 Age and sex impact the T cell reservoir

Figure 4.2 shows linear regression models of CD3+, CD8+ and CD4+ T cells frequencies. We identify a significant decline in the total frequency of CD3+ T cells with age in all subjects in our cohort (Figure 4.2A). These results are accompanied by a significant decline of CD8+ T cells with age (Figure 4.2B). On the contrary, CD4+ frequency increases significantly with age in all subjects, including males and females separately (Figure 4.2C). It is observed that males show no particular age-associated differences in the frequencies of either CD3+ or CD8+ cells, even though the age-dependent decrease of CD8+ T cells in males approaches the 0.05 coefficient *P* value (*P* = 0.0536, Figure 4.2D).

We then looked at each CD4+ and CD8+ subset separately and identified subsets as far as naïve (TN), central memory (TCM), effector memory (TEM) and terminal effector (TTEM). A sharp loss of naïve CD8+ cells was seen (Figure 4.3A), yet no significant age-associated alterations were identified for naïve CD4+ T cells (Figure 4.4A). CD8+ naïve T cells have a significant decline in females than in males (Figure 4.3A). This could suggest that males maintain the CD8+ TN reservoir better than females, however, it must be noted that the *P* value is close to the 0.05 coefficient value

(P = 0.078) and a negative slope value is also observed (-0.4228). Perhaps if our sample number increased for males we would reach the significance expected regarding the decreases CD8+ TN reservoir with age. In fact, recent transcriptomic and epigenomic studies have shown that T cell function deterioration is prominent in both sexes amongst the CD8+ TN cells (Moskowitz *et al.*, 2017; Ucar *et al.*, 2017; Márquez *et al.*, 2020).

The EM subsets increase significantly with age in the CD8 compartment (Figure 4.3C) , but not in the CD4 compartment (Figure 4.4C). Amongst the CD4+ subset only CM cells significantly increase with age (P = 0.0267 in CD4+ cells) (Figure 4.4B). These observations may suggest that there is a drastic and significant loss of CD8+ cells, thus resulting in the accumulation of TEM and end stage differentiated TTEM cells in the elderly for the CD8+ T cell compartment. The fact that CD4+ T cells show less significant changes than CD8+ T cells could suggest that the preservation of CD4+ T cell immune compartment acts as a survival mechanism for the elderly. To support our hypothesis, there are epigenetic studies that have determined that CD4+ T cells have a higher resilience of CD4+ T cells in comparison to CD8+ T cells with age (Hu *et al.*, 2020). Moreover, it has been demonstrated that homeostatic control mechanisms are very effective at maintaining a large and diverse subset of naïve CD4+ T-cells throughout lifetime, however these mechanisms eventually fail at a more advanced age compared to CD8+ T cells (Moro-García, 2013; Zhang, Weyand and Goronzy, 2021).

4.3.1.2 Senescence and exhaustion increase in T cells with age

The frequency of each T cell subset defines only a partial picture how the T cell immune compartment changes with age. Therefore, we categorised our cohort in three age groups (Young, 18-35, Middle 36-59, Old 60+) and analysed markers of senescence and exhaustion. Programmed cell death protein 1 (PD-1) is one of the most well-characterized exhaustion markers. We saw that PD1 significantly and progressively increases from young to old only among the CD8+ subsets and not amongst CD4+ T cells (Figure 4.5 A,B). Additionally, TIGIT, whose high expression on T cells is also associated with functional exhaustion, also profoundly increases from young to old, yet significantly only amongst the total CD8+ immune compartment. CD57 positive CD8+, but not CD4+, T cells from middle and old subjects increase significantly as well in comparison to young samples (Figure 4.5 A-B). This suggests that CD8+ T cells not only change in frequency but are also affected functionally during ageing. However, it can be argued that the age-dependent increase of PD1, TIGIT and CD57 is due to the fact that CD8+ TEM and TTEM subsets increase, as these are known as the subsets in which the expression of the above-mentioned markers is at its maximum (Dolfi *et al.*, 2013; Hutten *et al.*, 2018) . On the contrary, even though the frequency of CD4+ TCM increases with age, markers like PD1, TIGIT and CD57 do not increase amongst the CD4+ T cells.

To acquire a clearer picture, we dive deep into identifying how these markers change in each memory subset. Linear regression

models shown in figures 4.6 demonstrate that the increase of PD1 in the total CD8+ T cells (shown in figure 4.5A) is mainly driven by a significant increase in PD1 amongst CD8+ TCM and TTEM cell subsets (Figure 4.6A, 4.6D). On the other hand, CD8+ TEM remain somewhat functionally intact in the elderly, as their age-dependent increase is not associated to any significant change in the expression of the exhaustion marker PD1 (Figure 4.6A, 4.6D). Similarly, even though TIGIT increases significantly from young to old (shown in figure 4.6B), the significance is mainly driven by CD8+ TTEM cell subsets, although CD8+ TCM and TEM show an upward trend as well, with P values close to 0.05 ($P = 0.071$ and $P = 0.078$ respectively). CD57 also significantly increases mostly in CD8+ TTEM highlighting that these cells, which exert potent effector function after activation, are less functional in the elderly than the young (Figure 4.6C). Interestingly, even though we see no significant changes in the frequency of exhaustion and senescent markers amongst the total CD4+ T cell subsets, when looking closely to the CD4+ memory subsets we identify a significant increase of PD1 and TIGIT in TEM subsets, while PD1 also increases in TTEM subsets (Figure 4.7). These observations suggest that CD4+ T cells still lose some functional abilities with age yet not as significantly as CD8+ T cells. We therefore see that both compartments of the T cell immune response undergo senescence or exhaustion and many suggest that these observations are due to lifetime exposures to persistent pathogens and to constant homeostatic proliferation (Derhovanessian, Larbi and Pawelec, 2009; Saeidi *et al.*, 2018; Breznik *et al.*, 2022). Overall,

CD4+ T cells seem to remain more resistant to age-related phenotypic and functional changes than CD8+ T-cells, again enhancing our hypothesis that the CD4+ T cell immune compartment may be the elderlies' survival mechanism to fight infectious diseases, and that the CD8+ T cell compartment should be the focus for future research aiming at age related immune recovery (Moro-García, 2013; Moskowitz *et al.*, 2017; Ucar *et al.*, 2017; Hu *et al.*, 2020).

4.3.1.3 Age-related increase of rare CD8+ T cell subset

A newly defined T cell stem-like CD8+ memory T cell progenitor was recently discovered. This subset originally comes from antigen-specific progenitors with stem-like properties which are mainly responsible for the production of T cell memory subsets. The production of the memory subsets organised through developmental hierarchy is controlled by stem-cell memory T (TSCM), which undergo self-renewal to generate TCM and TEM subsets. TSCM are characterised as CCR7+, CD45RO- and CD95+ (Figure 4.1) (Roberto *et al.*, 2015). Within the CD8+ TSCM memory subset investigations were centred in order to help researchers understand why T cell differentiation is corrupted under conditions of persistent antigenic stimulation, chronic viral infections and progressive malignancies. Through these investigations, two stem-like CD8+ memory T cell subsets were discovered. One subset lacked PD1 and TIGIT, thus was committed to a functional lineage. The other one, expressing PD-1

and TIGIT, was instead committed to a dysfunctional, exhausted-like lineage (Tpex) (Galletti *et al.*, 2020). Our data shows that the frequency of Tpex cells increases with age in both males and females (Figure 4.8B), yet we see no significant changes in the CD8+ TSCM subset with age (Figure 4.8A) demonstrating that CD8+ T cell differentiation and self-renewal is an effect of Tpex accumulation and not due to a decrease of TSCM frequency as previously assumed.

4.3.1.4 Ageing T cells experience an increased mitochondrial oxidative phenotype

ROS mark as targets in measuring cellular functionality in the immune system and their accumulation has been found to correlated with disease progression, inflammatory diseases and ageing. For this reason, we applied here our novel polychromatic flow cytometry panel that measures redox-related markers (Chapter 3) on our cohort, to detect fine changes that could be occurring with age in different subpopulations of CD4+ and CD8+ T cell subsets. Figure 4.9 shows the gating strategy used to detect CD4+, CD8+ T cell and the subpopulations (upper panel). Within CD4+ and CD8+ T lymphocytes we follow T cell differentiation by gating against CCR7, CD45RO to define as previously TN, CM, EM and TEM. Within these subsets we were able to analyse markers related to the cellular redox status like MVG, MSR, TTV, NRF2 and SOD1 (Figure 4.9 – lower panel). To identify the true mitochondrial superoxide production of each cell we create a ratio

between the MFI of MSR, which measures mitochondrial superoxides, and MFI of MVG, which detects mitochondrial mass overall, independently of the status of the organelles themselves or of the cells. This is because MitoViewGreen appears to localize to mitochondria regardless of mitochondrial membrane potential and it can be used to normalize the MitoSOX median fluorescence intensity (that instead detects mainly mitochondrial ROS, specifically anion superoxide). In this way, whatever shift appears in the MitoSOX peak would be normalized for the mitochondrial mass, meaning that the residual relative differences among samples (comparing the ratios) would be really only ROS-dependent (and not due to a shift of the mitochondrial mass). In addition, to confirm that we are detecting true levels of superoxide we treated each subject with an optimal concentration of H_2O_2 to generate a redox-positive control for each subject (Chapter 3).

Our results show that the total CD8+ compartment, and all the T cell subsets (T naïve, TCM, TEM, TTEM) analysed individually demonstrate a significant increase in the normalised mitochondrial superoxide (Figure 4.10 A). Due to the previous result on senescence and exhaustion, such results were hypothesised to be highly prevalent for CD8+ T cells and not so prevalent for CD4+ T cells. However, we see similar results in CD4+ naïve and memory subsets (Figure 4.10 B). This indicates that even though the CD4+ T cell compartment appears to be less impaired with the aging compared to the CD8 compartment, the increased mitochondrial ROS production could still mark as a typical senescence feature. In

fact mitochondria of senescent cells demonstrate a decreased mitochondrial membrane potential, increased proton leak and increased generation of ROS (Callender *et al.*, 2020; Miwa *et al.*, 2022). These results are also confirmed when we compare normalised MSR with the three age groups of our cohort (Figure 4.11).

More precisely, it turned out that young and middle aged individuals in our cohort are more similar, from a mitochondrial fitness perspective, in comparison to old subjects. Ageing immune cells are able to keep mitochondrial ROS levels under control until late time in life. However, this is not true for CD4+ TCM cells, which show a faster mitochondrial deterioration, which appears in the middle ages of life and does not progress much further during old age. In fact, amongst the CD4+ TCM subset there are no significant changes in the expression of normalised MSR from middle to old aged subjects.

To counteract the accumulation of oxygen metabolites, which can damage essential cellular components, several antioxidant systems are used by the cells. Among the others, we selected SOD1, Nrf2 and glutathione. SOD1 is a mitochondrial superoxide dismutase responsible for destroying free superoxide radicals in the cell. In figure 4.12 we show that, in both CD4+ and CD8+ subsets, SOD1 expression has no significant changes with age. However, we see a negative slope, showing that there is a trend for SOD1 to decrease with age. The fact that a crucial antioxidant like SOD1 doesn’t

change in parallel to the accumulation of mitochondrial superoxide marks as an important functional problem for the T cells, suggesting a loss of oxidative balance with age. It is interesting to note that CD4+ TEM has the closest *P* value to 0.05 (P = 0.064) demonstrating a possible loss of SOD1, where CD4+ TEM was the only subset that acquired a significant increase in both PD1 and TIGIT with age (Figure 4.7). SOD1 is tightly connected with NF-E2-related factor-2 (Nrf2), a prototype transcription factor whose nuclear transport is redox regulated and master regulator of the expression of many antioxidants.

Nrf2 is normally bound to Keap1 in the cytosol. Following H_2O_2-dependent oxidation, Keap1 releases Nrf2 that can reach the nucleus and bind to antioxidant response elements in the promoter of target genes, inducing their expression.

In figure 4.13 we display similar regression models where no significant changes in the expression of NRF2 are detected with age in T cells. Interestingly, despite the lack of significance, the slope is negative for all the CD4+ T cells subsets, but not for CD8+ (Figure 4.13). Thus, as expected, Nrf2 shows parallel trends to SOD1, supporting an age-dependent functional impairment in counteracting oxidative stress in T cells. This results from the increase in mitochondrial superoxide, not sustained by a corresponding increase of some of the main antioxidant defence systems. Further investigation would be important to assess Nrf2

cytoplasmic-nuclear translocation, which provides a better understanding of this transcription factor functionality.

In order to further characterize the age-related redox reshaping of the adaptive immune cells,we then assessed reduced glutathione (TTV – Figure 4.14), a potent antioxidant and a convenient cofactor for enzymatic reactions. We define no significant changes with age other than the exception of CD8+ TCM (P = 0.0307) and TEM, which is close to the significant P value of 0.05 (P = 0.0552), also subsets that demonstrated an increase in markers of senescence and exhaustion (Figure 4.6). Reduced glutathione (GSH) is important to buffer excessive damage from ROS and to fuel the metabolic demand required after activation ((Mak *et al.*, 2017). In fact, non-aged early differentiated human CD8+T cells were shown to display substantial antioxidant capacity compared with more differentiated central and effector memory T cells (Pilipow *et al.*, 2018). However, as previously mentioned, ROS also regulate signaling pathways in multiple cell types. We could thus speculate that the increased GSH levels in CD8+ TCM and TEM in old individuals could imply lower activation capacity and partial or impaired effector functionality.

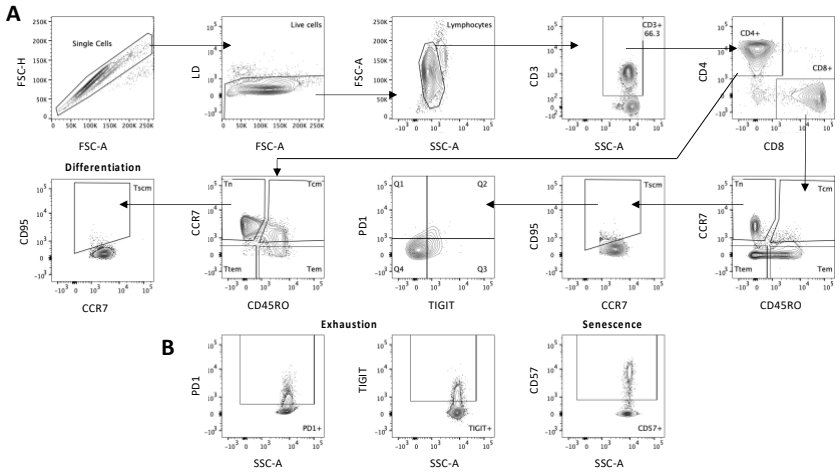

Figure 4.1: **Gating strategy used to analyse markers associated to differentiation, exhaustion, senescence and cytotoxicity in CD3+T cells. A)** First gate was set on the singlets followed by the identification of LD^- cells. Then, lymphocytes are identified using morphological parameters (FSC-A, SSC-A). CD3 positivity defines the T lymphocytes, among which we classify CD8+ and CD4+ T lymphocytes. Within CD4+ and CD8+ T lymphocytes, Naïve T (Tn) cells are defined as CCR7+, CD45RO-; central memory (Tcm) cells are CCR7+, CD45RO+; effector memory (Tem) cells are CCR7-, CD45RO+ and terminal effector (Ttem) are CCR7-, CD45RO-. Stem cell memory cells (Tscm) are gated against CD95 within the Tn subsets. **B)** Representative example of PD1, TIGIT and CD57 expression gated on the total lymphocytes.

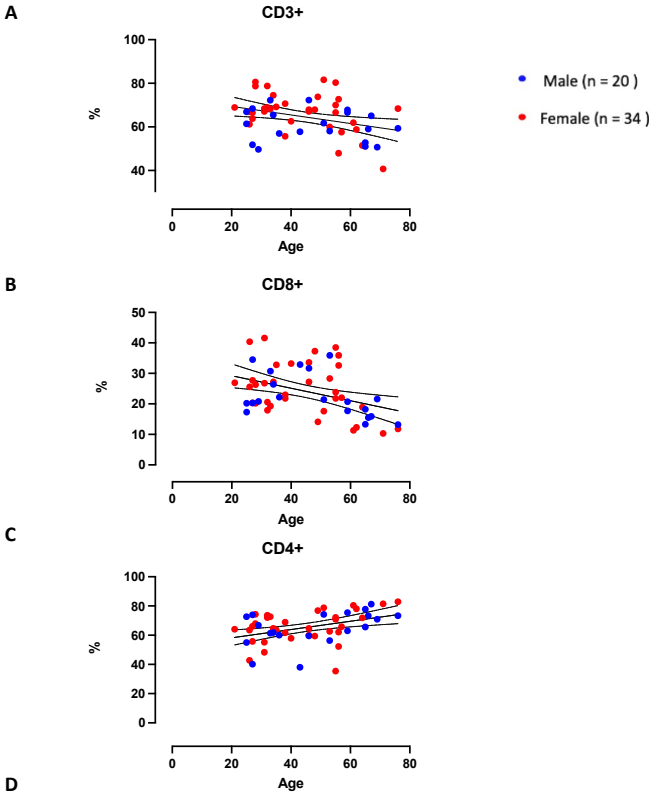

D

	ALL			Females			Males		
Population	R^2	P Value	Slope	R^2	P Value	Slope	R^2	P Value	Slope
CD3 +	0.1198	0.0103	-0.1966	0.1587	0.0196	-0.2485	0.0432	0.3790	-0.0861
CD8 +	0.1576	0.0030	-0.2044	0.1576	0.0196	-0.2128	0.1916	0.0536	-0.1793
CD4 +	0.1615	0.0026	0.2834	0.1323	0.0026	0.2697	0.2212	0.0364	0.3151

Figure 4.2: **Major T cell subsets with age and sex. A)** Scatter plot T cell (CD3+) frequency out of total lymphocytes of 54 participants in relation with participants' age, CD8+ **(B)** T cells frequency in relation with participants' age and CD4+ **(C)** T cells frequency in relation with participants' age. In A, B and C each dot represents one subject: red dots for female and blue dots for male. Linear regression models of the total are represented on each graph. **D)** Summary of the statistical values (R^2 , P Value and slope) of the linear regression analysis performed on data shown in A, B and C, for each population in all participants (ALL), and in female and male participants separately. P value lower than 0.05 are highlighted in grey and lighter grey if close. Coefficient interval bands – dotted lines (CI 95%) are also present to show where the true regression line lies at a certain level of confidence.

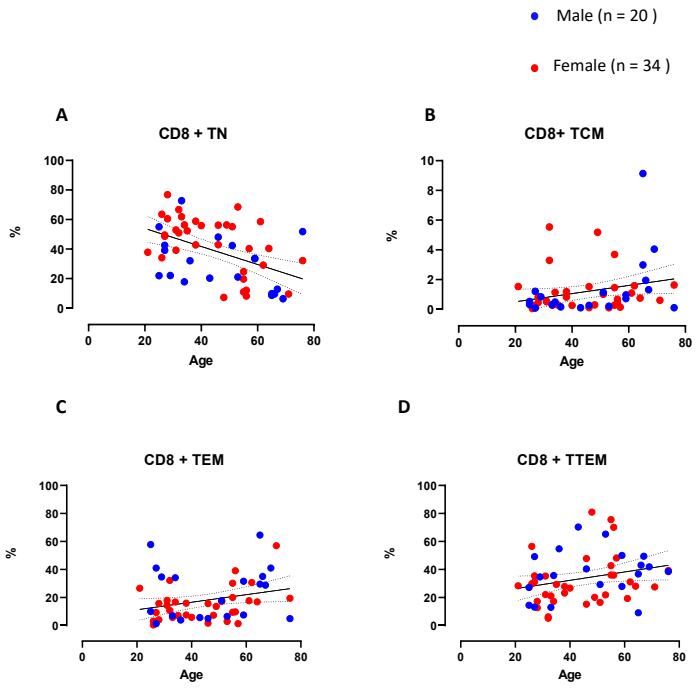

E

	ALL			Females			Males		
Population	R^2	P Value	Slope	R^2	P Value	Slope	R^2	P Value	Slope
CD8+ TN	0.2334	0.0002	-0.6097	0.2724	0.0015	-0.6810	0.1616	0.0789	-0.4228
CD8+ TCM	0.0671	0.0586	0.0275	0.0031	0.7549	0.0052	0.1985	0.0490	0.0543
CD8+ TEM	0.0737	0.0470	0.2695	0.1686	0.0158	0.3427	0.0104	0.6692	0.1125
CD8+ TTEM	0.0700	0.0531	0.2984	0.0757	0.1152	0.3375	0.0103	0.6691	0.2124

Figure 4.3: **The frequencies of the CD8+ T cell subsets with age and sex. A)** Scatter plots of CD8+ Naïve T (CCR7+CD45RO-), **B)** CD8 + TCM (CCR7+, CD45RO+), **C)** CD8+ TEM (CCR7- , CD45RO+) and **D)** CD8+ TTEM (CCR7- , CD45RO-) are shown. In A, B, C and D each dot represents one subject: red dots for female and blue dots for male. Linear regression models of the total are represented on each graph. **E)** Summary of the statistical values (R^2 , P Value and slope) of the linear regression analysis performed on data shown in A, B, C and D, for each population in all participants (ALL), and in female and male participants separately. P value lower than 0.05 are highlighted in grey and lighter grey if close. Coefficient interval bands – dotted lines (CI 95%) are also present.

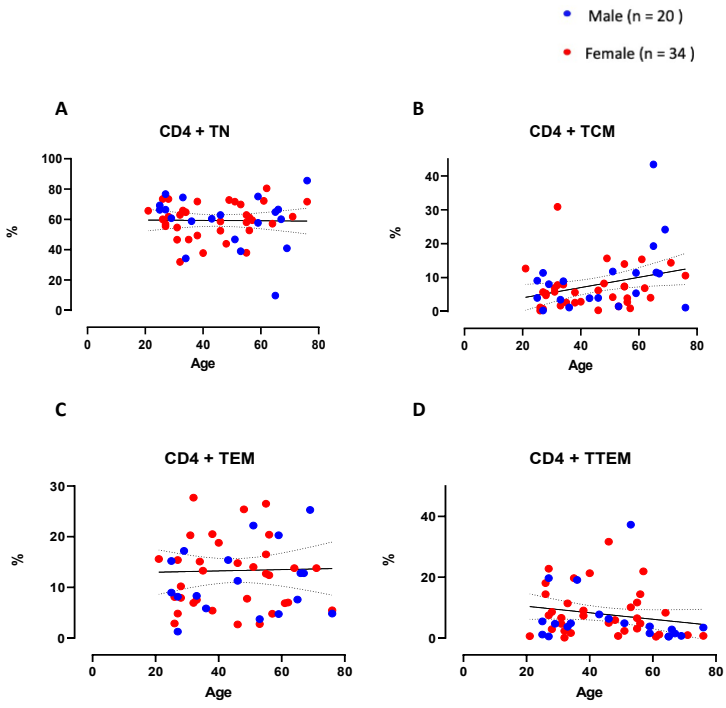

E

	ALL			Female			Male		
Population	R^2	P Value	Slope	R^2	P Value	Slope	R^2	P Value	Slope
CD4+ TN	0.0002	0.9198	-0.0125	0.0277	0.3462	0.1315	0.0339	0.4367	-0.1858
CD4+ TCM	0.0909	0.0267	0.1517	0.02058	0.4180	0.0601	0.1765	0.0651	0.2444
CD4+ TEM	0.0005	0.8668	0.0128	0.0074	0.6287	-0.0443	0.0158	0.5972	0.0744
CD4+ TTEM	0.0402	0.1462	-0.1068	0.0344	0.2937	-0.1004	0.0372	0.4150	-0.1010

Figure 4.4: **The frequencies of the CD4+ T cell subsets with age and sex. A)** Scatter plots of CD4+ Naïve T (CCR7+CD45RO-), **B)** CD4 + TCM (CCR7+, CD45RO+), **C)** CD4+ TEM (CCR7- , CD45RO+) and **D)** CD4+ TTEM (CCR7- , CD45RO-) are shown. In A, B, C and D each dot represents one subject: red dots for female and blue dots for male. Linear regression models of the total are represented on each graph. **E)** Summary of the statistical values (R^2 , P Value and slope) of the linear regression analysis performed on data shown in A, B, C and D, for each population in all participants (ALL), and in female and male participants separately. P value lower than 0.05 are highlighted in grey and lighter grey if close. Coefficient interval bands – dotted lines (CI 95%) are also present.

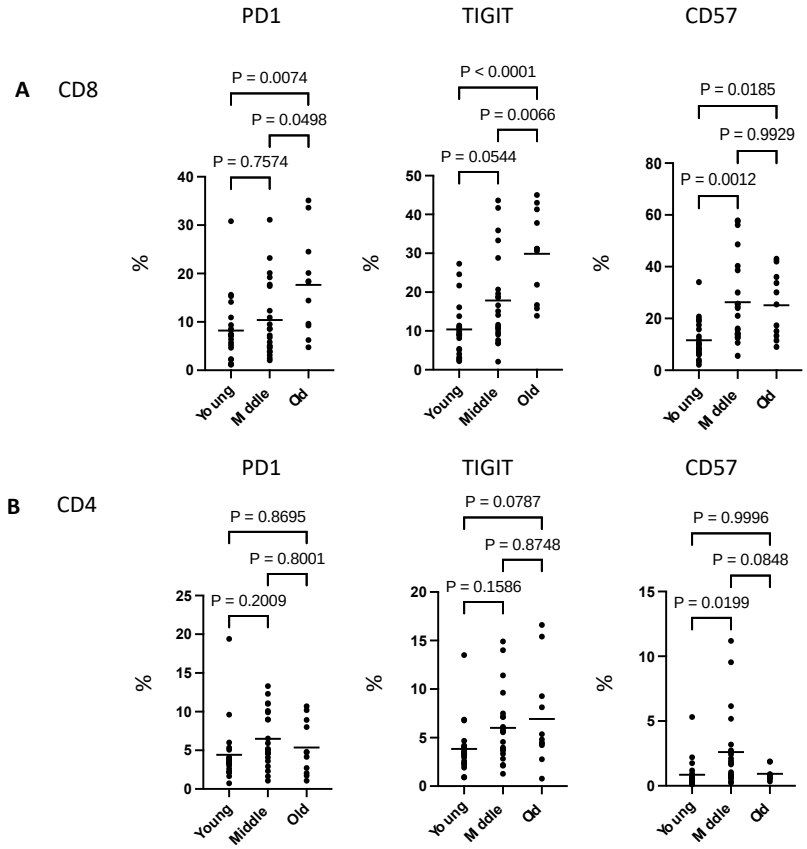

Figure 4.5: **The frequencies of exhaustion and senescence markers for young (18-35), middle (36-59) and old (60+) participants in CD8+ and CD4+ T cells.** Aligned scatter graphs showing how PD1, TIGIT and CD57 frequencies change amongst three age groups in CD8+ T cells **(A)** and CD4+ T cells **(B)**. All data represents individual values and error bars represent the mean (central bar). Statistical analysis was done by Ordinary one-way ANOVA multiple comparisons, comparing young vs old, young vs middle aged, old vs middle aged. P values are shown.

A

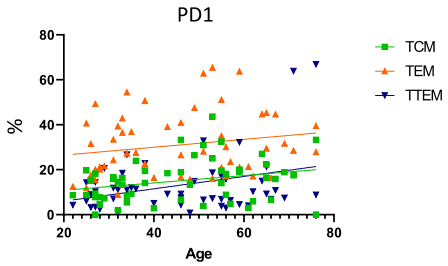

B

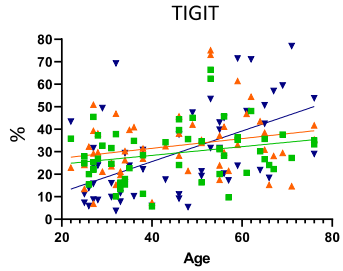

C

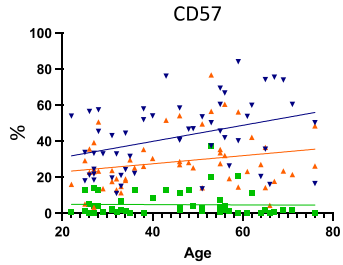

D

	PD1			TIGIT			CD57		
Population	R^2	P Value	Slope	R^2	P Value	Slope	R^2	P Value	Slope
TCM	0.0733	0.0476	0.1637	0.0617	0.0701	0.1939	0.0004	0.8891	-0.0087
TEM	0.0373	0.1615	0.1756	0.0584	0.0783	0.2171	0.0527	0.0949	0.2247
TTEM	0.1135	0.0127	0.2753	0.2871	<0.0001	0.6796	0.1326	0.0068	0.4457

Figure 4.6: **Senescence and exhaustion in CD8+ T cell memory subsets.** Scatter plot of participants' age versus frequencies of $PD1^+$**(A)**, $TIGIT^+$ **(B)** and $CD57^+$ **(C)** $CD8^+$ cells grouped per memory subsets (TCM in green, TEM in orange, TTEM in blue). **D)** R^2 , P Value and slope statistical values of the linear regression analysis for each graph in figure A, B and C. P values lower than 0.05 (significant results) are highlighted in grey.

A

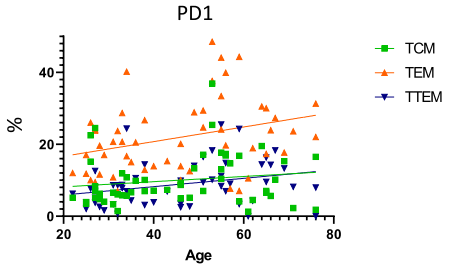

B

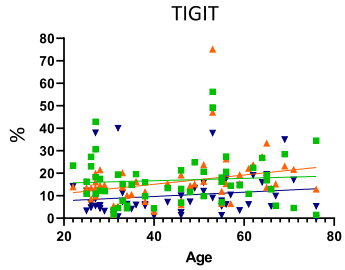

C

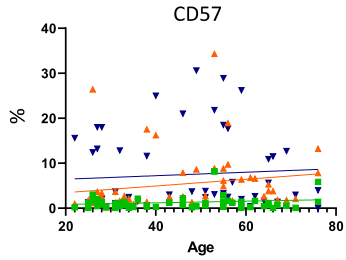

D

	PD1			TIGIT			CD57		
Population	R^2	P Value	Slope	R^2	P Value	Slope	R^2	P Value	Slope
TCM	0.0255	0.2481	0.0721	0.0053	0.5982	0.0525	0.0288	0.2197	0.0183
TEM	0.0988	0.0206	0.2037	0.0811	0.0369	0.2066	0.0311	0.2017	0.6093
TTEM	0.0878	0.0296	0.1161	0.0252	0.2515	0.0954	0.0051	0.0745	0.0388

Figure 4.7: **Senescence and exhaustion in CD4+ T cell memory subsets.** Scatter plot of participants' age versus frequencies of $PD1^+$**(A)**, $TIGIT^+$ **(B)** and $CD57^+$ **(C)** $CD4^+$ cells grouped per memory subsets (TCM in green, TEM in orange, TTEM in blue) **D)** R^2 , P Value and slope statistical values of the linear regression analysis for each graph in figure A, B and C. P values lower than 0.05 (significant results) are highlighted in grey.

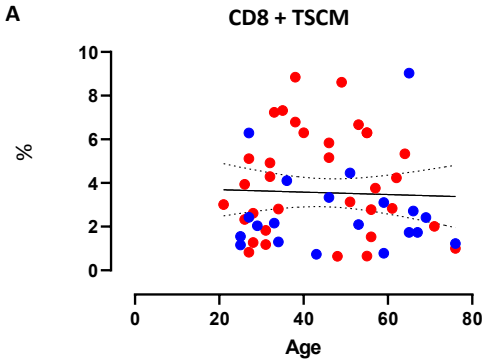

	ALL			Female			Male		
Population	R^2	P Value	Slope	R^2	P Value	Slope	R^2	P Value	Slope
CD8 + TSCM	0.0013	0.7885	-0.0056	0.0013	0.8385	-0.0059	0.0029	0.8187	0.0063

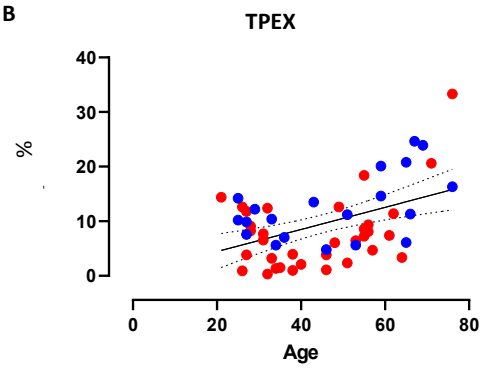

	ALL			Female			Male		
Population	R^2	P Value	Slope	R^2	P Value	Slope	R^2	P Value	Slope
Tpex	0.2137	0.0004	0.2029	0.1698	0.0154	0.1910	0.2731	0.0181	0.1833

Figure 4.8: **The frequencies of the CD8+ TSCM and TPEX T cell subsets with age and sex. A)** CD8+ TSCM (CCR7+,CD45RO-,CD95+) on the total of CD8+ T cells with age and sex amongst 54 healthy donors. **B)** From the same donors, the frequency of TPEX subset (CCR7+,CD45RO-, CD95+, TIGIT+, PD1+). R^2 , P Values and slope statistical values of the linear regression analysis model are presented in the table associated with the figure for each subset and for ALL, female and male participants. Coefficient interval bands – dotted lines (CI 95%) are also present to show where the true regression line lies at a certain level of confidence.

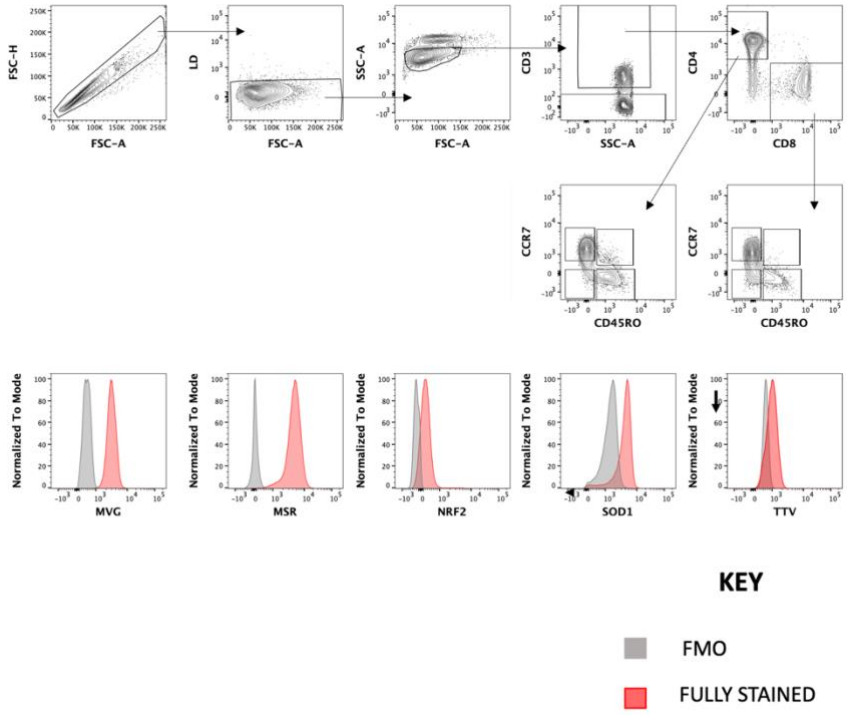

Figure 4.9: **Redox markers defined in T cells.** Gating strategy used to analyse markers related to reactive oxygen species (ROS) and to antioxidants. Identification of lymphocytes followed by the distinction of CD3+ and CD3- cells. On the CD3+ gate, plot against CD4 and CD8 defining the major T cell populations. In both CD4+ and CD8+, T naïve (TN CCR7+, CD45RO-), T central memory (CM CCR7+, CD45RO+), T effector Memory (EM CCR7-, CD45RO+), T terminal effector memory (TE CCR7-, CD45RO-) are defined. On the total lymphocyte gate histograms are displayed to define the fully stained (MVG - MitoView™ Green, MSR - MitoSOX™ Red, NRF2 (nuclear factor erythroid 2–related factor 2), SOD1 (superoxide dismutase 1), TTV (ThiolTracker™ Violet) - red peaks, and their Fluorescence Minus One (FMO) controls with the grey peaks.

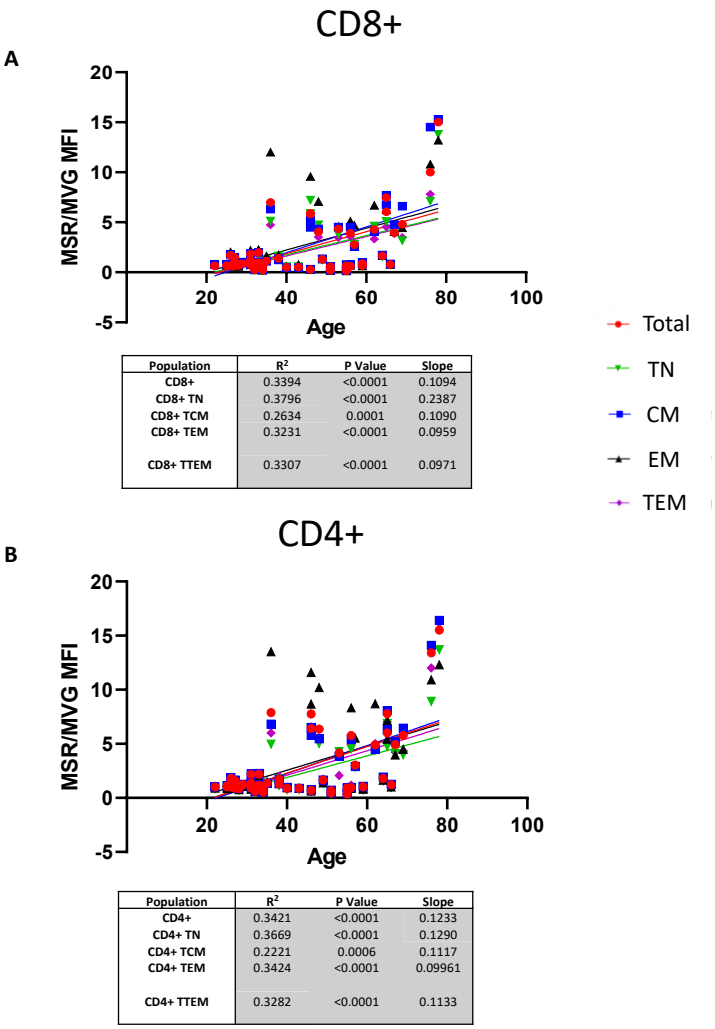

Population	R^2	P Value	Slope
CD8+	0.3394	<0.0001	0.1094
CD8+ TN	0.3796	<0.0001	0.2387
CD8+ TCM	0.2634	0.0001	0.1090
CD8+ TEM	0.3231	<0.0001	0.0959
CD8+ TTEM	0.3307	<0.0001	0.0971

Population	R^2	P Value	Slope
CD4+	0.3421	<0.0001	0.1233
CD4+ TN	0.3669	<0.0001	0.1290
CD4+ TCM	0.2221	0.0006	0.1117
CD4+ TEM	0.3424	<0.0001	0.09961
CD4+ TTEM	0.3282	<0.0001	0.1133

Figure 4.10: **Normalised MSR in CD8+ and CD4+ T cell subsets.** Linear regression models of normalised MFI vales of MSR is displayed for CD8+ **(A)** and CD4+ **(B)** subsets (Total -red, TN -green, CM-blue, EM-black and TEM-purple) against age. For all subsets there is a significant increase of the expression of normalised MSR with age. R^2, P Values and slope statistical values of the linear regression models are presented in the table associated with the figure for each graph. P values lower than 0.05 (significant level) are highlighted in grey.

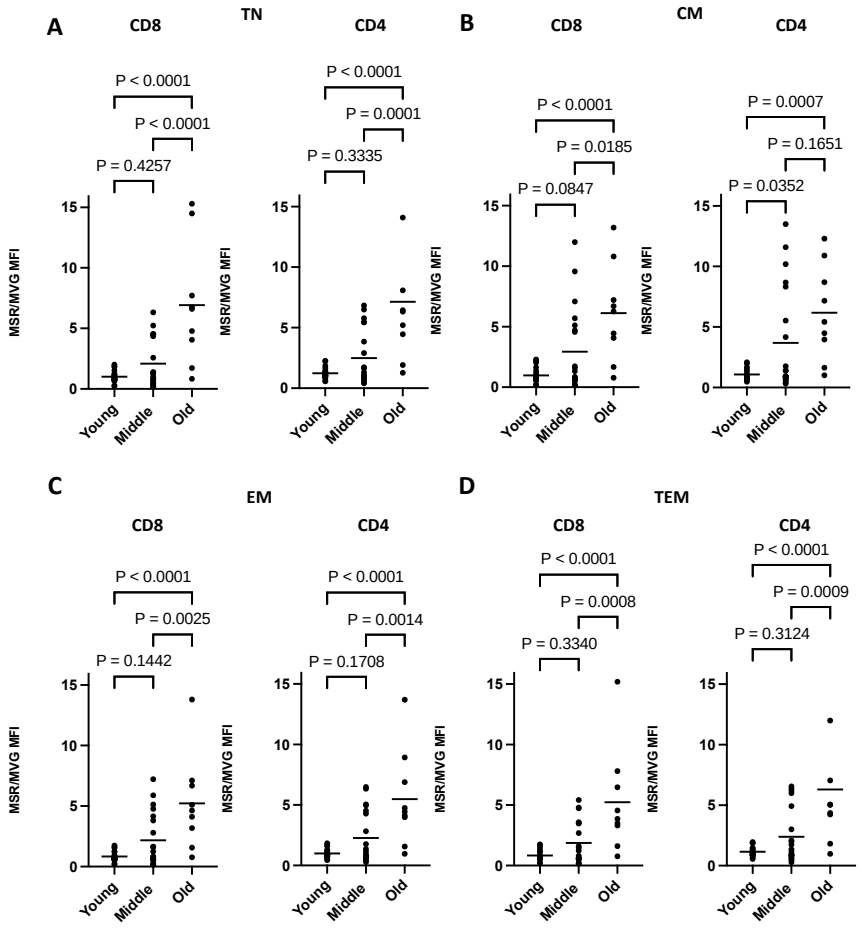

Figure 4.11: **The changes of normalised MSR in CD8+ and CD4+ T cell subsets displayed in age groups from young (18-35), middle (36-59) to old (60+) participants.** Aligned scatter plots of MFI targets of normalised MSR of different CD8+ and CD4+ T cell subsets TN **(A)**, CM **(B)**, EM **(C)**, TEM **(D)**. All data represents individual values and error bars represent the mean (central bar). Statistical analysis was done by Ordinary one-way ANOVA multiple comparisons test. P values are comparisons of young vs middle aged, young vs old aged and old aged vs middle. P values lower than 0.05 define a significant result.

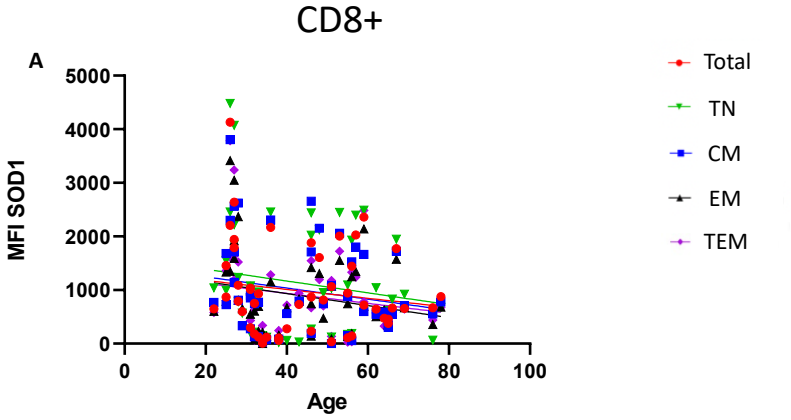

Population	R^2	P Value	Slope
CD8+	0.0231	0.2920	-8.287
CD8+ TN	0.0269	0.2552	-11.01
CD8+ TCM	0.0337	0.2018	-10.39
CD8+ TEM	0.0549	0.1015	-11.20
CD8+ TTEM	0.0345	0.1986	-9.253

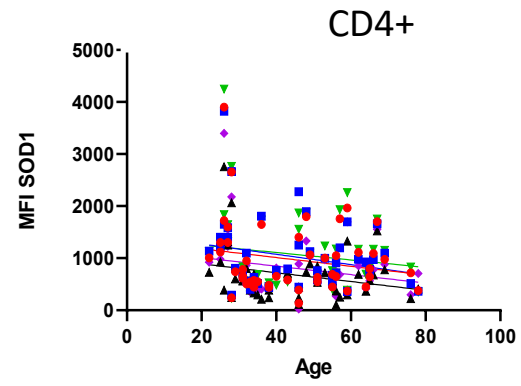

Population	R^2	P Value	Slope
CD4+	0.03711	0.1042	-8.414
CD4+ TN	0.0230	0.2926	-7.154
CD4+ TCM	0.0540	0.1042	-9.915
CD4+ TEM	0.0698	0.0637	-8.453
CD4+ TTEM	0.0505	0.1163	-8.145

Figure 4.12: **Antioxidant SOD1 in CD8+ and CD4+ T cell subsets.** Linear regression models MFI values of SOD1 displayed for CD8+ **(A)** and CD4+ **(B)** subsets (Total, TN, CM, EM and TEM) against age. Tabular results of simple linear regression analysis for each graph are shown. Tabular results of simple linear regression analysis (R^2 , P value and Slope) is shown for each graph. P values close to the 0.05 P value significant level are highlighted in light grey.

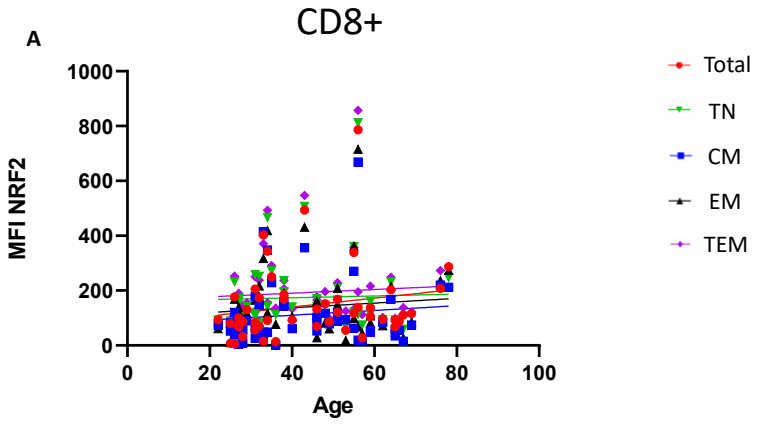

Population	R^2	P Value	Slope
CD8+	0.0342	0.1982	1.625
CD8+ TN	0.0014	0.7937	0.3373
CD8+ TCM	0.0121	0.4466	0.8676
CD8+ TEM	0.01067	0.4754	0.8580
CD8+ TTEM	0.0057	0.6031	0.6698

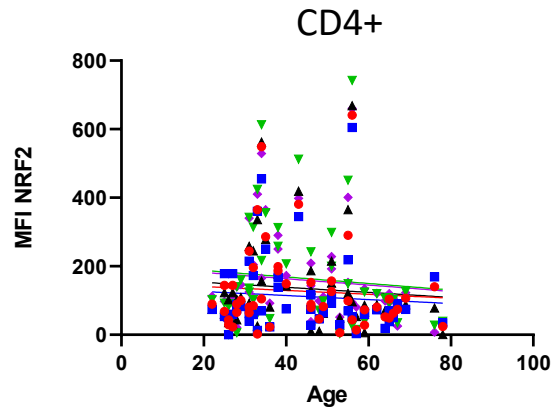

Population	R^2	P Value	Slope
CD4+	0.0045	0.6434	-0.5629
CD4+ TN	0.0082	0.5295	-0.95923
CD4+ TCM	0.0060	0.5922	-0.5869
CD4+ TEM	0.0071	0.5612	-0.7346
CD4+ TTEM	0.0112	0.4661	-0.9210

Figure 4.13: **Transcription factor NRF2 in CD8+ and CD4+ T cell subsets.** Linear regression models of MFI values of NRF2 displayed for CD8+ **(A)** and CD4+ **(B)** subsets (Total, TN, CM, EM and TEM) against age. Tabular results of simple linear regression analysis (R^2 , P value and Slope) is shown for each graph.

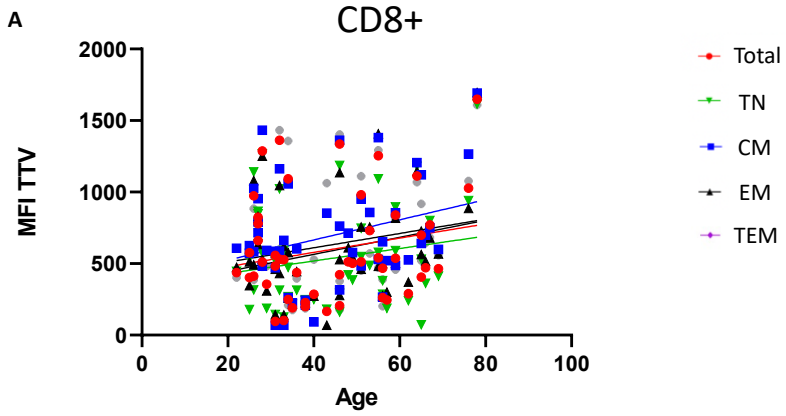

Population	R^2	P Value	Slope
CD8+	0.0446	0.1420	4.988
CD8+ TN	0.0411	0.1582	5.001
CD8+ TCM	0.0877	0.0367	7.033
CD8+ TEM	0.0744	0.0552	5.976
CD8+ TTEM	0.0360	0.1869	4.349

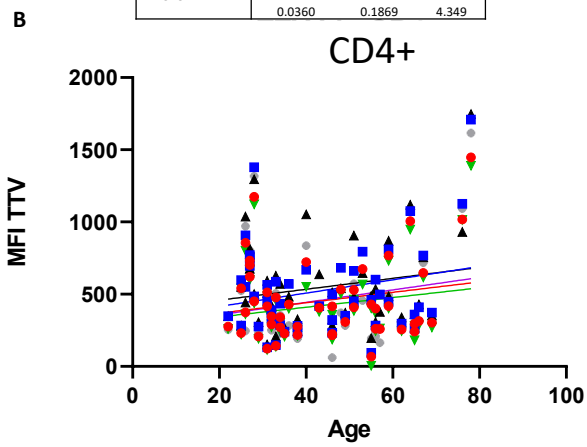

Population	R^2	P Value	Slope
CD4+	0.0397	0.1652	3.605
CD4+ TN	0.0366	0.1827	3.355
CD4+ TCM	0.0520	0.1111	4.611
CD4+ TEM	0.0351	0.1924	3.787
CD4+ TTEM	0.0423	0.1487	4.309

Figure 4.14: **Reduced glutathione in CD8+ and CD4+ T cell subsets.** Linear regression models of MFI values of TTV (ThiolTracker™ Violet) which measures reduced glutathione displayed for CD8+ **(A)** and CD4+ **(B)** subsets (Total, TN, CM, EM and TEM) against age. Tabular results of simple linear regression analysis (R^2 , P value and Slope) is shown for each graph. P values lower than 0.05 (significant level) are highlighted in grey.

4.3.2 B Cells

In addition to T cells, B lymphocytes represent the other crucial compartment of the adaptive immune response. For this reason we analyzed also changes that occur amongst the B cell response with age and sex of 41 healthy donors amongst our total cohort. As displayed in Figure 4.15, we identify the B cell subsets by doublet discrimination, followed by the identification of viable cells by using an LD dye. Then, we identify the lymphocytes based on the morphological parameters (FSC-A, SSC-A) and gate against CD20+, CD19+ to identify the total B cells. Following this, we define B cell differentiation by gaiting against CD21 and CD27.Specifically, naïve B cells are defined as (CD21+, CD27-), memory B cells (CD21+, CD27+) and exhausted B cells (CD21-, CD27-). In Figure 4.15 we show the gating strategy for determining immunoglobulins IgD, IgM and IgG, as well as transcription factors which are associated with B cell functionality PAX5 and XBP1. Positive populations are identified through the usage of FMX controls (Figure 4.15-lower panel).

4.3.2.1 B cell characterisation over lifetime

In figure 4.16 we see frequencies of Total B, Naïve B, Memory B and Exhausted B cells subsets, yet no significant changes are observed across individuals of different age and sex. However we can identify a declining trend with age amongst total B cells (Figure 4.16A) and Naïve B cells (Figure 4.16B). On the contrary, we see an increasing trend regarding memory and exhausted B cells. Specifically, the female compartment of the cohort seems to

acquire the closest value to the 0.05 significant coefficient value (*P* = 0.0773) for the increase of the exhausted phenotype. Higher accumulation of exhausted B cells has been previously reported in patients with autoimmune diseases like systemic lupus erythematosus, a disease mostly influencing females. CD21-CD27- B cells could thus represent a biomarker of increased inflammatory phenotype in females with aging (Horisberger *et al.*, 2022). This sexual-dimorphism in the human immune system, and in B cells in particular, could originate from sex-specific epigenetic changes. In fact B-cell specific chromatin loci were found open in women, yet in men they remain closed with age (Márquez *et al.*, 2020).

The expression of immunoglobulins (IgD, IgM and IgG) in the main B cell subsets we analysed above outlined no significant changes with age (Figure 4.17A,B,C). However, as already reported in the literature (Dirks *et al.*, 2023), IgD is more prominent in early B cell differentiation stages from all age groups (4.17A). Moreover, ageing memory B cells show a trend of slightly increased expression of IgM, whilst IgD and IgG stay quite constant (Figure 4.17). Memory responses are classically assigned to switched IgG memory B cells, whose unique cytoplasmic tail confers them enhanced reactivity. IgM memory B cells have been described almost 40 years ago, but their precise functional role remains as today ill-defined.

It was proposed that, despite the pentameric structure of the IgM antibody which increases its avidity, the lower affinity of IgM

memory B cells could in fact afford a wider cross-specific protection in front of mutating pathogens (Weill and Reynaud, 2020). The IgM+ memory B cell pool thus keeps a breadth of reactivity similar to that of naïve B cells, but with the advantage of being able to rapidly respond to antigen. The slight increase in the frequency of IgM+ memory B cells (Figure 4.17 B) could thus represent a way to compensate the loss in naïve B cells observed with age (Figure 4.16).

We were only able to assess the redox status in B cells subsets from 26 healthy subsets from our cohort. However, we were able to define a significant increase of normalised MSR with age in all B cell subsets analysed, as it occurs in T cells (Figure 4.18A and 4.10). Additionally, we also measured the MFI of SOD1, NRF2 and TTV, important antioxidant systems described before, and find that also in B cells there are no significant changes, thus, indicating a loss of oxidative balance also in B cell subsets with age.

4.3.2.2 Transcription factors associated to B cell development with age

Together with the frequency of the major B cell subsets, we also assessed two important transcription factors associated to B cell development. PAX5, responsible for activating B cell lineage-specific genes and XBP1, crucial for the development of antibody-secreting plasma cells by controlling unfolded protein responses, that relieves endoplasmic reticulum stress and permits

antibody release during B cell terminal differentiation (Todd *et al.*, 2009; O'Brien *et al.*, 2011).

In figure 4.19A we characterise the mean fluorescent intensity (MFI) of PAX5, which shows no significant changes among the total B, naïve, memory and exhausted B cells. In recent epigenetic studies PAX5 has shown to be downregulated with age in males only, an observation that we were not able to confirm (Márquez *et al.*, 2020). However further investigations are required to further understand the sex and age related PAX5 changes in B cells . On the contrary we define a significant decrease in the frequencies of XBP1 expression with age in all B cell subsets (Figure 4.19B). Specifically we see a significant drop in the expression of XBP1 after the age of 60 within our cohort. However when we classify our cohort into three age groups (young, middle and old aged) we define significant changes from both young to middle aged subjects and young to old from all B cell subsets. From middle aged to old we see no significant changes (Figure 4.20A). This observation has not been previously reported on B cells with age thus marking an important point for further investigation. It has been recently determined that the loss of XBP1 accelerates age-related decline in retinal function and neurodegeneration, thus indicating that lower XBP1 levels in ageing B cells could also be associated with a decreased functionality of B cells amongst old healthy subjects (McLaughlin *et al.*, 2018). Interestingly, in some *C. elegans* studies where the activation of XBP1 is encouraged in

neuronal expression, lifespan was improved (Henis-Korenblit et al., 2010; Taylor and Dillin, 2013).

XBP1 has also been linked to Systemic Lupus Erythematosus (SLE) and its blockade could be a potential strategy to treat autoimmune diseases (Piróg *et al.*, 2019). Autoimmune diseases are mostly prevalent in females as defined in the literature (Angum *et al.*, 2020), thus we assessed the expression of XBP1 in males and females in our cohort and found that women do in fact have a trend to express higher percentages of the transcription factor than men in all B cell subsets (Figure 4.20B), yet these results require further investigations.

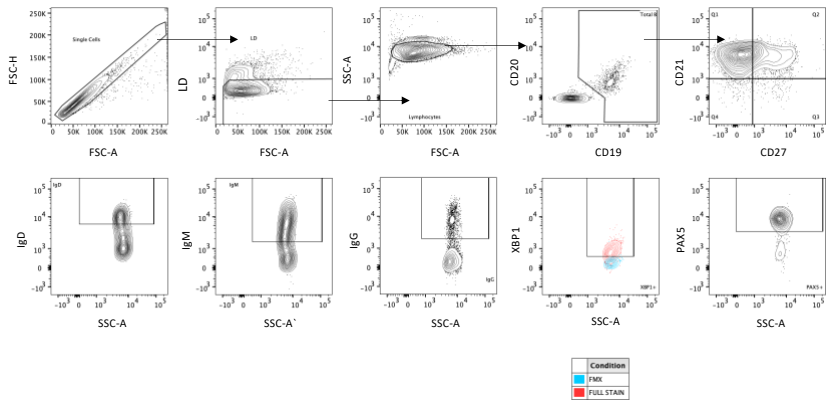

Figure 4.15: **Mature B cell subsets, immunoglobulins and transcription factors.** Gating strategy used to analyze markers associated to B cell differentiation, identification of immunoglobulins IgD, IgM and IgG and transcription factors associated to B cell maturation (PAX5, XBP1). Total B cells are defined by gating first on singlet (FSC-H vs FSC-A), live cells (LD^- cells), total lymphocytes (FSC-A vs SSC-A), $CD19^+$ and $CD20^+$.cells. Naïve B cells are then defined as CD21+, CD27- while memory B cells are identified as CD21+, CD27+ and exhausted memory B cells are defined as CD21-, CD27-. We include an fluorescent minus-X (FMX) control to define the gating strategy for XBP1 (blue is FMX and red is the fully stained).

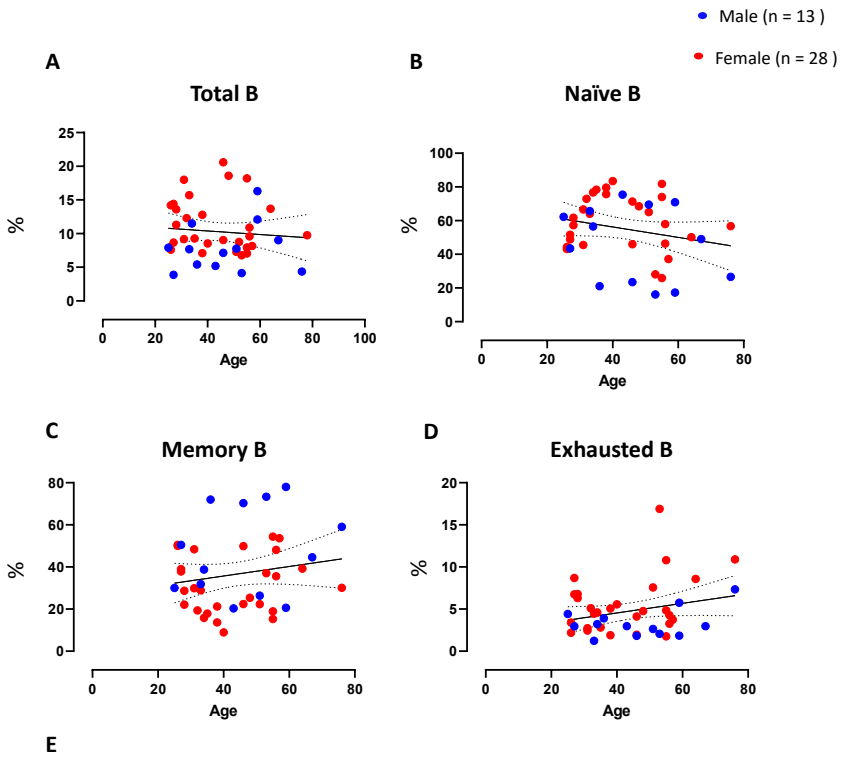

E

	ALL			Female			Male		
Population	R^2	P Value	Slope	R^2	P Value	Slope	R^2	P Value	Slope
Total B	0.0081	0.5755	-0.0264	0.0236	0.4346	-0.0447	0.0323	0.5570	0.04164
Naïve B	0.0529	0.1479	-0.3097	0.0194	0.4793	-0.1664	0.7717	0.3581	-0.3960
Memory B	0.0326	0.2590	0.2261	0.0052	0.7144	0.0732	0.0466	0.4784	0.2916
Exhausted B	0.0684	0.0984	0.0569	0.1151	0.0773	0.08470	0.1431	0.2024	0.0409

Figure 4.16: **Major B cell subsets with age and sex. A)** Scatter plots of the frequencies (%) of 41 healthy donors of their total B cell (CD20+. CD19+) distribution is displayed as a linear regression model. **B)** Naïve B (CD21+CD27-, **C)** Memory B cells (CD21+CD27+ and **D)** exhausted B cells are also show The R^2 , P Value and slope statistical values of the linear regression analysis model are presented in the table associated with the figure **(E)** for all subjects female and male participants separately. Coefficient interval bands – dotted lines (CI 95%) are also present to show where the true regression line lies at a certain level of confidence.

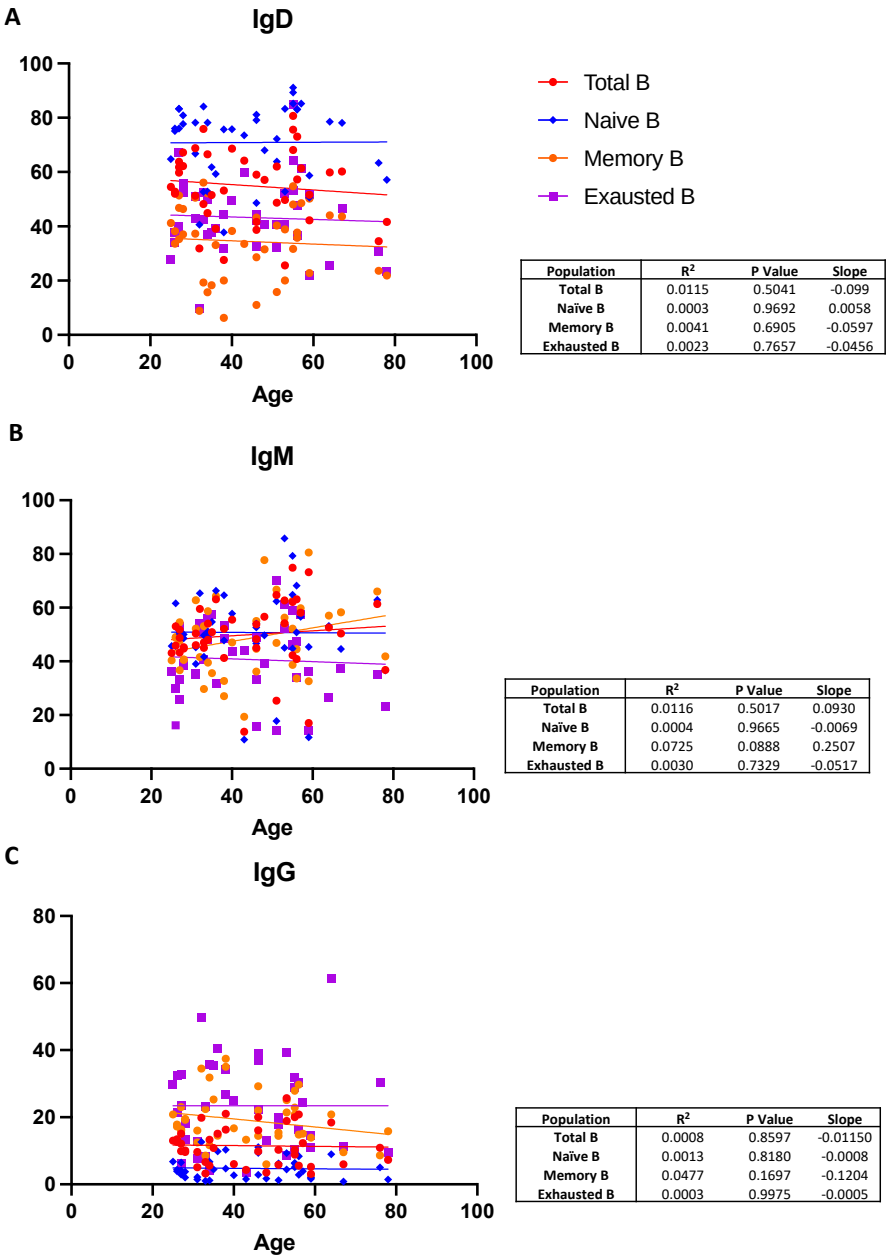

Population	R^2	P Value	Slope
Total B	0.0115	0.5041	-0.099
Naïve B	0.0003	0.9692	0.0058
Memory B	0.0041	0.6905	-0.0597
Exhausted B	0.0023	0.7657	-0.0456

Population	R^2	P Value	Slope
Total B	0.0116	0.5017	0.0930
Naïve B	0.0004	0.9665	-0.0069
Memory B	0.0725	0.0888	0.2507
Exhausted B	0.0030	0.7329	-0.0517

Population	R^2	P Value	Slope
Total B	0.0008	0.8597	-0.01150
Naïve B	0.0013	0.8180	-0.0008
Memory B	0.0477	0.1697	-0.1204
Exhausted B	0.0003	0.9975	-0.0005

Figure 4.17: **Immunoglobulin distribution with age.** Linear regression models of IgD **(A)**, IgM **(B)**, IgG **(C)** frequencies in relation to age of 41 healthy donors of Total B cells (red), Naïve B cells (blue), memory B cells (orange), exhausted B cells (purple). Tabular results of simple linear regression analysis for each graph are shown (R^2, P value, Slope).

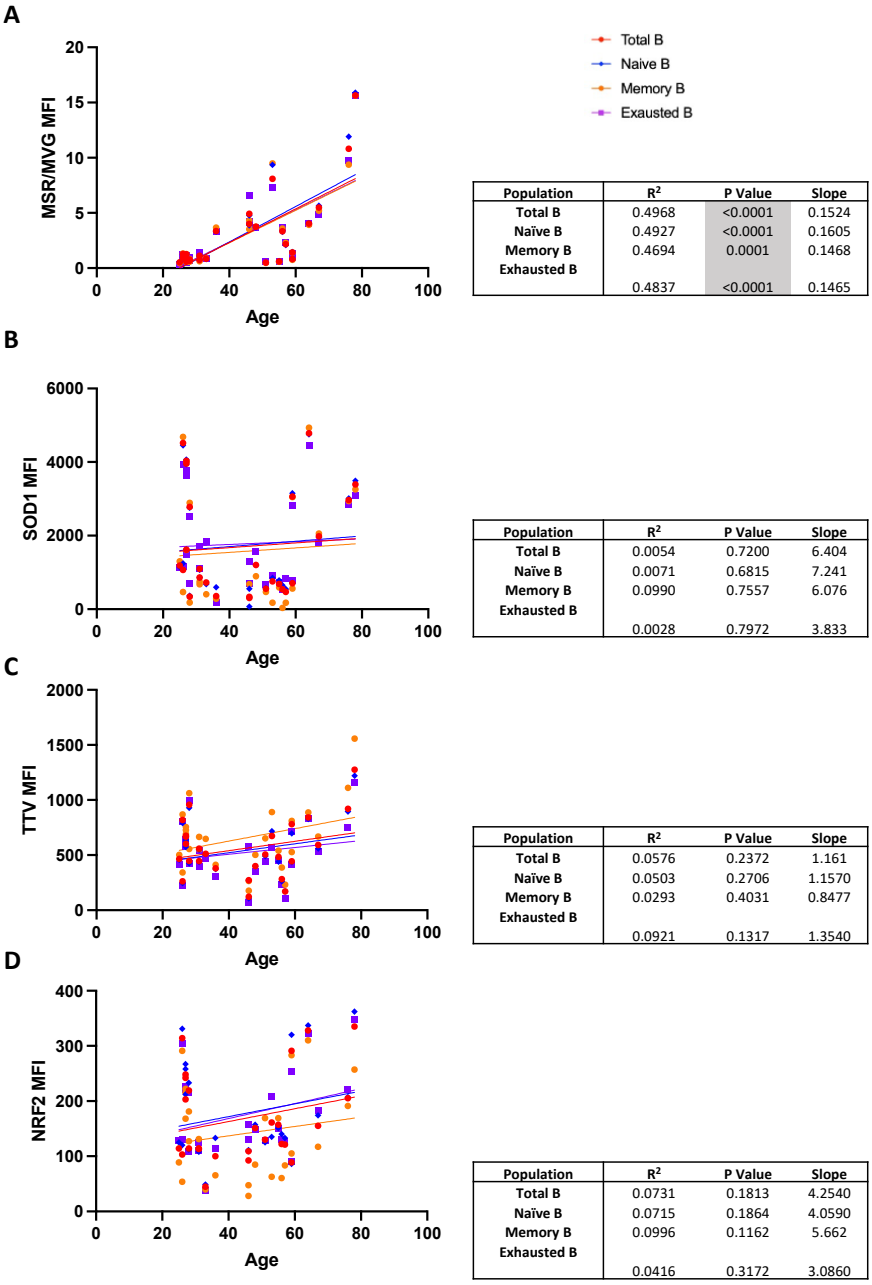

Population	R^2	P Value	Slope
Total B	0.4968	<0.0001	0.1524
Naïve B	0.4927	<0.0001	0.1605
Memory B	0.4694	0.0001	0.1468
Exhausted B	0.4837	<0.0001	0.1465

Population	R^2	P Value	Slope
Total B	0.0054	0.7200	6.404
Naïve B	0.0071	0.6815	7.241
Memory B	0.0990	0.7557	6.076
Exhausted B	0.0028	0.7972	3.833

Population	R^2	P Value	Slope
Total B	0.0576	0.2372	1.161
Naïve B	0.0503	0.2706	1.1570
Memory B	0.0293	0.4031	0.8477
Exhausted B	0.0921	0.1317	1.3540

Population	R^2	P Value	Slope
Total B	0.0731	0.1813	4.2540
Naïve B	0.0715	0.1864	4.0590
Memory B	0.0996	0.1162	5.662
Exhausted B	0.0416	0.3172	3.0860

Figure 4.18: **Redox related markers in B cell subsets.** Scatter plots of normalised MSR **(A)**, SOD1 **(B)**, TTV**(C)** and NRF2 **(D)** of 26 healthy donors amongst their Total B cells (red), Naïve B cells (blue), memory B cells (orange), exhausted B cells (purple). Tabular results of simple linear regression analysis for each graph are shown (R^2, P value, Slope), highlighted grey values indicate a P value lower than the 0.05 significance level.

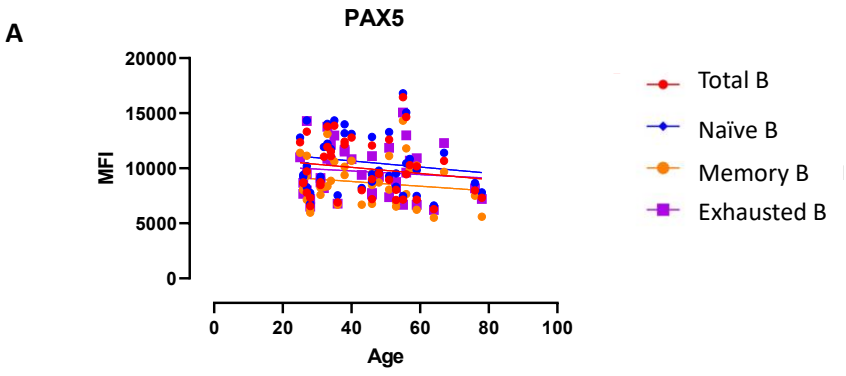

Population	R^2	P Value	Slope
Total B	0.0242	0.337	-27.70
Naïve B	0.0244	0.335	-27.98
Memory B	0.0217	0.363	-27.40
Exhausted B	0.0103	0.532	-16.55

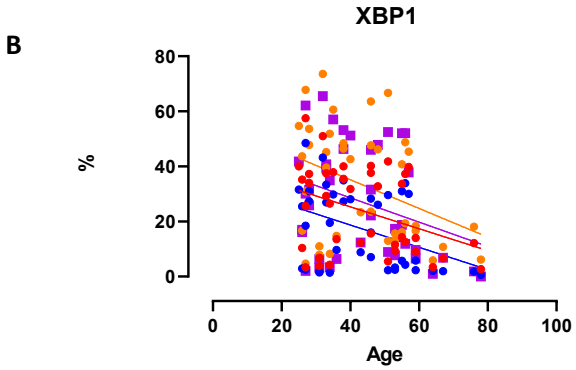

Population	R^2	P Value	Slope
Total B	0.1370	0.0187	-0.3973
Naïve B	0.1678	0.0087	-0.4051
Memory B	0.1342	0.0201	-0.5210
Exhausted B	0.0983	0.0488	-0.4417

Figure 4.19: **Transcription factors expressed in major B cell subsets with age. A)** Mean Fluorescence Intensity (MFI) values of transcription factor PAX5 shown via linear regression models to determine age related alternations in Total B (red line), Naïve B (blue line), Memory B (orange line) and Exhausted B (purple line) cells. **B)** Transcription factor XBP1 frequencies are also present The R^2 , P Value and slope statistical values of the linear regression analysis model are presented in the table associated with the figure for all subjects and highlighted grey values indicate a P value lower than the 0.05 significance level.

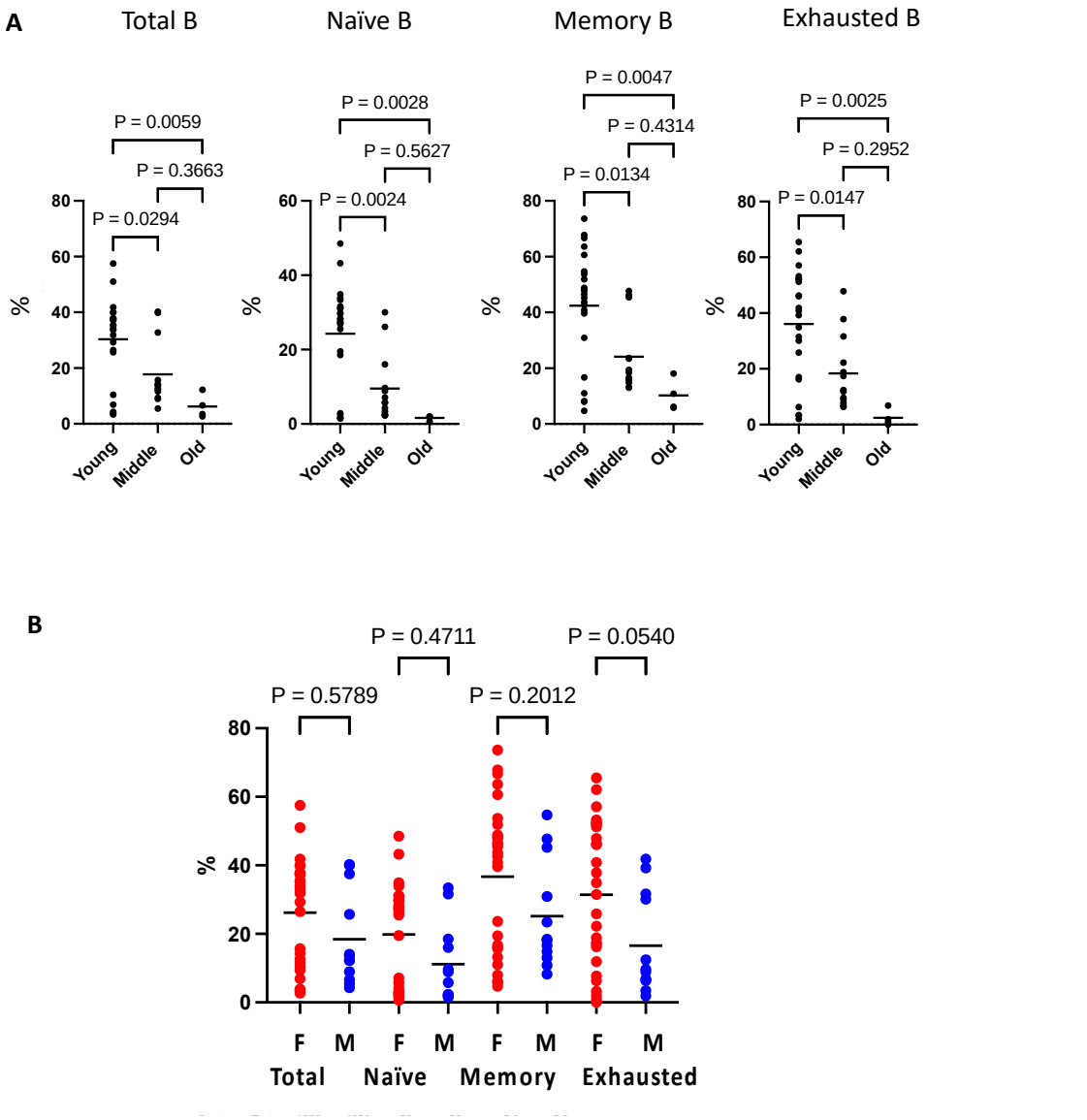

Figure 4.20: **Distribution of XBP1 frequencies in different age groups and sexes. A)** XBP1 frequencies are displayed in different age groups (Young 18-35, Middle 36-59, Old 60+) of all B cell subsets analysed (Total B, Naïve B, Memory B, and Exhausted B cells). Comparisons of each age group (Young vs Middle, Young vs Old, Middle vs Old) via ordinary one-way ANOVA multiple comparisons test (P values are displayed for each comparison). **B)** The distribution of XBP1 frequencies for each subject comparing females (red) and males (blue) in each B cell subset.

4.4 Conclusion

In the current chapter we utilised our standardised multiparametric flow cytometry panels in order to assess age related changes amongst 54 healthy donors in the adaptive immune response. Our panels were able to distinguish an age-related decline amongst naïve lymphocytes as well as an increase in memory lymphocytes with impaired immune function, due to the increased expression of exhaustion markers like PD1 and TIGIT. Additionally, CD4+ T cells seem to remain more resistant to age-related phenotypic and functional changes than CD8+ T-cells.

The CD8+ T cell compartment should be the focus for future research aiming at age related immune recuperation, as we defined it as the most hindered population. Studies further focusing on CD8+ T cell restoration with age should focus their attention on a newly defined CD8+ T cell subset, known as Tpex, since due to their exhausted phenotype they are known to obstructs T cell differentiation. For the first time we defined an increases frequency with age in Tpex cells, thus their restoration could remodulate the hindered age related differentiation in CD8+ T cell subsets.

Even though we saw no significant changes amongst B cells subsets, we identified a significant drop in the expression of transcription factor XBP1 in B cells with age. XBP1 is an important marker for age related neuron studies but has not been

yet considered in B cell aging. Being XBP1 one of the major drivers of terminal plasma cell differentiation and modulators of the unfolded protein response, the observed age-dependent decline might result in a failure of B cells to up-regulate UPR-related XBP1 target genes during terminal B cell differentiation. However, this hypothesis would need to be verified by analyzing XBP1 activity in the expression of genes required for biogenesis of the protein secretory pathway, protein folding and secretion, as well as clearance of misfolded proteins from ER.

Our novel redox panel is able to identify an increase of superoxide anions yet no significant changes amongst key antioxidants with age thus suggesting an impaired redox balance with age in T and B cells.
These findings are consistent with the mitochondrial oxidative stress theory of aging. However, we have to consider that other theories exist, claiming that increased superoxide generation might act as a signal in young cells to trigger changes of gene expression that prevent or attenuate the effects of subsequent aging. This would imply superoxide being generated as a protective signal in response to molecular damage sustained during aging and further studies would be required to justify that.

Although there has been significant progress in identifying age-associated changes in major lymphocyte subsets, more research is required to pinpoint age-associated alterations in T and B cells at the levels of gene expression, protein, and cellular organelles. New

lymphocyte subsets are constantly emerging thus our knowledge on age-related studies is limitless. A deeper comprehension of the mechanisms underlying the age-related changes in adaptive immune response will open up new possibilities for increasing the production of naive cells and preserving the memory-lymphocyte pool and its functionality. These further studies with then allow us to create vaccines and treatments that are more effective in older people.

4.5 Bibliography

Angum, F. *et al.* (2020) 'The Prevalence of Autoimmune Disorders in Women: A Narrative Review', *Cureus* [Preprint]. Available at: https://doi.org/10.7759/cureus.8094.

Berhanu, D. *et al.* (2003) 'Optimized lymphocyte isolation methods for analysis of chemokine receptor expression', *Journal of Immunological Methods*, 279(1–2), pp. 199–207. Available at: https://doi.org/10.1016/S0022-1759(03)00186-8.

Bertolotti, M. *et al.* (2013) 'Tyrosine Kinase Signal Modulation: A Matter of H 2 O 2 Membrane Permeability?', *Antioxidants & Redox Signaling*, 19(13), pp. 1447–1451. Available at: https://doi.org/10.1089/ars.2013.5330.

Bertolotti, M. *et al.* (2016) 'AQP8 transports NOX2-generated H2O2 across the plasma membrane to promote signaling in B cells', *Journal of Leukocyte Biology*, 100(5), pp. 1071–1079. Available at: https://doi.org/10.1189/jlb.2AB0116-045R.

de Biasi, S. *et al.* (2020) 'Marked T cell activation, senescence, exhaustion and skewing towards TH17 in patients with COVID-19 pneumonia', *Nature Communications*, 11(1), p. 3434. Available at: https://doi.org/10.1038/s41467-020-17292-4.

Breznik, J.A. *et al.* (2022) 'Cytomegalovirus Seropositivity in Older Adults Changes the T Cell Repertoire but Does Not Prevent Antibody or Cellular Responses to SARS-CoV-2 Vaccination', *The Journal of Immunology*, 209(10), pp. 1892–1905. Available at: https://doi.org/10.4049/jimmunol.2200369.

Callender, L.A. *et al.* (2020) 'Mitochondrial mass governs the extent of human T cell senescence', *Aging Cell*, 19(2). Available at: https://doi.org/10.1111/acel.13067.

Derhovanessian, E., Larbi, A. and Pawelec, G. (2009) 'Biomarkers of human immunosenescence: impact of Cytomegalovirus

infection', *Current Opinion in Immunology*, 21(4), pp. 440–445. Available at: https://doi.org/10.1016/j.coi.2009.05.012.

Dirks, J. *et al.* (2023) 'IgD shapes the pre-immune naïve B cell compartment in humans', *Frontiers in Immunology*, 14. Available at: https://doi.org/10.3389/fimmu.2023.1096019.

Dolfi, D. V *et al.* (2013) 'Increased T-bet is associated with senescence of influenza virus-specific CD8 T cells in aged humans', *Journal of Leukocyte Biology*, 93(6), pp. 825–836. Available at: https://doi.org/10.1189/jlb.0912438.

Galletti, G. *et al.* (2020) 'Two subsets of stem-like CD8+ memory T cell progenitors with distinct fate commitments in humans', *Nature Immunology*, 21(12), pp. 1552–1562. Available at: https://doi.org/10.1038/s41590-020-0791-5.

Goronzy, J.J. and Weyand, C.M. (2013) 'Understanding immunosenescence to improve responses to vaccines', *Nature Immunology*, 14(5), pp. 428–436. Available at: https://doi.org/10.1038/ni.2588.

Henis-Korenblit, S. *et al.* (2010) 'Insulin/IGF-1 signaling mutants reprogram ER stress response regulators to promote longevity', *Proceedings of the National Academy of Sciences*, 107(21), pp. 9730–9735. Available at: https://doi.org/10.1073/pnas.1002575107.

Horisberger, A. *et al.* (2022) 'Measurement of circulating CD21−CD27− B lymphocytes in SLE patients is associated with disease activity independently of conventional serological biomarkers', *Scientific Reports*, 12(1), p. 9189. Available at: https://doi.org/10.1038/s41598-022-12775-4.

Hu, B. *et al.* (2020) 'Distinct Age-Related Epigenetic Signatures in CD4 and CD8 T Cells', *Frontiers in Immunology*, 11. Available at: https://doi.org/10.3389/fimmu.2020.585168.

Hutten, T.J.A. *et al.* (2018) 'Increased Coexpression of PD-1, TIGIT, and KLRG-1 on Tumor-Reactive CD8+ T Cells During Relapse after Allogeneic Stem Cell Transplantation', *Biology of*

Blood and Marrow Transplantation, 24(4), pp. 666–677. Available at: https://doi.org/10.1016/j.bbmt.2017.11.027.

Mak, T.W. *et al.* (2017) 'Glutathione Primes T Cell Metabolism for Inflammation', *Immunity*, 46(4), pp. 675–689. Available at: https://doi.org/10.1016/j.immuni.2017.03.019.

Márquez, E.J. *et al.* (2020) 'Sexual-dimorphism in human immune system aging', *Nature Communications*, 11(1), p. 751. Available at: https://doi.org/10.1038/s41467-020-14396-9.

McLaughlin, T. *et al.* (2018) 'Loss of XBP1 accelerates age-related decline in retinal function and neurodegeneration', *Molecular Neurodegeneration*, 13(1), p. 16. Available at: https://doi.org/10.1186/s13024-018-0250-z.

Miwa, S. *et al.* (2022) 'Mitochondrial dysfunction in cell senescence and aging', *Journal of Clinical Investigation*, 132(13). Available at: https://doi.org/10.1172/JCI158447.

Moro-García, M.A. (2013) 'When aging reaches CD4+ T-cells: phenotypic and functional changes', *Frontiers in Immunology*, 4. Available at: https://doi.org/10.3389/fimmu.2013.00107.

Moskowitz, D.M. *et al.* (2017) 'Epigenomics of human CD8 T cell differentiation and aging', *Science Immunology*, 2(8). Available at: https://doi.org/10.1126/sciimmunol.aag0192.

O'Brien, P. *et al.* (2011) 'The *Pax-5* Gene: A Pluripotent Regulator of B-cell Differentiation and Cancer Disease', *Cancer Research*, 71(24), pp. 7345–7350. Available at: https://doi.org/10.1158/0008-5472.CAN-11-1874.

Pilipow, K. *et al.* (2018) 'Antioxidant metabolism regulates CD8+ T memory stem cell formation and antitumor immunity', *JCI Insight*, 3(18). Available at: https://doi.org/10.1172/jci.insight.122299.

Piróg, K.A. *et al.* (2019) 'XBP1 signalling is essential for alleviating mutant protein aggregation in ER-stress related skeletal

disease', *PLOS Genetics*, 15(7), p. e1008215. Available at: https://doi.org/10.1371/journal.pgen.1008215.

Roberto, A. *et al.* (2015) 'Role of naive-derived T memory stem cells in T-cell reconstitution following allogeneic transplantation', *Blood*, 125(18), pp. 2855–2864. Available at: https://doi.org/10.1182/blood-2014-11-608406.

Saeidi, A. *et al.* (2018) 'T-Cell Exhaustion in Chronic Infections: Reversing the State of Exhaustion and Reinvigorating Optimal Protective Immune Responses', *Frontiers in Immunology*, 9. Available at: https://doi.org/10.3389/fimmu.2018.02569.

Shive, C.L. *et al.* (2021) 'Markers of T Cell Exhaustion and Senescence and Their Relationship to Plasma TGF-β Levels in Treated HIV+ Immune Non-responders', *Frontiers in Immunology*, 12. Available at: https://doi.org/10.3389/fimmu.2021.638010.

Taylor, R.C. and Dillin, A. (2013) 'XBP-1 Is a Cell-Nonautonomous Regulator of Stress Resistance and Longevity', *Cell*, 153(7), pp. 1435–1447. Available at: https://doi.org/10.1016/j.cell.2013.05.042.

Todd, D.J. *et al.* (2009) 'XBP1 governs late events in plasma cell differentiation and is not required for antigen-specific memory B cell development', *Journal of Experimental Medicine*, 206(10), pp. 2151–2159. Available at: https://doi.org/10.1084/jem.20090738.

Ucar, D. *et al.* (2017) 'The chromatin accessibility signature of human immune aging stems from CD8+ T cells', *Journal of Experimental Medicine*, 214(10), pp. 3123–3144. Available at: https://doi.org/10.1084/jem.20170416.

Weill, J.-C. and Reynaud, C.-A. (2020) 'IgM memory B cells: specific effectors of innate-like and adaptive responses', *Current Opinion in Immunology*, 63, pp. 1–6. Available at: https://doi.org/10.1016/j.coi.2019.09.003.

Zhang, H., Weyand, C.M. and Goronzy, J.J. (2021) ‘Hallmarks of the aging T-cell system’, *The FEBS Journal*, 288(24), pp. 7123–7142. Available at: https://doi.org/10.1111/febs.15770.

Chapter 5

High-dimensional single cell analysis of NK cells with age and sex

5.1 Introduction

Natural killer (NK) cells are essential effector cells of the innate immune system whose defensive tactics include direct cytotoxicity by utilising cytotoxic granules and the release of immunoregulatory cytokines. They serve as the first line of defence against malignant and virally-infected cells (Hamerman, Ogasawara and Lanier, 2005; Waldhauer and Steinle, 2008; Michel *et al.*, 2016). Human NK cells are generally characterized by the expression of the $CD56^{+}$ surface marker. Based on differential surface expression of CD56 it is possible to identify two major subsets: CD56 bright ($CD56^{BRIGHT}$)and CD56 dim cells ($CD56^{DIM}$).

Less mature NK cells called $CD56^{BR}$ exhibit poor cytotoxicity, but produce a wide range of chemokines and cytokines to either aid cells of adaptive immune response or signal innate cells like dendritic cells to respond to invading pathogens. When in response to cellular stimuli, the more developed $CD56^{DIM}$ cells are powerful cytotoxic and cytokine-secreting cells (Hamerman, Ogasawara and Lanier, 2005; Poli *et al.*, 2009a; Michel *et al.*, 2016; Roberto *et al.*, 2018; Laskowski, Biederstädt and Rezvani, 2022).

NK cell immunesenescence, is a phenomenon coupled with the normal aging process, and is characterized by changes in the composition, phenotype, and functionality of NK cells (Judge, Murphy and Canter, 2020). An increased incidence and severity of viral infections, pneumonia, and infectious disease deaths are associated with decreased NK cell activity in elderly individuals (Ogata *et al.*, 2001; Waldhauer and Steinle, 2008; Hazeldine, Hampson and Lord, 2012; Hazeldine and Lord, 2013). In addition, a 2-fold increase in cancer was linked to low NK functionality (Imai *et al.*, 2000).

Here we developed a standardized polychromatic flow cytometry panel to assess age related changes in NK cell subsets of healthy donors and identify patterns of NK cell immunesenescence that increase the risk for cancer and infectious diseases.

5.2 Methods

5.2.1 Sample information

Peripheral blood mononuclear cells (PBMC's) were isolated by density gradient centrifugation from whole blood of forty-five healthy subjects. All subsets were free from infectious diseases, malignant conditions and immunodeficiencies. We categorised our cohort in three different age groups; Young (from 18 to 35), Middle (from 36 to 59) and Old (over 60 years old) (Lin *et al.*,

2020; Márquez *et al.*, 2020). Table 5.1 displays the composition of each group of subjects .

Table 5.1: Characteristics of healthy participants

Variable	Sex		
Age	Male	Female	Total
Young	3	10	13
Middle	7	16	23
Old	5	4	9
Total	15	30	45

5.2.2 Flow Cytometry

Single cell suspension of PBMC's were labelled initially with a viability dye by Invitrogen™ (LIVE/DEAD™ Fixable Aqua Dead Cell Stain Kit), for 405 nm excitation. Commercial monoclonal antibodies were used to stain cells for identification of all the markers necessary to NK cells characterization. CD14-BV510 , CD19-BV510, CD3-APCH7 were used to erase monocytes, B cells and T cells from the analysis. The following monoclonal antibody were used for NK cell characterization: CD56-BUV395, CD16-BV605, CD94-BUV495, NKG2D-PECF594, NKG2A-PEcy7, NKG2C-BUV805, NKp30-BV711, NKp46-BV786, DNAM1-PE, HLA-DR-PerCPcy5.5, CD107A-AF700, Granzyme B (GrB)-FITC, CD107A-AF700, PD1-BV42 and CD57-APC. The Cytofix/Cytoperm™ Fixation/Permeabilization was used for determining the intracellular markers GrB and CD107a. All the subjects were tested in 8 different experiments (around 6 donors

per experiment). An internal control was used in each experiment to test the experimental variability and avoiding experiment related bias.

Cells were acquired with a BD LSR Fortessa X-20 flow cytometer (BD, Biosciences, USA), fully equipped with blue, red, yellow/green, violet and UV lasers. The acquisition was performed using BD FACSDiva™ Software (V 8.0.3).

5.2.3 Analysis

Flow cytometry data analysis was performed using FlowJo software (V10.8.2). Considering the amount of markers to assess a computational analysis approach was conducted.

Total events were compensated while doublets and dead cells were eliminated. NK cells were defined as CD14–, CD19– and CD3– cells across all samples. Total NK cells from each subject were down-sampled using FlowJo Downsample v3.3.1 plugin to yield 5,000 cells per sample. Samples were then concatenated in a unique fcs file. The compensated concatenated FCS file was used to perform the FlowJo Uniform Manifold Approximation and Projection (UMAP) v3.1 plugin that offers a non-linear dimensionality reduction visual assessment of high dimensional data. (McInnes, Healy and Melville, 2018). For cluster identification, the FlowJo PhenoGraph v2.5.0 plugin was run with the default settings including the following parameters CD56, CD16, NKG2A, NKG2C,NKG2D, NKp30, NKp46, DNAM-1, Granzyme B (GrB), PD1, CD57, HLA-DR, CD94 and CD107A.

For evaluation of marker expression changes in the distinct clusters, integrated MFI (iMFI) scores were calculated by multiplying the positive frequency of each marker by the MFI of the positive population (Darrah *et al.*, 2007). The iMFI values were rescaled to values from 0 to 100 (Brummelman *et al.*, 2018).

5.2.4 Statistics

The statistical analysis was performed using GraphPad Prism software (V.9.5.1). Multiple comparisons t tests was completed to compare different age groups.

5.3 Results

5.3.1 High-dimensional single cell analysis of NK cells in healthy immunophenotypes

To characterize the diversity of $CD56^+$ NK cells in healthy subjects spanning different ages, we developed a polychromatic flow cytometry panel capable of simultaneously investigating 17 parameters on thousands of single cells from peripheral blood of forty-five healthy donors. Markers included in the panel, providing information on NK cell differentiation (CD56, CD16), NK cell receptor expression (CD94, NKG2C, NKG2D, NKp30, DNAM-1, NKp46, NKG2A), activation marker (HLA-DR), cytotoxicity (GrB, CD107A), exhaustion (PD1) and senescence (CD57). To reduce the dimensionality of the dataset and visualize high parameter datasets in a two dimensional space, UMAP algorithm was performed. Fig. 5.1A shows the UMAP plots of concatenated files on the total NK cells in all the 45 healthy subjects together with the expression level of the indicated functional and phenotypic NK markers. To gain a further insight on the immunophenotypes that preferentially characterize NK cells from the different group of subjects, PhenoGraph analysis was used (unsupervised clustering algorithm suitable for high-dimensional single cell data). PhenoGraph analysis identified 31 different NK subpopulations (“clusters;” visualized by using UMAP plots; Fig. 5.1B).

Figure 5.2A displays the frequency of each cluster for all 45 subjects. Clusters 8, 13, 14, 22, 23, 24, 29, 30 and 31 had frequencies less than or equal to $\leq$ 1%, therefore they were eliminated from the analysis to exclude biases.

To describe the phenotypic individuality of immunophenotypes resulting from PhenoGraph clustering, we calculated the iMFI values of each marker in each selected cluster and visualized these values in the form of a heat map (Figure 5.2B).

The UMAP analysis revealed slight changes in cluster representation and frequency in each age group (Young 18-35, Middle 36-59, Old 60+) (Fig. 5.3A). Therefore, to assess age related differences in the distribution of each cluster we investigated the cluster frequencies in all 45 subjects in each age group (Fig. 5.3B). Our analysis revealed that there are three clusters whose frequency significantly change with the aging.

5.3.2 NK cells loose adaptive communication with age

Cluster 3 significant increases from young to middle aged individuals ($p = 0.0434$), yet, it decreases from middle aged to old ($p = 0.0094$) – Fig. 5.3B. By cross referencing the heat map in Figure 5.2B, cells in cluster 3 expresses CD56, but they lack CD16. Indeed, they mainly belong to a subsets of $CD56^{BRIGHT}$ $CD16^{-}$ NK cells but also overlap with subset of $CD56^{DIM}CD16^{-}$

NK cells (Fig. 5.4). Cluster 3 acquires a high expression level of NK cell receptors as CD94, NKG2A, and NKG2C, dim levels of NKp30, NKp46 , and NKG2D. Consequently, in our cohort cells from cluster 3 exhibit a decrease with age from middle aged to old subsets, which are a subset aligned with $CD56^{BRIGHT}$ NK cell characteristics. $CD56^{BRIGHT}$ NK cells are prime secretors of immunoregulatory cytokines like IL-10 and IL-13 after antigen recognition where minimal production of these molecules is identified in $CD56^{DIM}$ NK cells (Michel *et al.*, 2016). The cytokine response by $CD56^{BRIGHT}$ NK cells is critical in the activation of the adaptive immune response by NK cells thus its diminished availability with age could contribute to the impaired immune regulation observed in elderly individuals (Chidrawar *et al.*, 2006; Poli *et al.*, 2009b; Almeida-Oliveira *et al.*, 2011). Studies have previously denoted that $CD56^{BRIGHT}$ NK cells do in fact decrease but also their cytokine production is substantially diminished (Hazeldine and Lord, 2013).

Cluster 3 also has a strong expression of CD94, which is an NK cell marker associated to NK cell development, and contributes to NK cell-mediated immunity to certain chronic infections including CMV (Gumá *et al.*, 2006; Yu *et al.*, 2010). CD94 covalently associates with members of the NKG2 family (NKG2A, B, C, E, and H), but insignificantly with NKG2D. Indeed, in the heatmap in figure 5.2B, we can see that cluster 3 is highly enriched in NKG2 family proteins, with NKG2D acquiring the least expression (Orr *et al.*, 2010; Yu *et al.*, 2010).

The ligand for CD94/NKG2 heterodimers is a MHC-I molecule, HLA-E in humans and categorised as an inhibitory receptor (Rosenberg and Huang, 2018). Under normal conditions, ligation of CD94/NKG2 to MHC-I HLA-E molecule, supress signalling activation, avoiding normal cell destruction. Downregulation of MHC I is common in tumour cells and has been denoted to associate with immune-evasion, that require MHC I signalling for activation (Rosenberg and Huang, 2018). Consequently NK cells have been targeted for immunotherapy in order to induce activation by inhibiting CD94/NKG2 heterodimers (André *et al.*, 2018). The decrease of cluster 3 implies a loss of adaptive and innate cell communication due to loss of cytokine production and in parallel the enriched expression of CD94/NKG2 heterodimers associates to immune evasion, increasing the risk for malignant disorders in the elderly. Further studies assessing whether the increase of $CD56^{BRIGHT}$ NK cells can rejuvenate the adaptive and innate communication with age, and in parallel inhibit highly expressed CD94/NKG2 heterodimers from triggering immune inhibition are required.

Another cluster whose frequency changes with age is cluster 11. The frequency of cluster 11 has a significant increase from middle aged to old aged subjects within the cohort as shown in Fig. 5.3B ($p= 0.0033$). Cells in cluster 11 also belong to $CD56^{BRIGHT}$ $CD16^{-}$

NK cell subsets, as cluster 3, however cells in cluster 11 are also closely associated to $CD56^{DIM}$ $CD16^{-}$ NK cells (Fig 5.4).

In comparison to cluster 3, cluster 11 mostly express NK cell receptors like NKp46 and has an enrichment of cells dim for NKG2C, NKG2A, NKp30 and low for CD94. NKp46 is a major NK cell-activating receptor that is involved in the direct elimination of target cells. Specifically, NK cells positive for NKp46 form different types of synapses that result in distinct functional outcomes associated with cytotoxic, inhibition and regulation (Poli *et al.*, 2009a; Hadad *et al.*, 2015).

An important observational difference amongst the two clusters is that cluster 3 acquires a stronger expression of CD107A than cluster 11 (Fig 5.2B). Throughout the process of degranulation, NK cells release cytolytic granules and membrane proteins like CD107A present to the surface and assess in the granule exocytosis mechanism. Due to these increased expression of CD107A in cluster 3 this may suggest that cells within this cluster acquire more functional characteristics than cluster 11. Additionally, studies have shown that NK cells that express more cytotoxic related ligands are a more differentiated NK cell subsets (Di Vito, Mikulak and Mavilio, 2019). This implies that cluster 3 belongs to a more differentiated NK subset than cluster 11.

5.3.3 A cluster negative for CD56 is enriched with age and its driven by males

Cluster 16 displays a significant increase in frequency from middle to old age subsets as shown in figure 5.3B (P = 0.0107). The cells present in cluster 16 show no expression of CD56, CD16, and other NK cell receptors (Fig 5.4, 5.2B). We confidently feel that these cells are neither dead cells, $CD3^+$ T cells, monocyte ($CD14^+$) nor B cell ($CD19^+$) contaminates, since these cells have been excluded from the analysis. On the basis of the heatmap in figure 5.2B, cluster 16 acquires an enrichment of PD1, yet no other marker.

Recent studies have shown that CD56 negative NK cells are an anomalous NK cell subset found in small numbers in healthy individuals and at elevated levels amounts individuals chronically infected with HIV-1, HCV, CMV and other chronic infections (Müller-Durovic *et al.*, 2019; Cocker *et al.*, 2022). It has been identified that individuals with such altered NK profiles respond differently to infections, vaccines and NK associated immunotherapies (Barker *et al.*, 2007). The first identification of CD56 negative NK cells was reported in a study associated with patients infected chronically with HIV-1, while further studies identified an enrichment in this cell subset amongst HIV-1 infected patients (Hu *et al.*, 1995; Mavilio *et al.*, 2005; Björkström, Ljunggren and Sandberg, 2010).

A recent studies on cancer patients positive for CMV has also demonstrated that leukemic patients acquire an enrichment of CD56 negative NK cells especially when treated with dasatinib (a drug that inhibits activated BCR-ABL) (Ishiyama *et al.*, 2021). The same study assessed the functionality of CD56 negative NK cells and identified a downregulation of NK-activating receptors, upregulation of PD-1, and decreased cytotoxicity and cytokine production, while functional studies showed that these cells are anergic and less functional. These findings suggest that CD56 negative NK cells are an exhausted population of NK cells (Ishiyama *et al.*, 2021). Indeed, cluster 16 does not express functional markers like GrB and CD107A, however highly expresses levels of PD1, a known maker of exhaustion (Cho *et al.*, 2020; Ishiyama *et al.*, 2021).

When assessing sexual dysmorphism in our cohort amongst the NK cell subsets, we saw no significant changes amongst middle and young males and females (data not shown). On the contrary, we conducted a multiple unpaired t test comparing old male and female subjects in our cohort and determined that there is a significant enrichment of cluster 16 and cluster 11 in males when compared to females (fig. 5.5A, B). In figure 5.5B we plot the results of the statistical analysis by using a volcano plot and we can determine that C16 and C11 acquire a significant difference with a -log10(P value) of -log10(P = 1.58) and -log10(P= 1.615) respectively. In gender related studies on NK cells, elderly men

have demonstrated to have less robust NK lymphocytes, while mature NK cells in females have a more vigorous cytotoxic granule response and thus are much more functional than males (Imai *et al.*, 2000; Al-Attar *et al.*, 2016; Huang *et al.*, 2021). The fact that cluster 16 is mostly enriched in males prompts that males in our cohort are more prone to lose vital NK receptors with age and uphold an exhausted NK phenotype. Additionally, males seem to also drive the enrichment of cluster 11 with age. As previously stated, cluster 11 acquires less functional markers and is prone to a more differentiated phenotype thus instigating that males obtain a less immunocompetent innate immune response than females amongst $CD56^{BRIGHT}$ NK cells. Nevertheless, a higher sample size is recommended in order to fully confirm these observations.

5.4 Conclusion

We developed and adopted an optimised flow cytometry panel and protocol capable to investigate the expression of 15 NK cells markers in human NK lymphocytes and define age and sex related changes in healthy donors. We applied a high-dimensional single cell approach to analyse and define phenotypic subpopulations that are preferentially enriched or diminished in healthy aging. Dimensionality reduction UMAP analysis is utilised to visualise the 31 clusters defined by PhenoGraph analysis and found that the frequency of $CD56^{BRIGHT}$ NK cells declines with age. $CD56^{BRIGHT}$ NK are efficient cytokine producers that signal other innate cells and adaptive immune cells and their diminished availability with age consequences to age related immunocopentances. Our analysis determined an enrichment of a CD56 negative population driven by males in our cohort. CD56 negative cells have been previously described in patients with chronic infections and are hypothesised to be an exhausted NK cell type with a terminally differentiated phenotype. Further studies, with a higher sample size are essential to understand the maturation status of CD56 negative NK cells and what cells are their precursors.

Figure 5.1: **UMAP representation of automated PhenoGraph clustering analysis on total NK cells of 45 donors. A)** UMAP plots of live, CD3-, CD19-, CD14- cells from 45 healthy donors (5,000 cells each), representing where each marker assessed is mostly enriched where red demonstrates high expression and blue is low expression. **B)** Visualization on UMAP plots of the 31 clusters determined by PhenoGraph analysis of live, CD3-, CD19-, CD14- cells from 45 healthy donors (5,000 cells each).

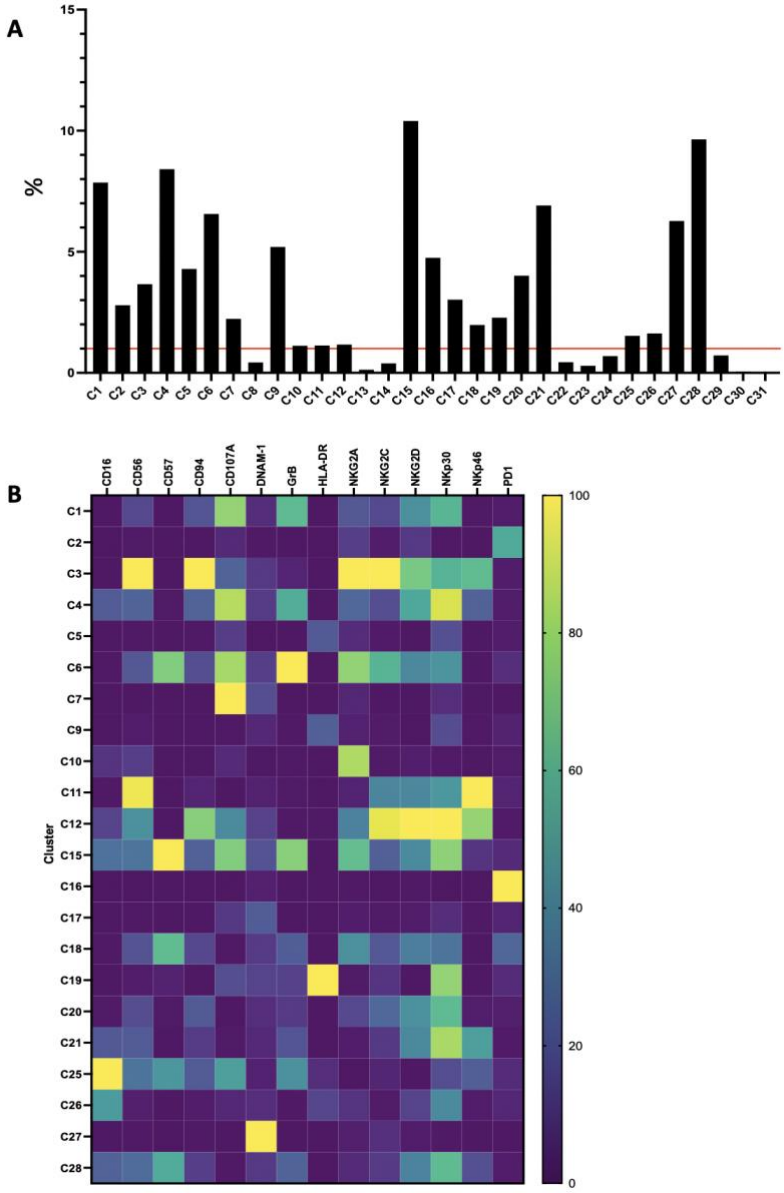

Figure 5.2: **Frequency and heatmaps of each clusters. A)** Bar graph representing the frequency of each cluster obtained by the PhenoGraph analysis. Red line indicates 1% of frequency (the threshold used for excluding clusters from further analysis due to very low frequencies. **B)** Heatmap representing the expression level of each marker of interest in all the clusters with frequency higher than 1%. The expression level is shown as an integrated MFI (iMFI) rescaled to values from 0 to 100.

A

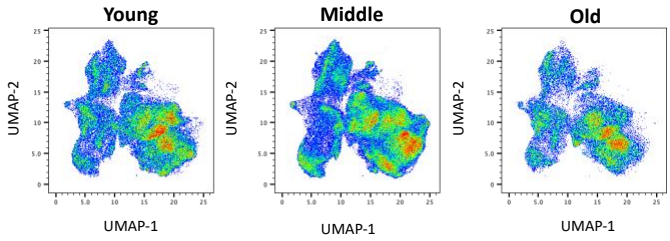

B

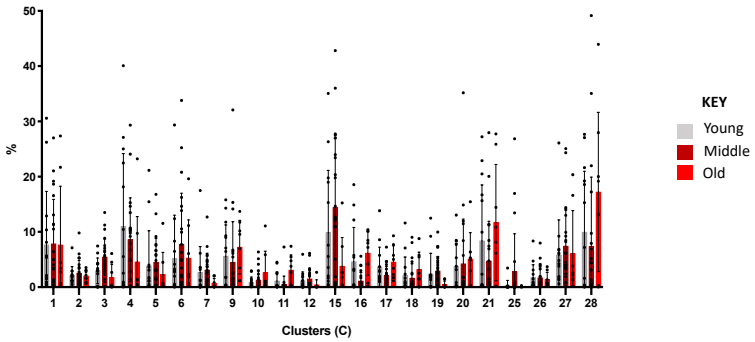

Cluster	Young vs. Middle	Summary	Young vs. Old	Summary	Middle vs. Old	Summary
1	0.9993	ns	>0.9999	ns	0.9996	ns
2	0.8661	ns	>0.9999	ns	0.8989	ns
3	***0.0434***	*	0.7197	ns	***0.0094***	*
4	0.8496	ns	0.3733	ns	0.6884	ns
5	0.9717	ns	0.8608	ns	0.6283	ns
6	0.757	ns	>0.9999	ns	0.8525	ns
7	0.9807	ns	0.4762	ns	0.2577	ns
9	0.9457	ns	0.9213	ns	0.672	ns
10	0.9245	ns	0.1949	ns	0.3406	ns
11	0.6839	ns	0.0518	ns	**0.0033**	**
12	0.8769	ns	0.6666	ns	0.2737	ns
15	0.5576	ns	0.5472	ns	0.0778	ns
16	***0.0387***	*	0.7679	ns	***0.0107***	*
17	0.2155	ns	0.8366	ns	0.0755	ns
18	0.9513	ns	0.7962	ns	0.4954	ns
19	0.9286	ns	0.3528	ns	0.1202	ns
20	0.9932	ns	0.9544	ns	0.9864	ns
21	0.5403	ns	0.7843	ns	0.1713	ns
25	0.3809	ns	0.9996	ns	0.4755	ns
26	>0.9999	ns	0.9742	ns	0.9749	ns
27	0.8627	ns	0.9997	ns	0.9486	ns
28	0.9035	ns	0.4783	ns	0.1702	ns

Figure 5.3: **Age related changes on NK cells after computational analysis. A)** UMAP plot of automated analysis of all NK cells from 46 healthy separated by age (Young 18-35, Middle 36-59, Old 60+). **B)** Frequencies (%) on selected cluster per young 18-35 (grey), middle 36-59 (dark red) and old 60+ (red) age groups. Each dot represents a subject, mean frequency is displayed as a bar chart and error bars indicate the standard deviation for each bar. The table displays the p values and statistical summary of the multiple t test analysis comparing each age group per cluster.

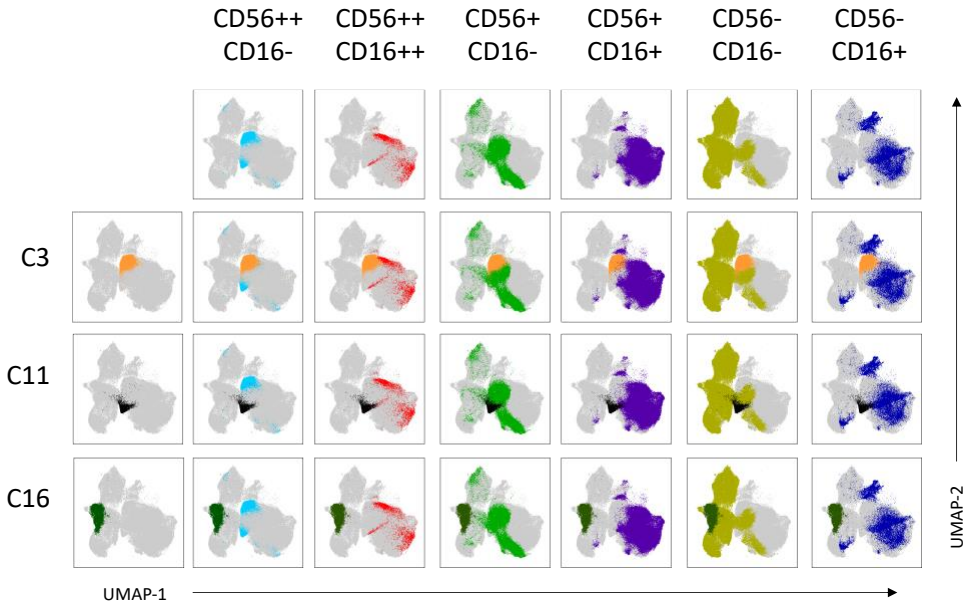

Figure 5.4: **Six major NK cell subsets in cluster 3, 11 and 16.** UMAP plots showing where six different NK subsets are displayed and how close in proximity they are with cluster 3, 11, and 16. The NK subsets are CD56++CD16- ($CD56^{BRIGHT}$), CD56++CD16++, CD56+CD16-, CD56+CD16+ ($CD56^{DIM}$), CD56-CD16- and CD56-CD16+.

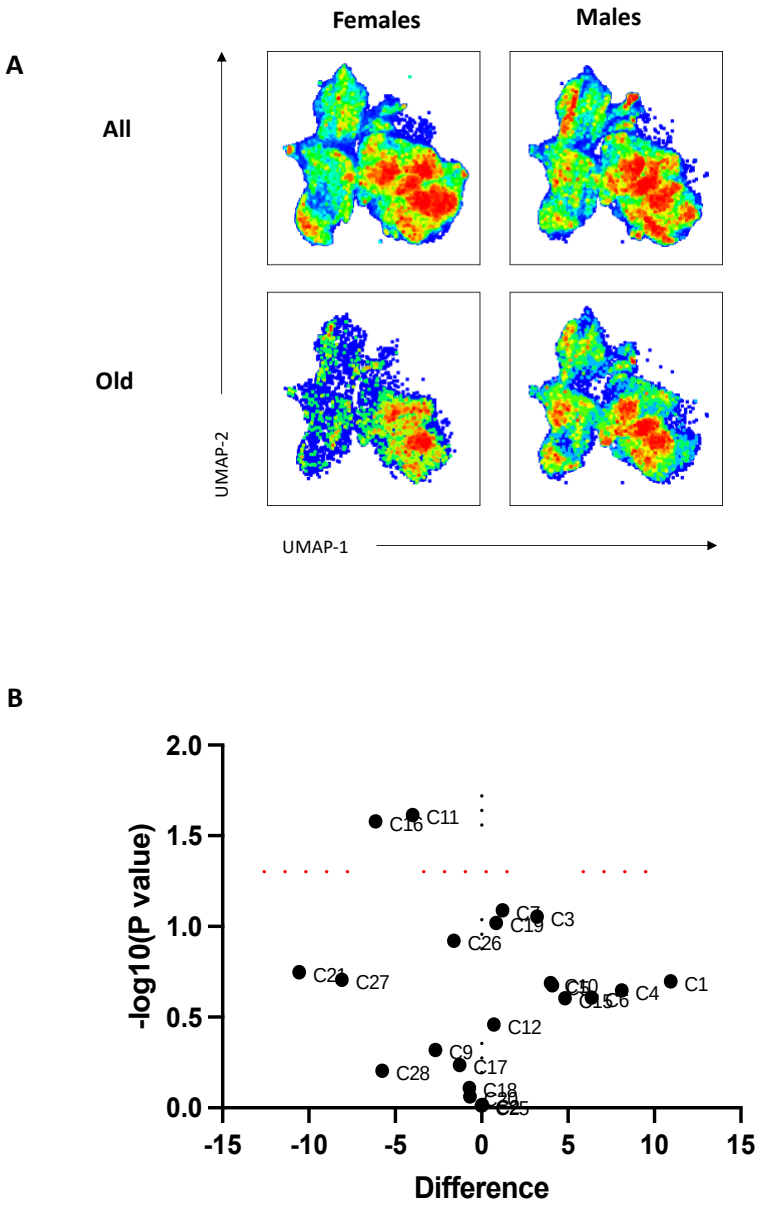

Figure 5.5: **Old males and female changes of NK cell subsets after computational analysis. A)** UMAP plot of automated analysis of all NK cells from 45 healthy donors and the old subjects below (60+) where males are on the right and females on the left. **B)** Volcano Plot comparing old females vs old male frequencies of each cluster where the X axis plots the difference between means. A dotted grid line is shown at X=0 that means no difference. The Y axis demonstrates the -log 10 of the p (0.05). The threshold of significance ($-\log_{10}(0.05) = 1.3$) is indicated with a horizontal dotted red line.

5.5 Bibliography

Al-Attar, A. *et al.* (2016) 'The effect of sex on immune cells in healthy aging: Elderly women have more robust natural killer lymphocytes than do elderly men', *Mechanisms of Ageing and Development*, 156, pp. 25–33. Available at: https://doi.org/10.1016/j.mad.2016.04.001.

Almeida-Oliveira, A. *et al.* (2011) 'Age-related changes in natural killer cell receptors from childhood through old age', *Human Immunology*, 72(4), pp. 319–329. Available at: https://doi.org/10.1016/j.humimm.2011.01.009.

André, P. *et al.* (2018) 'Anti-NKG2A mAb Is a Checkpoint Inhibitor that Promotes Anti-tumor Immunity by Unleashing Both T and NK Cells', *Cell*, 175(7), pp. 1731-1743.e13. Available at: https://doi.org/10.1016/j.cell.2018.10.014.

Barker, E. *et al.* (2007) 'Dysfunctional natural killer cells, in vivo, are governed by HIV viremia regardless of whether the infected individual is on antiretroviral therapy', *AIDS*, 21(17), pp. 2363–2365. Available at: https://doi.org/10.1097/QAD.0b013e3282f1d658.

Björkström, N.K., Ljunggren, H.-G. and Sandberg, J.K. (2010) 'CD56 negative NK cells: origin, function, and role in chronic viral disease', *Trends in Immunology*, 31(11), pp. 401–406. Available at: https://doi.org/10.1016/j.it.2010.08.003.

Brummelman, J. *et al.* (2018) 'High-dimensional single cell analysis identifies stem-like cytotoxic CD8+ T cells infiltrating human tumors', *Journal of Experimental Medicine*, 215(10), pp. 2520–2535. Available at: https://doi.org/10.1084/jem.20180684.

Chidrawar, S.M. *et al.* (2006) 'Ageing is associated with a decline in peripheral blood CD56bright NK cells', *Immunity & Ageing*, 3(1), p. 10. Available at: https://doi.org/10.1186/1742-4933-3-10.

Cho, M.M. *et al.* (2020) 'Programmed cell death protein 1 on natural killer cells: fact or fiction?', *Journal of Clinical*

Investigation, 130(6), pp. 2816–2819. Available at: https://doi.org/10.1172/JCI137051.

Cocker, A.T.H. *et al.* (2022) 'CD56-negative NK cells: Frequency in peripheral blood, expansion during HIV-1 infection, functional capacity, and KIR expression', *Frontiers in Immunology*, 13. Available at: https://doi.org/10.3389/fimmu.2022.992723.

Darrah, P.A. *et al.* (2007) 'Multifunctional TH1 cells define a correlate of vaccine-mediated protection against Leishmania major', *Nature Medicine*, 13(7), pp. 843–850. Available at: https://doi.org/10.1038/nm1592.

Gumá, M. *et al.* (2006) 'Expansion of CD94/NKG2C+ NK cells in response to human cytomegalovirus-infected fibroblasts', *Blood*, 107(9), pp. 3624–3631. Available at: https://doi.org/10.1182/blood-2005-09-3682.

Hadad, U. *et al.* (2015) 'NKp46 Clusters at the Immune Synapse and Regulates NK Cell Polarization', *Frontiers in Immunology*, 6. Available at: https://doi.org/10.3389/fimmu.2015.00495.

Hamerman, J.A., Ogasawara, K. and Lanier, L.L. (2005) 'NK cells in innate immunity', *Current Opinion in Immunology*, 17(1), pp. 29–35. Available at: https://doi.org/10.1016/j.coi.2004.11.001.

Hazeldine, J., Hampson, P. and Lord, J.M. (2012) 'Reduced release and binding of perforin at the immunological synapse underlies the age-related decline in natural killer cell cytotoxicity', *Aging Cell*, 11(5), pp. 751–759. Available at: https://doi.org/10.1111/j.1474-9726.2012.00839.x.

Hazeldine, J. and Lord, J.M. (2013) 'The impact of ageing on natural killer cell function and potential consequences for health in older adults', *Ageing Research Reviews*, 12(4), pp. 1069–1078. Available at: https://doi.org/10.1016/j.arr.2013.04.003.

Hu, P.F. *et al.* (1995) 'Natural killer cell immunodeficiency in HIV disease is manifest by profoundly decreased numbers of CD16+CD56+ cells and expansion of a population of CD16dimCD56- cells with low lytic activity.', *Journal of acquired*

immune deficiency syndromes and human retrovirology : official publication of the International Retrovirology Association, 10(3), pp. 331–40.

Huang, Z. *et al.* (2021) 'Effects of sex and aging on the immune cell landscape as assessed by single-cell transcriptomic analysis', *Proceedings of the National Academy of Sciences*, 118(33). Available at: https://doi.org/10.1073/pnas.2023216118.

Imai, K. *et al.* (2000) 'Natural cytotoxic activity of peripheral-blood lymphocytes and cancer incidence: an 11-year follow-up study of a general population', *The Lancet*, 356(9244), pp. 1795–1799. Available at: https://doi.org/10.1016/S0140-6736(00)03231-1.

Ishiyama, K. *et al.* (2021) 'Programmed cell death 1-expressing CD56-negative natural killer (NK) cell expansion is a hallmark of chronic NK cell activation during dasatinib treatment', *Cancer Science*, 112(2), pp. 523–536. Available at: https://doi.org/10.1111/cas.14692.

Judge, S.J., Murphy, W.J. and Canter, R.J. (2020) 'Characterizing the Dysfunctional NK Cell: Assessing the Clinical Relevance of Exhaustion, Anergy, and Senescence', *Frontiers in Cellular and Infection Microbiology*, 10. Available at: https://doi.org/10.3389/fcimb.2020.00049.

Laskowski, T.J., Biederstädt, A. and Rezvani, K. (2022) 'Natural killer cells in antitumour adoptive cell immunotherapy', *Nature Reviews Cancer*, 22(10), pp. 557–575. Available at: https://doi.org/10.1038/s41568-022-00491-0.

Lin, Z. *et al.* (2020) 'Establishment of age group classification for risk stratification in glioma patients', *BMC Neurology*, 20(1), p. 310. Available at: https://doi.org/10.1186/s12883-020-01888-w.

Márquez, E.J. *et al.* (2020) 'Sexual-dimorphism in human immune system aging', *Nature Communications*, 11(1), p. 751. Available at: https://doi.org/10.1038/s41467-020-14396-9.

Mavilio, D. *et al.* (2005) 'Characterization of CD56 $^{-}$ /CD16 $^{+}$ natural killer (NK) cells: A highly dysfunctional NK subset expanded in HIV-infected viremic individuals', *Proceedings of the National Academy of Sciences*, 102(8), pp. 2886–2891. Available at: https://doi.org/10.1073/pnas.0409872102.

McInnes, L., Healy, J. and Melville, J. (2018) 'UMAP: Uniform Manifold Approximation and Projection for Dimension Reduction'.
Michel, T. *et al.* (2016) 'Human CD56 ^{bright} NK Cells: An Update', *The Journal of Immunology*, 196(7), pp. 2923–2931. Available at: https://doi.org/10.4049/jimmunol.1502570.

Müller-Durovic, B. *et al.* (2019) 'CD56-negative NK cells with impaired effector function expand in CMV and EBV co-infected healthy donors with age', *Aging*, 11(2), pp. 724–740. Available at: https://doi.org/10.18632/aging.101774.

Ogata, K. *et al.* (2001) 'Association between natural killer cell activity and infection in immunologically normal elderly people', *Clinical and Experimental Immunology*, 124(3), pp. 392–397. Available at: https://doi.org/10.1046/j.1365-2249.2001.01571.x.

Orr, M.T. *et al.* (2010) 'Development and Function of CD94-Deficient Natural Killer Cells', *PLoS ONE*, 5(12), p. e15184. Available at: https://doi.org/10.1371/journal.pone.0015184.

Poli, A. *et al.* (2009a) 'CD56 ^{bright} natural killer (NK) cells: an important NK cell subset', *Immunology*, 126(4), pp. 458–465. Available at: https://doi.org/10.1111/j.1365-2567.2008.03027.x.

Poli, A. *et al.* (2009b) 'CD56 ^{bright} natural killer (NK) cells: an important NK cell subset', *Immunology*, 126(4), pp. 458–465. Available at: https://doi.org/10.1111/j.1365-2567.2008.03027.x.

Roberto, A. *et al.* (2018) 'The early expansion of anergic NKG2A ^{pos} /CD56 ^{dim} /CD16 ^{neg} natural killer represents a therapeutic target in haploidentical hematopoietic stem cell transplantation', *Haematologica*, 103(8), pp. 1390–1402. Available at: https://doi.org/10.3324/haematol.2017.186619.

Rosenberg, J. and Huang, J. (2018) 'CD8+ T cells and NK cells: parallel and complementary soldiers of immunotherapy', *Current Opinion in Chemical Engineering*, 19, pp. 9–20. Available at: https://doi.org/10.1016/j.coche.2017.11.006.

Di Vito, C., Mikulak, J. and Mavilio, D. (2019) 'On the Way to Become a Natural Killer Cell', *Frontiers in Immunology*, 10. Available at: https://doi.org/10.3389/fimmu.2019.01812.

Waldhauer, I. and Steinle, A. (2008) 'NK cells and cancer immunosurveillance', *Oncogene*, 27(45), pp. 5932–5943. Available at: https://doi.org/10.1038/onc.2008.267.

Yu, J. *et al.* (2010) 'CD94 surface density identifies a functional intermediary between the CD56bright and CD56dim human NK-cell subsets', *Blood*, 115(2), pp. 274–281. Available at: https://doi.org/10.1182/blood-2009-04-215491.

Chapter 6

Concluding Remarks of the Thesis

6.1 Conclusion

The challenges brought by the accelerated aging of the global population are felt in almost every nation, and have been certainly highlighted during the COVID-19 pandemic. A rise in age-related diseases, many of which have an immune component, is a result of the increased aged population. Understanding the pathophysiology of aging-related diseases amongst the immune system is therefore more crucial than ever.

The aim of this project was to develop and optimise standardised PFC panels that have the capability to detect age and sex related changes amongst T, B and NK lymphocytes, their subsets, and assess their functionality by evaluating their redox status.

As expected, this thesis has demonstrated that flow cytometry is a gold standard and robust technique for evaluating the phenotypic and functional characterisation of the immune system. Flow cytometry can measure multiple markers simultaneously on more than a thousand cells per second, which makes it possible to collect high throughput and high dimensional data from both a small and large volume of samples. Overall, our panels allow a deep characterisation of intracellular and functional components of

a variety of lymphocyte populations. Besides, our novel redox panel is noteworthy, as for the first time, multiple redox markers can be measured at a single cell level simultaneously with other phenotypic markers, something that traditional techniques like immunoblotting and microscopy can't do.

Specifically, by using our newly designed panels, we were able to identify that CD4+ T cells remain more resistant to age-related phenotypic and functional changes than CD8+ T cells, which exhibits a profound decrease in frequency and present an exhausted and senescent phenotype. For the first time we demonstrated that TPEX cells, a newly defined exhausted subset of stem cell memory T cells, increases with age in males and females, thus suggesting that their increased presence restricts CD8+ T cell differentiation and functionality (Galletti *et al.*, 2020). Consequently, further studies are necessary to elucidate CD8+ T cell loss of function with age, and further investigate mechanisms that could delay T cell senescence and exhaustion.

We are also able to clearly identify transcription factors that have been associated with age related changes in genomic studies. For example in B cells we identified a loss of XBP1 in all B cell subsets. XBP1 controls the transcription of UPR target genes involved in protein folding and consequently B cell plasma secretion (Grootjans *et al.*, 2016). Loss of XBP1 has been found to accelerate age-related decline in retinal function and neurodegeneration, thus confirming that XBP1 could potentially

be a target for B cell aging (McLaughlin *et al.*, 2018). By taking advantage of our Redox panel we demonstrated that among all T and B cell subsets, there is a loss of oxidative balance with age due to an increase of superoxide anions (ROS), while antioxidants like SOD1 and NRF2 don't change. This result signifies a loss of oxidative balance with age.

The comprehensive analysis of our NK cell panel revealed a decline of $CD56^{BRIGHT}$ NK cells with age. $CD56^{BRIGHT}$ NK cells are important correspondents towards the adaptive immune response by secreting cytokines thus their loss with age highlights the loss of communication amongst adaptive and innate cells with age (Michel *et al.*, 2016). Furthermore, we observed a significant enrichment of lymphocytes that lack CD56 but express high level of PD-1. We believe that further studies should emphasise on CD56 negative NK cells that seem to become enriched in healthy aging and how their recovery could convalesce the NK immune response.

In conclusion, our PFC panels demonstrated that the immune system is generally impaired with the aging, with a higher expression of exhaustion markers in T and NK cells, a loss of XBP-1 in B cells, and an overall loss of oxidative balance in T and B cells. Therefore the panels developed in this thesis can be used not only to asses major age and sex related changes but can be exploited by clinical trials to help the scientific community unravel information regarding T, B, NK cells and their redox status.

6.2 References

Grootjans, J. *et al.* (2016) "The unfolded protein response in immunity and inflammation," *Nature Reviews Immunology*, 16(8), pp. 469–484. Available at: https://doi.org/10.1038/nri.2016.62.

McLaughlin, T. *et al.* (2018) "Loss of XBP1 accelerates age-related decline in retinal function and neurodegeneration," *Molecular Neurodegeneration*, 13(1), p. 16. Available at: https://doi.org/10.1186/s13024-018-0250-z.

Michel, T. *et al.* (2016) "Human CD56 ^{bright} NK Cells: An Update," *The Journal of Immunology*, 196(7), pp. 2923–2931. Available at: https://doi.org/10.4049/jimmunol.1502570.

Epilogue

HemaSphere

EHA EUROPEAN HEMATOLOGY ASSOCIATION

Editorial
Open Access

A Journey Into the Unknown: PhD Students in a European Training Network on Age-related Changes in Hematopoiesis Conduct Their Project During a Global Pandemic

Christina Pitsillidou[1,2], Sandra Alonso-Rubido[1,3], Andrea Ávila-Ávila[4,5], Mari Carmen Romero-Mulero[6], Agata Labedz[1], Athanasios Oikonomou[7,8], Ludovica Proietti[9], Maria Eleni Psychoyiou[10], Clara Tellez-Quijorna[11], Maniriho Hillary[12], Eirini Sofia Fasouli[1,13], Guillermo Fernández-Rodríguez[14], Natalia Giner-Laguarda[15], Natalia Skinder[16], Chiara Taroni[17], John Strouboulis[10], Eleni Katsantoni[13], Antonella Ellena Ronchi[1]

Correspondence: Christina Pitsillidou (c.pitsillidou@campus.unimib.it).

[1]Dipartimento di Biotecnologie e Bioscienze, Università degli Studi Milano-Bicocca, Milano, Italy
[2]FlowMetric Europe, Milan, Bresso, Italy
[3]Diagenode SA, Ougrée, Belgium
[4]Institute Curie, Orsay, France
[5]Centre National de la Recherche Scientifique UMR3348, Centre Universitaire, Orsay, France
[6]Max Planck Institute of Immunobiology and Epigenetics, Freiburg, Germany
[7]Fondazione Tettamanti, Centro di Ricerca Tettamanti, Centro Maria Letizia Verga, Monza (MB), Italy
[8]Dipartimento di Medicina e Chirurgia, Università degli Studi Milano-Bicocca, Monza (MB), Italy
[9]Institute of Medical Biochemistry, University of Veterinary Medicine, Vienna, Austria
[10]Molecular Haematology, Comprehensive Cancer Centre, School of Cancer and Pharmaceutical Sciences, King's College London, United Kingdom
[11]Team of Epigenetics in Normal and Abnormal Hematopoiesis, CRCM (Centre de Recherche en Cancérologie de Marseille), France
[12]Department of Human Molecular Genetics and Biochemistry, Sackler Faculty of Medicine, Tel Aviv University, Tel Aviv-Yafo and Schneider Children's Medical Centre of Israel, Petach, Tikvah
[13]Basic Research Center, Biomedical Research Foundation, Academy of Athens, Greece
[14]Department of Biology and Biotechnology "Charles Darwin", Sapienza University of Rome, Italy
[15]Department of Cellular and Molecular Biology, Centro de Investigaciones Biológicas Margarita Salas, Madrid, Spain
[16]European Research Institute for the Biology of Ageing, University Medical Center Groningen, University of Groningen, Netherlands
[17]Institut de Génétique et de Biologie Moléculaire et Cellulaire (IGBMC), Institut National de la Santé et de la Recherche Médicale (INSERM) U1258, Centre National de la Recherche Scientifique (CNRS) UMR 7104, Université de Strasbourg, Illkirch, France
CP, SA-R, AÁ-Á, and MCR-M have contributed equally to this work.

HemaSphere (2022) 6:8(e763).
http://dx.doi.org/10.1097/HS9.0000000000000763.

The age-related changes in hematopoiesis (ARCH) project is part of the Innovative Training Network (ITN) of the Marie-Sklodowska Curie Actions (MSCA) program, which provides doctorate training of excellence based on the exchange of ideas and competencies from the academic and private sectors.[1] The ARCH project intends to outline hematopoietic stem cell (HSC) alterations with aging, how hematopoietic cell individuality is controlled at the transcriptional and epigenetic levels in normal hematopoiesis and in leukemias, and understand the crosstalk between intrinsic and extrinsic indications that support the proliferation of preleukemic and leukemic cells within the hematopoietic niche.

We are 15 PhD students funded by this network, based around Europe, and our common aim is to understand functional changes in the hematopoietic system with age, how these changes link to the development of age-associated diseases and in parallel work towards the development of new treatments.[2] Our projects kicked off just when the severe acute respiratory coronavirus-2 (SARS-CoV-2) emerged. Two and a half years later, SARS-CoV-2 continues to infect millions of people and has taken the lives of at least 6 million people worldwide.[3] The COVID-19 outbreak brought along social isolation and feelings of uncertainty to everyone around the world, including doctorate students.[4,5] Ironically, our projects have been more relevant than ever, as the pandemic has highlighted the important relationship between age-related changes in hematopoiesis and disease severity. Below, we aim to discuss the timeline of the ARCH project throughout the pandemic and how we managed to courageously pull through the hardships of doing research during a global pandemic within different settings (academia/institutes and industry). We provide recommendations to future PhD students on how to manage their PhD projects during global emergencies.

PANDEMIC TIMELINE OF ARCH

The rapid spread of SARS-CoV-2 at the beginning of 2020 in Europe led the World Health Organization to declare a global pandemic on March 11, 2020. The ARCH opening conference,

planned for the same month was canceled. At the same time, the first lockdowns were put in place around Europe, while most of us were just starting our new project or were moving to a different country to begin. Some of us started on this project during or after the first lockdown, causing further delays, which led to a multiphasic pattern of recruitment (Figure 1). During the first lockdown, we individually set up our strategies to progress our research projects at home by either reading scientific literature, writing review papers,[6,7] or planning experiments for when we would eventually return to work. By summer 2020, many of us began to slowly get back to the laboratory in shifts or for a limited time to avoid overcrowding of spaces. Times were still uncertain and the pandemic was of great concern to the global scientific community. With the whole world waiting for vaccine developments to stop the pandemic, our slow training process commenced. However, by fall, new lockdown measures were set against a new surge of infections and deaths (Figure 1). This second lockdown stretched until Christmas, marking the completion of our first year with minimal hands-on training and very limited experimental progress. This brings us to today, where most of us have entered the final year of our projects and it seems that COVID-19 is here to stay.

COVID-19: PHDS INTO THE UNKNOWN

Engaging in a PhD project on its own is stressful and overwhelming. The main objectives when beginning a 3-year PhD project are to develop new laboratory, academic, and research-based skills, yet we were unable to advance on any of these. Close and continuous supervision is required to meet these goals. Communication with supervisors at the beginning of our PhDs, which coincided with the pandemic, made our start more challenging than expected. Coming out of isolation in the summer of 2020, we did not expect those upcoming months would continue to affect our projects and to make us experience how vulnerable we are.

Working hours were adjusted to allow for social distancing, while meetings were still being held online. Even when we were physically at the laboratory, there was an inability for close supervision due to safety restrictions. In addition to communication challenges, technical difficulties were also at play during the first lockdown. For example, students that had already begun to breed mice a few weeks before the lockdown were forced to interrupt their experiments and redirect their projects as it would take too much time to re-establish mouse breeding. The high demand for equipment, reagents, and consumables for the advancement of COVID-19 research and diagnosis added to

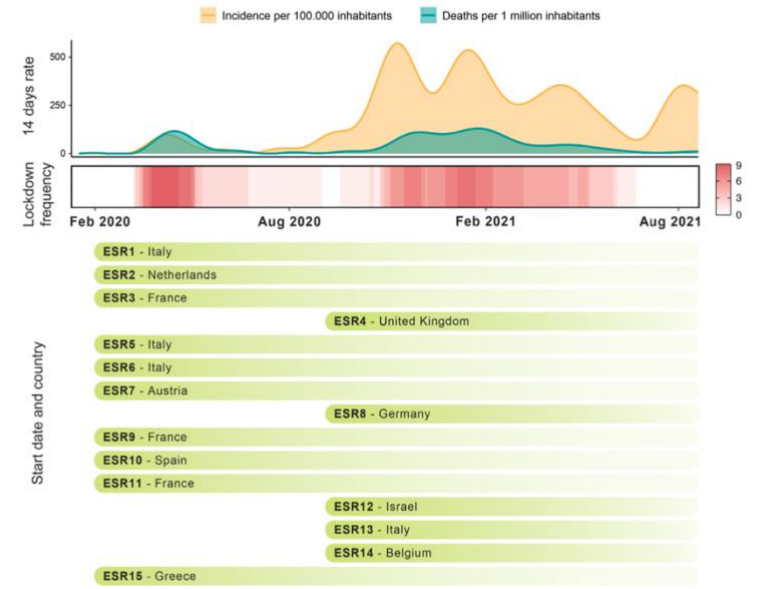

Figure 1. Timeline of the ARCH project during the COVID-19 pandemic. Average 14-day notification rates of newly reported COVID-19 cases per 100,000 inhabitants and COVID-19 related deaths per 1 million inhabitants in the participating countries of the ARCH project are represented during the first year and a half of the pandemic in Europe (top graph). By fall 2020, there is an all-time high of the infection and death rates. The lockdown frequency considered as the daily number of ARCH participating countries under measurements of lockdown is shown in a heat-map along the same period (middle graph). Starting time and country of the beneficiary institution where each early stage researcher (ESR) performs the PhD project is shown in bars (bottom graph). These data have been collected from official governmental reports from each country. The lockdown definition and concrete measures differ between countries and regions within the countries.

these difficulties and made it challenging for us to obtain the necessary consumables for our research. Reagents and consumables were not the only shortage, but also sample availability. As our projects are based on hematology, many of our experiments require fresh samples from healthy or diseased participants to progress. Such fresh materials were merely impossible to find as clinics halted unnecessary visits and hospitals gave sole priority to COVID-19 patients. Again, this inevitably led to the redirection of some projects and added to the uncertainties and delays of the projects.

Some institutions acknowledged the loss of time for many PhD students and offered time extensions for thesis submissions. In some institutions, time extensions were only applicable to students that were enrolled in their second and third year, a situation that we consider is not justified as the pandemic had a strong impact on all PhD projects regardless of the year of enrollment. However, those that were offered an extension were offered no additional financial support. This made us feel that our PhD training status was overlooked and shows once more that PhD positions are a precarious form of employment. As these are typically 3 to 4 year training periods, where PhD students need to provide evidence of strong scientific skills, not being able to work is a major limitation not only to obtain the PhD degree, but also for the success in making next step in the career.

COVID-19 repercussions created disruptions also to life science companies. Twenty percent of ARCH students work in the private sector. Companies had to adapt to the COVID-19 pandemic to survive, thus made COVID-19 research and treatment innovation their uppermost priority. Industry supervisors were understandably busy involved in clinical research projects to meet client requests. Lockdown measures stalled many investigations, having a domino effect on doctorate projects based there. At the same time, the detachment of industry PhDs from research institutions and universities negatively affected their learning progress.

The main scientific activities were mostly virtual and we missed the stimulus of having an audience present, while many such events were inadequately organized and prone to technical glitches. Virtual learning left gaps in milestone competencies like collaboration and the development of a critical approach to research questions and results. However, we are thankful for online platforms. Regardless of the complexity of our position, many of us took advantage of the lockdown by completing online courses and taking part in virtual conferences. Virtual platforms at least allowed us to have some communication and to develop more valuable computational skills than ever before, which were also applied to our projects.

WHAT PHD STUDENTS CAN DO DURING GLOBAL EMERGENCIES?

Doctorate students aim to find the answers to complex scientific problems and need to excel in critical thinking and correct decision-making, which already imposes pressure on them. Experiencing external pressures through a global pandemic makes it harder to face the challenges associated with research. Here we offer our advice to students that could be experiencing similar global emergencies:

Mental wellbeing is one of the biggest challenges one will face when conducting a PhD project in such peculiar times. Even under the best circumstances, one cannot be productive at all times. Therefore, we recommend PhD students to avoid harsh self-criticism if they are lack motivation. We strongly encourage PhD students to share feelings with their peers and colleagues in the same consortium or institution and thus to be open and talk about all problems. We created a group chat where we shared our thoughts and worries. This exercise made us realize that we were not alone and others could relate to our emotions, which was comforting. It is important to rely on other students and researchers to find personal support. Do not hesitate to reach out to your supervisor for help regarding your mental wellbeing as this can have an impact on your work. Good supervision and communication are crucial for the proper development and success of your project.

To make the most out of a PhD project we recommend that PhD students take advantage of all opportunities and plan. Design experiments to be performed during times when you can enter the laboratory and plan to generate enough data that you can analyze if a new lockdowns arises. We recommend students to start writing anything related to their research field. For example, write the introduction of the PhD thesis, methodologies that will be used, write a review article, and so on. PhD students will have to write at some point, so they should not hesitate to start even with no results or experience in the field they have just embarked on. Additionally, online seminars can be followed as well as online courses, for example to develop new computational or experimental skills.

CONCLUSION

Despite all the difficulties, we feel fortunate to be part of the ARCH MSCA ITN program. In December 2021, after 2 years of travel restrictions, we finally met for the first time in person in Rome. Here students and supervisors used this opportunity to begin collaborations, present projects, discuss, and overcome limitations.

The COVID-19 pandemic continues to have a significant impact on scientists. PhD students completing their projects throughout the global pandemic have suffered immense isolation and anxiety. Despite recurring delays throughout our project, we feel we have emerged as efficient workers, excellent planners and have developed strong social skills virtually and in person. Those experiencing similar global emergencies should share their experience with peers and colleagues, and find ways to efficiently transit towards effective solutions.

Finally, we hope that PhD students experiencing such situations are acknowledged for the time lost and hope that funding agencies recognize that time extensions should be accompanied by financial compensation.

DISCLOSURES

The authors have no conflicts of interest to disclose.

SOURCE OF FUNDING

This project has received funding from the European Union's Horizon 2020 Research and Innovation Program under the Marie Skłodowska-Curie grant agreement no. 813091 (ARCH, age-related changes in hematopoiesis).

REFERENCES

1. Marie Sklodowska-Curie Actions. *MSCA: Developing talents, advancing research*. [Online]. Available at: https://marie-sklodowska-curie-actions.ec.europa.eu Accessed April 12, 2022.
2. Age-related changes in hematopoiesis: ARCH project. [Online]. Available at: https://arch-project.eu/ Accessed March 20, 2022.
3. Wang H, Paulson K, Pease S, Watson S, Comfort H, Zheng P et al. Estimating excess mortality due to the COVID-19 pandemic: a systematic analysis of COVID-19-related mortality, 2020–21. *Lancet*. 2022;399:1513–1536.
4. Keszei Z, Vendrell X, Soultsioti M, Molina P, Wirth L, Weiss H, et al. 100 days of solitude: The spring of COVID-19 through the eyes of 15 young virologists of the INITIATE program. *Virus Res*. 2020;287:198093.
5. Gavriilaki E, Maiques-Diaz A. "Long COVID-19" of researchers: what to do next? *HemaSphere*. 2022;6:e673.
6. Barbarani G, Łabedz A, Ronchi A. β-Hemoglobinopathies: the test bench for genome editing-based therapeutic strategies. *Front Genome Ed*. 2020;2:571239.
7. Barbarani G, Labedz A, Stucchi S, Abbiati A, Ronchi A. Physiological and aberrant γ-globin transcription during development. *Front Cell Dev Biol*. 2021;9:640060.
8. Giner-Laguarda N, Vidal M. Functions of polycomb proteins on active targets. *Epigenomes*. 2020;4:17.
9. Fasouli E, Katsantoni E. JAK-STAT in early hematopoiesis and leukemia. *Front Cell Dev Biol*. 2021;9:669363.